

**A Comparison of Analytical Models and Experimental Results
for the Acoustic Response in a Non-rigid-wall Enclosure**

by

James Mumaw


Thesis submitted to the Faculty of the
Virginia Polytechnic Institute and State University
in partial fulfillment of the requirements for the degree of

MASTERS OF SCIENCE

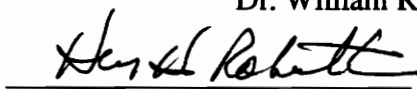
IN

MECHANICAL ENGINEERING

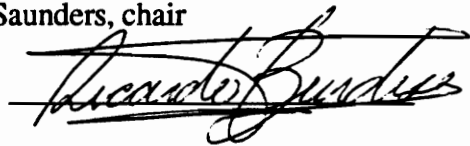
APPROVED:



Dr. William R. Saunders, chair



Dr. Harry S. Robertshaw



Dr. Ricardo A. Burdisso

December, 1996

Blacksburg, Virginia

Keywords: Acoustic, Enclosure, Modeling, Impedance, Control

LD
5655
V855
1986
M863
C.2

**A Comparison of Analytical Models and Experimental Results
for the Acoustic Response in a Non-rigid-wall Enclosure**

by

James Mumaw

Committee Chairman: Dr. William R. Saunders

Mechanical Engineering

(ABSTRACT)

The work presented in this thesis was motivated by the need for an accurate modeling approach for the acoustic response in a non-rigid-wall enclosure. The acoustic response in any enclosure is determined by the boundary conditions at the interior surface of the enclosure walls, and the types of sources present. The analyses presented in this thesis assumed that the sources were either at the surface of the enclosure, or interior to the enclosure walls.

Three different analytical modeling approaches were investigated and presented in this thesis for the acoustic response in a rectangular enclosure. A reference model assumed that the walls of the enclosure were rigid, corresponding to an infinite acoustic impedance boundary condition. The acoustic pressure response was expressed in terms of the characteristic rigid wall acoustic modes of the enclosure. The second modeling

approach used a finite acoustic impedance boundary condition to model the influence of non-rigid walls on the acoustic response. The third modeling approach treated the vibration of the enclosure walls as additional sources which were constructed from the *in vacuo* structural modes of the enclosure. The acoustic pressure was expressed in terms of the rigid-wall acoustic modes. High-dimensional state variable and transfer function models are presented, along with discussions of their validity and performance as model parameters vary. The frequency response functions generated using these three models were compared to the actual acoustic frequency response function obtained experimentally for a non-rigid-wall, plexiglass enclosure. It was found that the finite impedance model generated an acoustic response which best matched that of the actual acoustic response in magnitude and frequency; however, further development of this model is needed to account for structural resonances of the enclosure.

For Mom and Dad...

Acknowledgments

I would like to thank my advisor, Dr. William Saunders, for his guidance and encouragement when difficulties arose in my research, and for giving me the opportunity to work on several interesting projects. I would also like to thank the other members of my committee, Dr. Ricardo A. Burdisso and Dr. Harry Robertshaw, for reviewing my work, and offering their comments.

Thanks to the guys I shared an office with, who offered help when they could.

Table of Contents

Abstract.....	ii
Dedication	iv
Acknowledgments.....	v
Table of Contents.....	vi
List of Figures.....	ix
List of Tables	xiii
List of Variables.....	xiv
Chapter 1. Introduction.....	1
Overview of Thesis	3
Chapter 2. Literature Review.....	5
2.1 Early Years	5
2.2 Advancements in Active Sound Control	8
2.2.1 Feedforward Control of Sound (General)	9
2.2.2 Feedback Control of Sound (General)	10
2.2.3 Active Sound Control in an Acoustic Duct	12
2.2.4 Active Control of Enclosed Sound.....	15
2.3 Modeling of Enclosure Acoustics	21
2.3.1 Transducer Dynamics.....	23

Chapter 3. Model Formulation for Enclosure Acoustics	25
3.1 Rigid-wall Boundary Condition (Infinite Acoustic Impedance).....	25
3.1.1 Solution for Rigid-wall Eigenvalues and Eigenfunctions	29
3.2 Non-rigid-wall Boundary Condition (Finite Acoustic Impedance).....	35
3.2.1 Solution for Non-rigid-wall Eigenvalues and Eigenfunctions.....	36
3.3 Coupled Modal Approach	46
3.4 Transducer Dynamics Model.....	54
Chapter 4. Comparison of Numerical Results for Acoustic Models and Experimental Results	56
4.1 Experimental Set-up and Results	56
4.2 Infinite Impedance Model (Rigid Wall).....	59
4.3 Finite Impedance Model (Non-rigid Wall)	62
4.3.1 Influence of Impedance Value and Frequency on Eigenvalue	62
4.4 Coupled Modal Approach	71
Chapter 5. Conclusions and Future Work	76
5.1 Assessment of Acoustic Models	77
5.1.1 Rigid-wall Model	77
5.1.2 Finite Acoustic Impedance Model.....	78

5.1.3 Coupled Model	78
5.2 Future Work	79
Bibliography	81
Appendix A. Experimental Enclosure Characteristics.....	86
Vita	122

List of Figures

Figure 2.1 Lueg's Patent	6
Figure 2.2 Olson and May's Electronic Absorber.....	7
Figure 2.3 Placement of Active Sound Absorbers in Room.....	7
Figure 2.4 Elements of Active Sound Control Design.....	20
Figure 3.1 Rigid Wall Acoustic Eigenfunction	33
Figure 4.1 Experimentally Measured Speaker Frequency Response	57
Figure 4.2 Frequency Response of Sensor Microphone.....	57
Figure 4.3 Experimental Acoustic Frequency Response (a) Collocated, (b) Non-collocated.....	58
Figure 4.4 Comparison of Experiment to Rigid-wall Model Acoustic Frequency Response (a) Collocated, (b) Non-collocated	61
Figure 4.5 k_x vs. k	63
Figure 4.6 k_x (odd) vs. Impedance Ratio (a) Magnitude, (b) Real Part, (c) Imag. Part...	64
Figure 4.7 k_x (even) vs. Impedance Ratio (a) Magnitude, (b) Real Part, (c) Imag. Part..	65
Figure 4.8 k_x (odd) vs. Real Impedance Ratio.....	66
Figure 4.9 k_x (odd) vs. Imaginary Impedance Ratio	66
Figure 4.10 Magnitude of Eigenfunction for Infinite Impedance Ratio	67
Figure 4.11 Magnitude of Eigenfunction When Impedance Ratio is Real	68
Figure 4.12 Magnitude of Eigenfunction When Impedance Ratio is Imaginary	68

Figure 4.13 Comparison of Experiment to Finite Impedance Model Acoustic Frequency Response (a) Collocated, (b) Non-collocated 69

Figure 4.14 Experimentally Estimated Acoustic Impedance Ratio..... 70

Figure 4.15 Comparison of Experiment to Coupled Model Acoustic Frequency Response (a) Collocated, (b) Non-collocated 74

Figure A.1 Enclosure (Note: Holes Sealed When Not in Use)..... 87

Figure A.2 Left End of Enclosure..... 87

Figure A.3 Right End of Enclosure..... 88

Figure A.4 Front of Enclosure..... 88

Figure A.5 Top of Enclosure..... 89

Figure A.6 Bottom of Enclosure 89

Figure A.7 Dynaco Amplifier Frequency Response..... 90

Figure A.8 Speaker 1, Collocated Microphone 91

Figure A.9 Speaker 1, Microphone 1..... 92

Figure A.10 Speaker 1, Microphone 5..... 93

Figure A.11 Speaker 1, Microphone 7..... 94

Figure A.12 Speaker 1, Microphone 8..... 95

Figure A.13 Speaker 1, Microphone 11..... 96

Figure A.14 Speaker 1, Microphone 12..... 97

Figure A.15 Speaker 2, Microphone Collocated With Speaker 1 98

Figure A.16 Speaker 2, Microphone 1..... 99

Figure A.17 Speaker 2, Microphone 2.....	100
Figure A.18 Speaker 2, Microphone 6.....	101
Figure A.19 Speaker 2, Microphone 9.....	102
Figure A.20 Speaker 2, Microphone 10.....	103
Figure A.21 Speaker 2, Microphone 11.....	104
Figure A.22 Speaker 2, Microphone 13.....	105
Figure A.23 Speaker 2, Microphone Collocated	106
Figure A.24 Speaker 3, Microphone 1.....	107
Figure A.25 Speaker 3, Microphone 2.....	108
Figure A.26 Speaker 3, Microphone 5.....	109
Figure A.27 Speaker 3, Microphone 7.....	110
Figure A.28 Speaker 3, Microphone 8.....	111
Figure A.29 Speaker 3, Microphone 11.....	112
Figure A.30 Speaker 3, Microphone 13.....	113
Figure A.31 Speaker 4, Microphone 1.....	114
Figure A.32 Speaker 4, Microphone 2.....	115
Figure A.33 Speaker 4, Microphone 5.....	116
Figure A.34 Speaker 4, Microphone 7.....	117
Figure A.35 Speaker 4, Microphone 8.....	118
Figure A.36 Speaker 4, Microphone 9.....	119
Figure A.37 Speaker 4, Microphone 11.....	120

Figure A.38 Speaker 4, Microphone 12..... 121

List of Tables

Table 4.1 Modeled Impedance Ratio Values.....	70
---	----

List of Variables

Acoustic model variables:

a_n	acoustical mode contribution factor
A_x, B_x	harmonic solution coefficients of acoustic response for rigid-wall case
C_x, D_x	harmonic solution coefficients of acoustic response for non-rigid-wall case
c	speed of sound in fluid medium (for air $c \cong 345$ m/s)
E	Young's modulus of structural material
$f(\mathbf{r}_s)$	force per unit area
h	wall thickness
i	complex variable
k	wave number, equal to ω/c
k_n	eigenvalue corresponding to acoustical mode n
k_x, k_y, k_z	eigenvalues corresponding to x , y , and z directions, respectively
L_x	x dimension of rectangular enclosure
L_y	y dimension of rectangular enclosure
L_z	z dimension of rectangular enclosure
n	used to define normal direction
n	mode number
n_x, n_y, n_z	modal integers corresponding to x , y , and z directions, respectively
p	acoustic pressure
p_x, p_y	structural mode integers corresponding to x and y directions, respectively

q	volume velocity of source
\mathbf{r}	response field point, in Cartesian coordinates it is equivalent to (x, y, z)
\mathbf{r}_0	source field point, in Cartesian coordinates it is equivalent to (x_0, y_0, z_0)
t	time
V	enclosure volume
w	normal displacement of wall
w_p	structural mode contribution factor
$X(x)$	part of acoustical eigenfunction corresponding to the x direction
$Y(y)$	part of acoustical eigenfunction corresponding to the y direction
$Z(z)$	part of the acoustical eigenfunction corresponding to the z direction
Z	specific acoustic impedance equivalent to p/v_n
ρ	density of fluid medium (for air $\rho \cong 1.2 \text{ kg/m}^3$)
$\Psi_n(\mathbf{r})$	acoustical eigenfunction corresponding to mode n, for position \mathbf{r}
ω	frequency in rad/sec
ω_n	natural frequency in rad/sec
Λ_n	normalization factor for mode n
ζ_n	viscous damping coefficient corresponding to mode n
δ_n	imaginary part of complex acoustic eigenvalue is equal to δ_n/c
v_n	air particle velocity normal to surface
ζ	acoustical impedance ratio, which is equal to $Z/\rho c$
$\Phi_p(\mathbf{r})$	structural eigenfunction corresponding to mode p, for position \mathbf{r}

ρ_m	density of wall material
ν	Poisson's ratio of structural material

Speaker model variables:

B	magnetic flux density in driver air gap
C_{AS}	acoustic compliance of driver suspension
l	length of the voice-coil conductor in magnetic field of air gap
M_{AS}	acoustic mass of driver diaphragm assembly including voice coil and air load
R_{AS}	acoustic resistance of driver suspension losses
R_{AT}	total acoustic resistance
R_E	dc resistance of driver voice coil
R_g	output resistance of source
\dot{q}	volume acceleration of source
S_D	effective projected surface area of driver diaphragm
V_{in}	input voltage to the speaker

Chapter 1. Introduction

Several techniques have been investigated for the active control of sound. All of these techniques fall under one or both of two basic approaches, feedforward control or feedback control.

Feedforward control requires a reference signal that is coherent with the sound to be controlled. This reference signal can be used with a controller to produce a secondary signal to destructively interfere with the primary noise signal. Adaptive feedforward control uses an error signal to adjust the controller gains in order to minimize the controlled signal. When a reference signal is not available then feedback control can be used.

Feedback control design uses the response of the plant. To simulate and design the controller for the controlled system response, a model of the plant dynamics is required. Two types of models are sought after. The first is an accurate transfer function model, which can be used to generate magnitude and phase frequency response plots from which the gain and phase margins of the system can be found. These are an indication of when the controlled system will be unstable. The second is a pole-zero model that can be used to generate a pole-zero plot from which any unstable, right-half-plane poles can be seen. These models can be easy to generate for relatively simple plants, but become more difficult for increasing plant complexity. One such complex plant is a non-rigid-wall enclosure.

If the boundaries of the enclosed sound field are rigid, then the model for the dynamics is not difficult to formulate. This is assuming that the enclosure is simple in shape, and the sources are well defined. The effect of non-rigid walls on the acoustic response within the enclosure is more difficult to model, especially for non-uniform structures.

When the walls of the enclosure are not rigid, there will be a resulting acoustic response due to the vibration of the walls. The vibration of the enclosure walls may be due to mechanical inputs or may be induced by the enclosed sound field itself. The development of an accurate model of the dynamics of this coupled system must account for the changed acoustic wall impedance, which results from the wall motions. There is no mechanism available in the rigid-wall model to account for the vibration of the walls. Therefore, other modeling approaches are needed.

The purpose of this thesis is to compare three different analytical models for the acoustic response in an enclosure. The first model is for the acoustic response in a rigid-wall enclosure. This model assumes that the acoustic impedance at the interior surface of the enclosure walls is approximately infinite. The acoustic pressure is expressed in terms of the characteristic acoustic modes of the enclosure. The other two models are for the response in a non-rigid-wall enclosure. The first model uses finite complex acoustic impedance values for each pair of walls. The corresponding eigenvalues and eigenfunctions are then calculated based on this finite impedance value. The acoustic pressure is expressed in terms of complex modes. The second model for a non-rigid-wall enclosure treats the vibration of the enclosure walls as additional sources, which are

expressed in terms of the *in vacuo* modes of the structure. The pressure is expressed as an expansion of the rigid wall acoustic modes of the enclosure. It will be shown how the steady-state and transient responses predicted by each of these models is different. The acoustic frequency responses which are given by these three models are then compared to the actual frequency response which is found in an experimental, non-rigid-wall enclosure.

It was found that the rigid-wall model did not produce a frequency response function that accurately represented the frequency response functions measured experimentally. This was not unexpected and was due to the fact that there was no mechanism to account for the influence of the wall flexibility, as mentioned earlier. The frequency response generated using the coupled modal modeling approach did not match the actual frequency response, due to the inaccuracy of the structural modes that were available for those calculations. The finite impedance modeling approach produced an acoustic frequency response that best matched the actual frequency response. However, detailed analysis of this approach shows that a fundamental assumption is made, which requires that the acoustic impedance increase linearly with frequency. In addition, this modeling approach would need further development in order to predict accurate wall velocities of the enclosure.

Overview of Thesis

This thesis is divided into five chapters. Chapter 2 is a review of literature covering the development of active sound control, particularly concerning the modeling of

enclosed sound fields. It begins with the patent presented by Lueg (1936) introducing the concept of active sound control and ends with the most recent papers dealing with new techniques and applications for the active control of sound. Chapter 3 gives an in-depth formulation of each of the analytical models mentioned previously. Chapter 4 presents some numerical results using the models formulated in Chapter 3. The results calculated using each of the formulated models are compared to each other, as well as to experimental data which was collected for an actual enclosure. Representative experimental frequency response plots are included in Chapter 4, and additional experimental results are included in Appendix A. Chapter 5 presents conclusions based on the numerical results which were found, and discusses future work.

Chapter 2. Literature Review

There are two basic approaches for active sound control. These include feedforward and feedback control strategies. The effectiveness of either control strategy is determined by the type of system to be controlled and the availability of key physical parameters. For example, if a reference signal that is coherent with the signal to be controlled is not available, then feedforward control is not possible. Feedback control can be used, but the stability of the controlled system must be ensured. One way to analyze the stability of the controlled system is to develop its frequency response, with the use of an accurate model. An accurate frequency response model will give magnitude and phase plots of the system response, and the gain and phase margins of the system can be found. A pole-zero plot will show any right-half plane poles which cause instability, based on the specific feedback control law.

This chapter presents a review of the literature dealing with the active control of acoustic systems. The chapter is divided into several sections. These sections cover the earliest attempts at active sound control, advancements in both active feedforward and active feedback sound control, active sound control in a duct, active control of enclosed sound, and modeling of the dynamics involved in an enclosed acoustic system.

2.1 Early Years

The theory on which active sound control is based has been in place for several decades (Lueg, 1936). In his patent, Lueg presented the theory that a sound wave could

be canceled by another sound wave with the same amplitude and opposite phase.

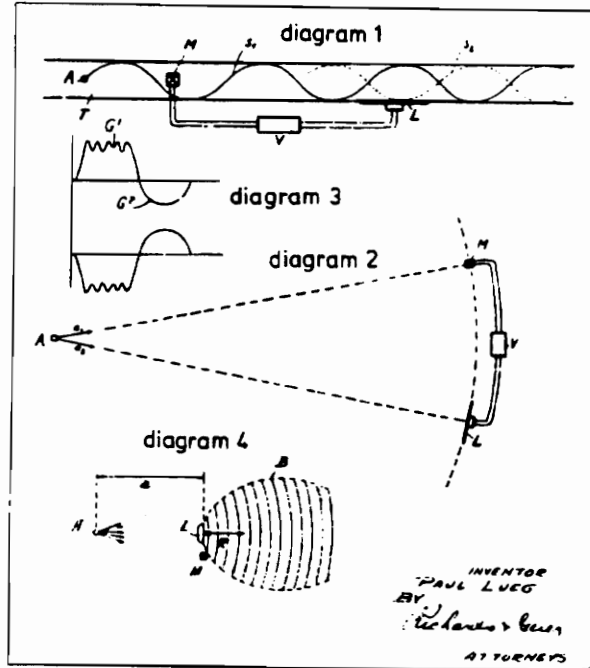


Figure 2.1 Lueg's Patent

In Figure 2.1 taken from his patent, Lueg showed the setup which could be used to reduce the sound pressure level in a duct downstream of a noise source (diagram 1). His method incorporated a feedforward control approach, in which the sound to be attenuated was sensed with a microphone (M) upstream of the control speaker (L). The sensed signal was then fed forward through a controller (V) to the control speaker; which produced a sound wave with the same frequency, amplitude, and the appropriate phase to cancel the unwanted sound wave. One problem associated with this technique is the sensing upstream of the compensating signal. Lueg does not discuss how to remedy this problem.

Olson and May (1953) were two of the first to suggest the use of a volume

velocity source as an acoustic absorber or local sound reducer.

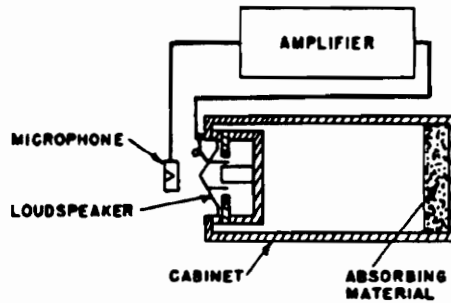


Figure 2.2 Olson and May's Electronic Sound Absorber

As shown in Figure 2.2 taken from their paper, their design consisted of a sensor microphone, a loudspeaker, and an amplifier connecting the two in a negative feedback manner. The electronic sound absorber, as they referred to it, was a feedback system which worked to reduce the sound pressure at the sensor microphone, by reducing the acoustical impedance. They envisioned several of these sources being placed on the walls on an enclosure as shown in Figure 2.3, much like conventional passive absorption materials would be used.

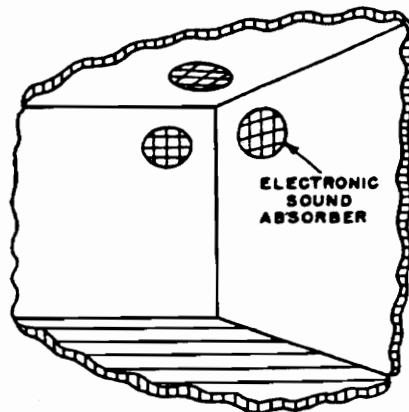


Figure 2.3 Placement of Active Sound Absorbers in Room

Olson wrote an additional paper (Olson, 1956), in which he further discussed the

electronic sound absorber, as well as an electronic vibration reducer. He listed several applications, including the local reduction of sound pressure near a passenger's head in an airplane or automobile compartment, or near a noisy machine operator's head. These applications involved the reduction of low frequency noise, which is not suitable for reduction using passive means. He also presented the idea of using a feedback noise reducer in a headset configuration, or helmet configuration. The noise at the wearer's ears would be reduced locally.

Bleazey (1962) used an 'electronic sound absorber,' to decrease the noise level produced by an air conditioning unit. He used a feedback control approach similar to Olson's device. He found that the sound was reduced best for the frequency range between 150 and 300 Hz.

Due to hardware limitations, the practical implementation of active sound control systems was limited. The correct amplitude and phase relationship between the primary and secondary source sound waves was difficult to achieve. Also, the dynamics of the different acoustical systems were not fully understood or easily modeled.

2.2 Advancements in Active Sound Control

Several papers have been written documenting the progression of noise control technology (Warnaka (1982), Guicking and Rollwage (1984), Leitch and Tokhi.(1987), Elliott and Nelson (1990), Tichy (1994), Eriksson (1994), Alves et al. (1995), Fuller and von Flotow (1995)). In addition to these papers, the book Active Control of Sound, by

P.A. Nelson and S.J. Elliott, is an excellent source for descriptions of the physical architectures and concepts related to the active control of sound.

As stated earlier, two basic approaches are used in the active control of sound. These include feedforward and feedback approaches. The specific system dynamics and disturbance inputs determine which of the two control strategies should be used.

2.2.1 Feedforward Control of Sound (General)

The feasibility of implementing feedforward active sound control is determined by the amount of information available from the acoustic system. Feedforward control requires the measurement of a reference signal that is coherent with the sound to be controlled. Numerous applications where this is possible have been investigated.

Ross (1981) used a digital feedforward control strategy (single degree of freedom) to reduce the low frequency sound entering an anechoic chamber through a set of doors. The sound to be attenuated was measured with a microphone located outside of the anechoic chamber. A loudspeaker was mounted at the entrance to the anechoic chamber, and provided the necessary control output to reduce the unwanted sound. In another paper, Ross (1982 I) described a feedforward control approach used to reduce the level of acoustic plane waves traveling through a duct. He reported reductions of 15 to 25 dB in the frequency range 25 to 350 Hz. Also in 1982 (II), Ross used an adaptive feedforward control method to reduce the sound level in a wind tunnel caused by the fan motor. Reductions of 11.2 dB in the frequency range from 40 to 160 Hz were obtained.

Chaplin (1983) described a technique using “waveform synthesis,” used to produce a control signal to cut down periodic noise and vibration. The system described by Chaplin was an adaptive feedforward approach. Essentially, the controller used past noise signal information to predict future noise signal information, and from this a control signal with the correct gain and phase relationship was produced.

Nelson et al. (1987 I) proposed using optimization theory to determine the point secondary source strength outputs needed to minimize the combined power output from a point primary source and several secondary sources. They found that in order to obtain substantial reductions in the total power output, the secondary sources needed to be located within half of a wavelength of the primary source.

The active control of stationary random sound fields was discussed by Nelson et al. (1988,1990). These papers analyzed the performance limits of active noise control systems in the time domain, for stationary random sound fields. Frequency domain methods often do not work for this type of sound field, due to the fact that the optimal secondary sources which are found are required to act non-causally.

If there is not access to a reference signal, then this form of feedforward active sound control is not feasible. Also, if it is intended to change the dynamics of the system, such as the addition of damping, feedback control must be used.

2.2.2 Feedback Control of Sound (General)

Feedback controller designs have an advantage over feedforward control

approaches, due to the fact that a reference noise signal need not be known. Stability of the controller must however be ensured. Balas (1978, 1979) discussed the stability of feedback controllers when the response of a flexible system was modeled by a finite number of modes. This is directly related to the feedback control of sound, due to the fact that the controller is most often designed on the basis of a model composed of a finite number of acoustic modes. The effect of unmodeled dynamics in the system must be understood. One way to minimize the effect of unmodeled dynamics is to filter their contribution out of the signal to be entered into the controller.

Short (1980) discussed a control approach in which a feedback control device is placed close to the noise source in order to reduce the acoustic energy produced by the source. When the secondary source was located 10 centimeters from the primary source, reductions in the radiated power were achieved between 40 and 250 Hz. As the source frequency was increased, the separation distance between the primary and secondary sources was comparable to or greater than a wavelength. Reduction in the radiated power was not possible due to the significant phase shift which occurred between the two sources.

Guicking et al. (1983) used feedback control to actively control the acoustic impedance of a wall. The system consisted of loudspeakers which were fed by adjusted signals from sensor microphones in such a way that the acoustic input impedance was controlled to a specific value.

Minimizing the total combined power output from an array of primary and secondary sources, and the absorption of sound power were both investigated by Elliott et

al. (1991). They found that in free-space, the secondary sources are well coupled to the primary source if they are located within a quarter of a wavelength of the primary source. This is also true in an enclosure excited near the natural frequency of a lightly damped acoustic mode, which will be discussed further in Section 2.3.4.

Dowling et al. (1995) looked at an adaptive digital feedback control system to control the output of a non-minimum phase acoustic plant. The ideal compensated system would be equivalent to a pure time delay and could reduce the system power by 96%. This was not possible for the non-minimum phase plant, and their controller design incorporated a compensator that produced an all-pass function when put in series with the plant. This controller was able to reduce the acoustic power of the system by 74%.

2.2.3 Active Sound Control in an Acoustic Duct

In order to gain a better understanding of the active control of sound in a three dimensional enclosure, several researchers have investigated the active control of sound in a one dimensional duct. For frequencies below the cut on frequency of the duct, the sound consists of only plane waves. This reduces the complexity of the model needed to simulate the acoustic response.

Swinbanks (1973) proposed a method to reduce the amplitude of a plane wave propagating through a one-dimensional duct. His method was much like the one proposed by Lueg (1936), although Swinbanks used an array of sensors and actuators. By using an array of sensors and actuators, he was able to measure and generate sound waves which

traveled in the down stream direction only. This eliminated the problem of sensing the secondary waves at the upstream sensors.

Curtis et al. (1987) discussed three different methods which can be used to reduce the acoustic energy in a one-dimensional, finite length duct. These included the acoustical virtual earth, the absorbing termination, and the minimization of acoustic energy. The virtual earth method uses a secondary source which maintains zero sound pressure directly in front of itself. In the absorbing termination method, the secondary source is driven so that no reflections occur off of its surface. The minimization of the acoustic energy is accomplished by setting the differential of the energy with respect to the source strength to zero. For this method, the acoustic energy after control is found to be half of that found for the absorbing termination method.

Dohner and Shoureshi (1989 I) developed a state space model for a one-dimensional rigid-walled duct which had a finite impedance termination. Using this state space model, they were able to design a single input, single output feedback controller and simulate the response of the system. A state observer was created in order to estimate the unmeasured states of the plant, which included the pressures at present and past times on the end boundary of the duct.

Hull et al. (1991) used modern state space control theory to design a feedback controller to be used in an one dimensional, hard-walled duct. They used the wave equation to model the air particle displacement in the duct. The states were not directly measurable in their state space model, therefore an observer was developed in order to estimate the values of the individual states. A single sensor and single control speaker

were used. The estimated state values were used with a state feedback controller, and a 58% reduction in the noise level at all points in the duct was obtained.

Wu et al. (1995) developed another state space model for a one-dimensional duct system by directly discretizing the wave equation modeling the acoustic pressure. They used the finite difference method and the state variables preserved their physical meanings. A full state feedback controller design was simulated and the feedback gains were found using optimal control theory. Two acoustic pressure sensors were used to measure two of the states corresponding to the acoustic pressure at two different locations. A state estimator was developed in order to estimate the values of the pressures at the other locations corresponding to the unmeasured states. Reductions of more than 30 dB were achieved.

Hong et al. (1996) also looked into feedback control of the sound pressure propagating in a duct. They developed a state-space model for the acoustic pressure propagating in a duct, with the inclusion of the microphone and control speaker dynamics. The effect of transducer dynamics can be substantial depending on the frequency range of interest, and should be included in the system model if the model is expected to represent reality accurately. They used experimental identification of the duct to obtain the parameters used for controller synthesis.

As more dimensions are added to the active control problem, the complexity of the system increases. The sound can no longer be assumed to consist of only plane waves. Further analysis of the sound field is required.

2.2.4 Active Control of Enclosed Sound

S.J. Elliott and P.A. Nelson have investigated several different techniques for the reduction of noise inside an enclosure. Much of their work has focused on the control of steady state sound in a lightly damped enclosure, allowing certain simplifying assumptions, which will be discussed later.

In a three part series of articles (Nelson et al. (1987 II), Bullmore et al. (1987), Elliott et al. (1987)), they investigated both local and global control strategies. They found that there are constraints related to the physical aspects of the enclosure that determine when global sound control can be easily achieved or not. When the sound field in an enclosure consist of frequencies where distinct acoustic modes control the sound pressure level, then global sound control is accomplished by reducing the levels of those acoustic modes. If the sound field consists of many non-distinct acoustic modes, then true global sound control is not achievable for typical applications.

At relatively low frequencies, the overall sound pressure level can be dominated by distinct acoustic modes. If the pressure response due to these modes can be attenuated, then a reduction in the sound pressure throughout the enclosure will be achieved. This is referred to as modal control. It requires that the modes can be sensed and relatively few modes participate in the response.

The point where the frequency content is considered high is determined by the Schroeder frequency of the enclosure (Schroeder (1962), Joseph et al. (1994 I)). The

Schroeder frequency is determined by the dimensions of the enclosure, as well as the absorption of the walls. It is an indication of the modal density in the frequency range of interest. The Schroeder frequency is defined as:

$$f_{Schroeder} = 2000\sqrt{T_{60}/V} \quad (2.2.1)$$

where $f_{Schroeder}$ Schroeder frequency in Hz
 T_{60} reverberation time in sec
 V room volume in m³

The frequency limit under which global active sound control is realizable is at discrete frequencies approximately one-third the Schroeder frequency. For a typical 5m x 5m x 3m room with a T_{60} time of 1 second, the Schroeder frequency is approximately 230 Hz.

Nelson et al. (1987 II) used a controller design approach in which the secondary source strengths were chosen in order to minimize the acoustic potential energy at several sensors. For the case in which the frequency content in the enclosure is above the Schroeder limit, the secondary sources must be located within half a wave length of the primary noise source. Of course, this is only possible when the primary sources are inside the enclosure and relatively compact in dimension.

The situation is different for the case of low modal density. In order to achieve good global control, the secondary sources must be located at the modal antinodes of the enclosure. The corner location ensures that a secondary source is located at antinodes of all of the acoustic modes of the enclosure.

In their 1988 paper, Elliott et al. used a control strategy similar to the one described in their 1987 paper. Engine noise experienced in the interior compartment of an automobile was reduced by adjusting the strengths of two secondary sources. An optimization algorithm was used to find the secondary source strengths which reduced the squared outputs of 4 microphones. Global reductions of 10 - 15 dB were achieved.

Tohyama and Suzuki (1987) discussed the active power minimization of an acoustic source in a closed space. In this paper, they described the response in an enclosure in terms of its acoustic modes, and developed the power output of the source in terms of this description. They formulated the secondary source strengths needed to obtain the minimum power response (MPR) of the sources in the enclosure.

In another paper, Dohner and Shoureshi (1989 II) developed a state space model for a three-dimensional acoustic plant. The formulation was for a finite space with well-damped boundaries. They used a linear quadratic Gaussian control approach to build a feedback filter. The filter was chosen to minimize the following performance index:

$$IP = E \left[\int_0^{\infty} [\mathbf{x}^T \mathbf{Q} \mathbf{x} + s u^2] dt \right] \quad (2.2.2)$$

where \mathbf{x} is the vector of state magnitudes, u is the control input, \mathbf{Q} is a matrix which weights the state feedback gains accordingly, and s is a scalar. A full order observer was used to estimate the response of the states, which were the Fourier coefficients and their derivatives. When a broadband source was excited in the box, some modal amplitudes were amplified when the controller was turned on. Reductions in the sound pressure level were obtained for a primary source which was band limited to below 100 Hz.

One application of digital feedback control of noise is presented by Costin et al. (1989). He used a feedback control strategy to reduce the noise in an automobile interior due to the road noise from the tires. Two different feedback control strategies were tested; proportional integral, and a generalized minimum variance controller, which gave the best reduction of the two. The GMV controller gave a reduction of 10-20 dB between 25 and 60 Hz.

Batta et al. (1990) described the use of direct digital feedback control to reduce the sound level generated by a noise source in a room. The control sensor and actuator were located close to the noise source in order to attempt to get global reduction. A reduction of 13 dB was achieved at the disturbance frequency of 200 Hz, throughout the room. The amplitude of the frequency content below and above the disturbance frequency was increased, but remained much lower than the disturbance signal.

Johnson and Elliott (1993) discussed the use of the acoustic power measurement from a secondary source in order to decrease the total power output of the primary and secondary sources. When the total power output from the primary and secondary sources is minimized, the acoustic power output of the secondary source is zero. To achieve optimal results the volume velocity of the secondary source must be adjusted to be 180° out of phase with that of the primary source. The adjustment of the secondary source strength was done manually, but could be done using an adaptive feedforward control strategy. Using the acoustic power as a means of sound control only requires the measurement of the sound local to the sources. This eliminates the need for large microphone arrays, which are needed for other control approaches, such as the

minimization of the acoustic potential energy.

Yang et al. (1993) discussed the feedback control of sound in a reverberant enclosure. They used an H_{∞} design approach to obtain a robust controller. The effects of both unmodeled dynamics and sensor noise were accounted for in the controller design. Large reductions in the response to a disturbance were found near the acoustic resonances of the enclosure. The sound pressure level was slightly increased at frequencies between the acoustic resonances.

Joseph et al. (1994 I) investigated the reduction of sound in the near field of an acoustic source. As stated earlier, the effective global control of sound in an enclosure is dependent on the modal density in the frequency range of interest. High modal density corresponds to high modal overlap, which means many modes contribute to the sound pressure level at a certain frequency. The Schroeder frequency can be used to determine the nature of the sound field in the enclosure, i.e. is it diffuse or not? Joseph pointed out that this is a simplified analysis of the effectiveness of global vs. local sound control. It does not take into account the degree of coupling between the secondary sources and the acoustic modes, the distribution of natural frequencies in the room, or the exact mix of axial, tangential, and oblique room modes. He stated that it is still a good analysis tool.

For a sound field of high modal density, a zone of quiet can be formed around a sensor microphone using a single control speaker. In this zone of quiet the sound pressure level can be attenuated by 10 dB or more. Joseph found that the dimensions of the zone of quiet could be increased by increasing the diameter of the control speaker and the distance between the sensor microphone and the control speaker. However, as the zone

of quiet was increased in size, the sound pressure at locations away from the control point were increased.

In an additional paper, Joseph et al. (1994 II) further investigated the low and high frequency limits of the active control of enclosed sound in terms of the statistical properties of the sound field. For low modal density, global sound control can be achieved using a single secondary source. Two requirements must be met for good global control. These include positioning the secondary source so that it is well coupled with the important modal contributions of the room, and also so that it does not overly excite the residual sound field.

For a sound field of high modal density, global sound control is not feasible, and local zones of quiet around a point can be achieved. The average acoustic potential energy throughout the enclosure is increased, although it may be negligible if the error microphone is within the radius of reverberation for the secondary source.

Elliott (1994) summarized the active control of sound in an enclosure. He presented a figure similar to Figure 2.4, which shows the three important elements that need to be considered in the design of an active sound control system.

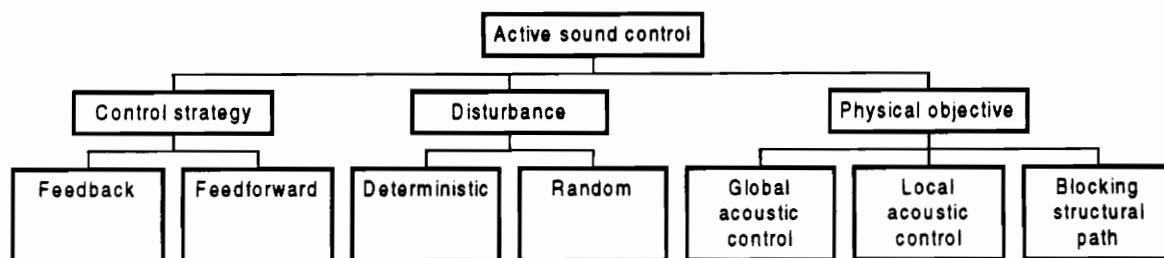


Figure 2.4 Elements of Active Sound Control Design

These elements include the control strategy, the type of disturbance, and the physical objective of the controller. Elliott discussed how each of these elements determines the controller design needed in order to achieve the best results possible.

Clark et al. (1995) analyzed a direct rate feedback control approach to reduce the sound pressure level in an enclosure. By using feedback control, damping can be added to the resonant frequencies of the enclosure. Added damping will reduce the sound pressure levels at the resonant frequencies, and thus reduce the overall sound pressure in the enclosure. Stability must be ensured when designing a feedback controller, but it is often difficult to develop an accurate model of the system dynamics, in order to perform stability analyses. The acoustic properties of the system, as well as the acoustic-structural interaction must be understood. In addition, the dynamics of the sensors, transducers, and amplifiers, and their influence on the stability of the system need to be modeled accurately.

2.3 Modeling of Enclosure Acoustics

One of the first to look into the theory of room acoustics was Morse (1939). He assumed that the walls of the enclosure are locally reactive, and he stated that the property which best represents the interaction of the enclosure walls with the sound field is the normal acoustic impedance. The normal acoustic impedance is the ratio of pressure to the normal air velocity at the surface of the material. Morse assumed that each wall was uniformly covered with absorbing material. He developed expressions for the acoustic modal frequencies and reverberation times in terms of the wall impedances. Morse

discovered that the waves traveling parallel to a wall were not absorbed as much as waves traveling perpendicular to a wall.

Schroeder (1962) investigated the random nature of sound in rooms when it is modally dense. He stated that this occurs when the average spacing between the acoustic resonant frequencies is less than one third of their bandwidth.

Dowell et al. (1977) investigated the interaction of the walls of an enclosure and its interior sound field. The primary concern of the paper was the theoretical development of the acoustic response in an enclosure caused by the vibration of one of its walls. They used a coupled approach, in which the *in vacuo* structural modes and the rigid-walled acoustic modes are coupled in order to get the overall response of the enclosure. They called this interaction “acoustoelasticity.” A flexible panel was mounted to the side of a rigid-walled cavity. The structural modes of the vibrating panel were calculated assuming a clamped boundary condition, and the acoustic response in the cavity was estimated. Then, the acoustic response of multiply connected cavities was formulated.

In another paper by Dowell (1978), he derived a theoretical model for the reverberation time of an enclosure in terms of the impedance of the absorption materials on the walls. Dowell stated that if the pressure time history is dominated by a single mode, then the reverberation time is equal to the reverberation time of that mode.

Jie and Bies (1988) qualitatively investigated the interaction between the walls of a reverberation chamber and the sound enclosed by the chamber. They concluded that the interaction in an enclosure is determined through modal coupling of the acoustic modes and the structural modes of the enclosure walls.

Boone et al. (1995) used an expression for the acoustic response in an enclosure in the frequency domain, in order to develop an expression in the time domain. This is not possible in a general sense, but is possible if the source type is known. Boone et al. developed expressions for the response for a harmonic source, as well as for an impulse source. They found good agreement between theoretical and experimental results.

There have been several attempts to develop an accurate model for the acoustic response in an enclosure, as presented in the previous paragraphs. A single document which compares these models was not located. A detailed formulation of three different models for the acoustic response in an enclosure will be presented in the Chapter 3. These models take into account both the boundary conditions and the type of acoustic source present in the enclosure. In addition to the acoustic dynamics associated with an active sound control system, there are transducer dynamics that influence the overall system response. A brief discussion of these dynamics is presented in the next section.

2.3.1 Transducer Dynamics

Small (1972) developed expressions for the analysis of direct-radiator loudspeaker systems. In his paper, Small described how simple experimentally measured values can be used to predict the response of a loudspeaker. The accuracy of the transfer function found with Small's approach is dependent on the accuracy of the speaker parameters which determine the transfer function coefficients. The actual form of the transfer function found using Small's approach, which relates the volume velocity of the speaker to the input

voltage to the speaker, is discussed in Chapter 3. It should be pointed out that there are many treatments of speaker dynamics, and Small's transfer function model is only one of them.

In addition to the dynamics associated with the loudspeakers in an active acoustic control system, there are also dynamics associated with the sensor microphones. These dynamics will be discussed further in Section 4.1 Experimental Set-up and Results.

Chapter 3. Model Formulation for Enclosure Acoustics

To correctly simulate the response of an acoustic feedback control system, an accurate model of the important dynamics of the system is needed. Several textbooks present theories on enclosure acoustics with varying levels of complexity (Beranek, et al. (1992), Kuttruff (1991), Fahy (1985), Morse (1936), Morse, et al. (1968), Nelson, et al. (1993), Pierce (1989)). In the following sections, we will assume that the sources are located on the boundary or interior to the enclosure. The sound field that is established inside any enclosure is dependent on the boundary conditions as well as the type of sources present. This chapter presents the formulation of three different modeling approaches, which will be compared in Chapter 4.

The first method assumes that the walls of the enclosure are rigid. This is equivalent to assuming that the acoustic impedance at the enclosure walls is infinite, and greatly simplifies the equations governing the acoustic response inside the enclosure. The second method incorporates a finite complex acoustic impedance value at the boundaries to account for the interaction between the vibration of the walls and the acoustic response of the enclosed fluid. The third method uses the *in vacuo* structural modes of the enclosure, along with the rigid wall acoustic modes of the enclosed fluid, in a coupled formulation in order to calculate the modes of the combined system.

3.1 Rigid-wall Boundary Condition (Infinite Acoustic Impedance)

The sound field in any enclosure is governed by the inhomogeneous wave equation

presented below.

$$\nabla^2 p(\mathbf{r}, t) - \frac{1}{c^2} \frac{\partial^2 p(\mathbf{r}, t)}{\partial t^2} = -\rho \frac{\partial q(\mathbf{r}_0, t)}{\partial t} \quad (3.1.1)$$

where

c	speed of sound in fluid medium
p	acoustic pressure
q	source strength
\mathbf{r}	response field point (x_r, y_r, z_r)
\mathbf{r}_0	source field point (x_0, y_0, z_0)
t	time
ρ	density of fluid medium

The acoustic pressure response can be expressed as the sum of the contributions of each of the characteristic acoustic modes of the enclosure, which will be developed later. These acoustic modes are a result of standing waves which are created by constructive interference between reflected waves at the walls of the enclosure.

$$p(\mathbf{r}, t) = \sum_{n=0}^{\infty} \Psi_n(\mathbf{r}) a_n(t) \quad (3.1.2)$$

where

$\Psi_n(\mathbf{r})$ value of eigenfunction at response point \mathbf{r} , corresponding to mode n

$a_n(t)$ modal contribution factor corresponding to mode n

The modal contribution factor for each mode can be solved for by the derivation given below. First, the expression for the acoustic pressure given in Eq. (3.1.2) can be

inserted into the inhomogeneous wave equation.

$$\nabla^2 \left\{ \sum_{n=0}^{\infty} \Psi_n(\mathbf{r}) a_n(t) \right\} - \frac{1}{c^2} \frac{\partial^2 \left\{ \sum_{n=0}^{\infty} \Psi_n(\mathbf{r}) a_n(t) \right\}}{\partial t^2} = -\rho \frac{\partial q(\mathbf{r}_0, t)}{\partial t} \quad (3.1.3)$$

$$\sum_{n=0}^{\infty} \nabla^2 \Psi_n(\mathbf{r}) a_n(t) - \frac{1}{c^2} \sum_{n=0}^{\infty} \Psi_n(\mathbf{r}) \frac{d^2 a_n(t)}{dt^2} = -\rho \frac{\partial q(\mathbf{r}_0, t)}{\partial t} \quad (3.1.4)$$

Now, the homogeneous wave equation for a specific mode is

$$\nabla^2 \Psi_n(\mathbf{r}) a_n(t) - \frac{1}{c^2} \frac{\partial^2 \{ \Psi_n(\mathbf{r}) a_n(t) \}}{\partial t^2} = 0 \quad (3.1.5)$$

Eq. (3.1.5) simplifies to the homogeneous Helmholtz equation for harmonic excitations.

$$\nabla^2 \Psi_n(\mathbf{r}) + k_n^2 \Psi_n(\mathbf{r}) = 0 \quad (3.1.6)$$

$$k_n = \frac{\omega_n}{c}$$

The variable k_n is the eigenvalue corresponding to the n^{th} mode. The natural frequency of the n^{th} mode is given by ω_n . Using the expression for $\nabla^2 \Psi_n$ given by Eq. (3.1.6) in Eq. (3.1.4) gives:

$$\sum_{n=0}^{\infty} \left(-k_n^2 \Psi_n(\mathbf{r}) a_n(t) \right) - \frac{1}{c^2} \sum_{n=0}^{\infty} \Psi_n(\mathbf{r}) \frac{d^2 a_n(t)}{dt^2} = -\rho \frac{\partial q(\mathbf{r}_0, t)}{\partial t} \quad (3.1.7)$$

$$\sum_{n=0}^{\infty} \left(-k_n^2 \Psi_n(\mathbf{r}) a_n(t) \right) - \frac{1}{c^2} \sum_{n=0}^{\infty} \Psi_n(\mathbf{r}) \ddot{a}_n(t) = -\rho \frac{\partial q(\mathbf{r}_0, t)}{\partial t} \quad (3.1.8)$$

The acoustic eigenfunctions are orthogonal over the volume, V , of the enclosure as expressed by Eq. (3.1.9).

$$\int_v \Psi_n(\mathbf{r})\Psi_m(\mathbf{r})dV = \begin{cases} 0, m \neq n \\ \Lambda_n, m = n \end{cases} \quad (3.1.9)$$

For the rigid wall case, the eigenfunctions can be normalized by the enclosure volume so that $\Lambda_n = V$. The fact that the acoustic eigenfunctions are orthogonal can be used to further simplify Eq. (3.1.8). First, multiply Eq. (3.1.8) for the acoustic response by $\Psi_m(\mathbf{r})$ and integrate over the enclosure volume.

$$\int_v \Psi_m(\mathbf{r}) \sum_{n=0}^{\infty} (-k_n^2) \Psi_n(\mathbf{r}) a_n(t) dV - \int_v \Psi_m(\mathbf{r}) \frac{1}{c^2} \sum_{n=0}^{\infty} \Psi_n(\mathbf{r}) \ddot{a}_n(t) dV = \dots$$

$$\int_v \Psi_m(\mathbf{r}) (-\rho) \frac{\partial q(\mathbf{r}_0, t)}{\partial t} dV \quad (3.1.10)$$

$$\int_v \Psi_m^2(\mathbf{r}) (-k_m^2) a_m(t) dV - \int_v \Psi_m^2(\mathbf{r}) \frac{1}{c^2} \ddot{a}_m(t) dV = \dots$$

$$-\rho \int_v \Psi_m(\mathbf{r}) \frac{\partial q(\mathbf{r}_0, t)}{\partial t} dV \quad (3.1.11)$$

Using the orthogonality condition of the eigenfunctions, we can write Eq. (3.1.11) as follows:

$$V(-k_m^2)a_m(t) - V\frac{1}{c^2}\ddot{a}_m(t) = -\rho \int_v \Psi_m(\mathbf{r}) \frac{\partial q(\mathbf{r}_0, t)}{\partial t} dV \quad (3.1.12)$$

Multiply by $-c^2/V$ to get:

$$\ddot{a}_m(t) + \omega_m^2 a_m(t) = \frac{\rho c^2}{V} \int_v \Psi_m(\mathbf{r}) \frac{\partial q(\mathbf{r}_0, t)}{\partial t} dV \quad (3.1.13)$$

Replace m with n to get:

$$\ddot{a}_n(t) + \omega_n^2 a_n(t) = \frac{\rho c^2}{V} \int_v \Psi_n(\mathbf{r}) \frac{\partial q(\mathbf{r}_0, t)}{\partial t} dV \quad (3.1.14)$$

There is no dissipation of energy in Eq. (3.1.14). Energy dissipation in the enclosed fluid can be added to the differential equation governing the acoustic modal contribution factor through the use of a viscous damping coefficient, which is added to the left hand side of the equation.

$$\ddot{a}_n(t) + 2\zeta_n \omega_n \dot{a}_n(t) + \omega_n^2 a_n(t) = \frac{\rho c^2}{V} \int_V \Psi_n(\mathbf{r}) \frac{\partial q(\mathbf{r}_0, t)}{\partial t} dV \quad (3.1.15)$$

Another possible method to add damping to the mode, which is not used here, is to define the speed of sound in the fluid, c , as a complex number.

This equation can be implemented in a state-space model to find the acoustic response in the enclosure. If the source is assumed to be a point harmonic source, then a single input, single output (SISO) transfer function relating a_n to q_0 can be developed.

$$\frac{a_n}{q_0 \omega i} = \frac{\Psi_n(\mathbf{r}_0) \rho c^2}{V[\omega_n^2 - \omega^2 + 2\zeta_n \omega_n \omega i]} \quad (3.1.16)$$

To find the overall pressure response, the eigenvalues and eigenfunctions of the system must be developed. These are determined by the exact acoustic boundary conditions at the interior of the enclosure walls.

3.1.1 Solution for Rigid-wall Eigenvalues and Eigenfunctions

The solutions for the eigenvalues and eigenfunctions of the enclosed acoustical system are dependent on the boundary conditions. They determine the resonant frequencies of the enclosure. The resonant frequencies of a rigid-wall enclosure will be different than those for a non-rigid-wall enclosure, due to the interaction of the fluid with

the boundaries. This section concentrates on the development of the acoustic eigenvalues and eigenfunctions for a rectangular enclosure with rigid walls.

For an enclosure with rigid walls, the boundary condition at the interior of the enclosure walls is given by Eq. (3.1.17).

$$\frac{\partial p}{\partial n} = 0 \quad (3.1.17)$$

where n stands for the direction normal to the wall surface.

For a rectangular enclosure, this boundary condition can be expressed in terms of Cartesian coordinates, (x , y and z) for each of the characteristic acoustic modes of the enclosure. For example,

$$\frac{\partial \Psi_n}{\partial x} = 0 \quad \text{at } x = 0, L_x \quad (3.1.18)$$

where

n mode number

L_x length of enclosure in the x direction.

The boundary conditions are similar for the y and z directions in the enclosure. Separation of variables is assumed to be valid for the acoustic eigenfunctions, so that

$$\Psi_n(x, y, z) = X(x)Y(y)Z(z) \quad (3.1.19)$$

The expression for the eigenfunction can be inserted into Eq. (3.1.18) for the boundary conditions to find:

$$\frac{\partial \Psi_n}{\partial x} = \frac{\partial X}{\partial x} Y(y)Z(z) \quad \text{and} \quad \frac{\partial^2 \Psi_n}{\partial x^2} = \frac{\partial^2 X}{\partial x^2} Y(y)Z(z) \quad (3.1.20)$$

Similar expressions hold for the y and z directions.

Substitution of Eq. (3.1.20) along with similar equations for the y and z directions into the homogeneous Helmholtz equation gives Eq. (3.1.21).

$$\frac{\partial^2 X(x)}{\partial x^2} Y(y) Z(z) + X(x) \frac{\partial^2 Y(y)}{\partial y^2} Z(z) + X(x) Y(y) \frac{\partial^2 Z(z)}{\partial z^2} = -k_n^2 X(x) Y(y) Z(z) \quad (3.1.21)$$

Divide Eq (3.1.21) by $X(x)Y(y)Z(z)$ to get

$$\frac{\partial^2 X(x)}{\partial x^2} \frac{1}{X(x)} + \frac{\partial^2 Y(y)}{\partial y^2} \frac{1}{Y(y)} + \frac{\partial^2 Z(z)}{\partial z^2} \frac{1}{Z(z)} = -k_n^2 \quad (3.1.22).$$

Each term on the left side of Eq. (3.1.22) is dependent on a different variable and therefore should be equal to three different constants:

$$\frac{\partial^2 X(x)}{\partial x^2} \frac{1}{X(x)} = -k_x^2 \quad \frac{\partial^2 Y(y)}{\partial y^2} \frac{1}{Y(y)} = -k_y^2 \quad \frac{\partial^2 Z(z)}{\partial z^2} \frac{1}{Z(z)} = -k_z^2$$

leading to the Helmholtz equation in each coordinate direction:

$$\frac{\partial^2 X(x)}{\partial x^2} + X(x)k_x^2 = 0$$

$$\frac{\partial^2 Y(y)}{\partial y^2} + Y(y)k_y^2 = 0 \quad (3.1.23 \text{ a,b,c})$$

$$\frac{\partial^2 Z(z)}{\partial z^2} + Z(z)k_z^2 = 0$$

Assume harmonic solutions for each of the previous equations.

$$X(x) = A_x e^{ik_x x} + B_x e^{-ik_x x}$$

$$Y(y) = A_y e^{ik_y y} + B_y e^{-ik_y y}$$

$$Z(z) = A_z e^{ik_z z} + B_z e^{-ik_z z} \quad (3.1.24 \text{ a,b,c})$$

Use the boundary conditions specified in Eq. (3.1.18) and solve for the coefficients A_x and B_x .

$$\Psi_n(x, y, z) = (A_x e^{ik_x x} + B_x e^{-ik_x x}) Y(y) Z(z) \quad (3.1.25)$$

$$\frac{\partial \Psi_n}{\partial x} = ik_x (A_x e^{ik_x x} - B_x e^{-ik_x x}) Y(y) Z(z) \quad (3.1.26)$$

At $x = 0$

$$0 = ik_x Y(y) Z(z) (A_x - B_x).$$

For a non-trivial solution $ik_x Y(y) Z(z) \neq 0$

$$\therefore A_x = B_x$$

At $x = L_x$

$$0 = ik_x Y(y) Z(z) (A_x e^{ik_x L_x} - B_x e^{-ik_x L_x}).$$

For a non-trivial solution $ik_x Y(y) Z(z) \neq 0$

$$\therefore A_x e^{ik_x L_x} - B_x e^{-ik_x L_x} = 0$$

$$A_x e^{ik_x L_x} - A_x e^{-ik_x L_x} = 0$$

$$0 = e^{ik_x L_x} - e^{-ik_x L_x}$$

$$0 = \sin(k_x L_x) \quad (3.1.27)$$

The distinct values for k_x which satisfy Eq. (3.1.27) are the acoustic eigenvalues for the enclosure. Similar expressions hold for the y and z directions. Solving for k_x , k_y , and k_z , the rigid wall eigenvalues are given by:

$$k_x = \frac{n_x \pi}{L_x} \quad n_x = 0, 1, 2, 3, \dots$$

$$k_y = \frac{n_y \pi}{L_y} \quad n_y = 0, 1, 2, 3, \dots$$

$$k_z = \frac{n_z \pi}{L_z} \quad n_z = 0, 1, 2, 3, \dots \quad (3.1.28 \text{ a,b,c})$$

The modal integers n_x , n_y and n_z determine the number of nodal planes in the x, y and z directions, respectively. This is shown one-dimensionally in Fig. 3.1, where the magnitude of the x-directed eigenfunction is plotted corresponding to $n_x = 3$.

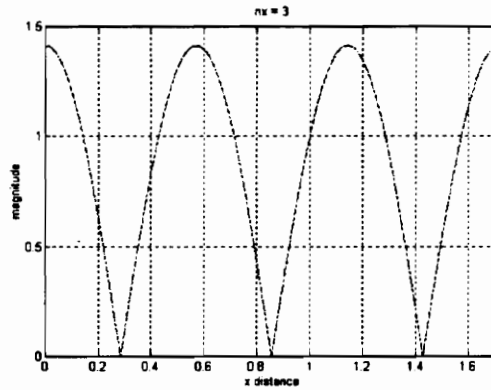


Figure 3.1 Rigid Wall Acoustic Eigenfunction

The eigenfunctions for the rigid wall system are found by substituting the eigenvalues given in Eq. (3.1.28 a,b,c) into Eq. (3.1.24 a,b,c):

$$X(x) = A_x e^{ik_x x} + A_x e^{-ik_x x} = 2A_x \cos(k_x x)$$

$$Y(y) = 2A_y \cos(k_y y)$$

$$Z(z) = 2A_z \cos(k_z z)$$

To ensure that the eigenfunctions are normalized with respect to the volume of the enclosure, let:

$$2A_x 2A_y 2A_z = \sqrt{\epsilon_{nx} \epsilon_{ny} \epsilon_{nz}}$$

Therefore, for a rectangular enclosure with rigid walls:

$$\Psi_n(x, y, z) = \sqrt{\epsilon_{nx} \epsilon_{ny} \epsilon_{nz}} \cos(k_x x) \cos(k_y y) \cos(k_z z) \quad (3.1.29)$$

where

$$\epsilon_{nx} = 1 \quad \text{if } n_x = 0$$

$$\epsilon_{nx} = 2 \quad \text{if } n_x > 0.$$

Similar results are obtained for the modal integers corresponding to the y and z directions.

It is easily seen from the equations, that the rigid wall eigenvalues are real. Their corresponding eigenfunctions are also real. This is not the case for non-rigid-wall eigenfunctions, as will be shown in Sec. 3.2.

To summarize, the rigid-wall eigenvalues and eigenfunctions have been found in terms of wavenumbers, spatially periodic quantities, or natural frequencies:

$$k_n = \sqrt{k_x^2 + k_y^2 + k_z^2} \quad \text{eigenvalue} \quad (3.1.30)$$

$$\omega_n = k_n c \text{ (rad/sec)} \quad \text{natural frequency}$$

$$f_n = \frac{\omega_n}{2\pi} \text{ (Hz)} \quad \text{eigenfrequency} \quad (3.1.31 \text{ a,b}).$$

Numerical results for the acoustic response in a specific rigid-wall enclosure will be presented in Chapter 4. The formulations for the non-rigid-wall eigenvalues and eigenfunctions are not quite as simple. This is primarily because of the inherent fluid-structure interaction which occurs for flexible walls. The next two sections present two alternative modeling approaches which account for that interaction in different ways.

3.2 Non-rigid-wall Boundary Condition (Finite Acoustic Impedance)

When the acoustic impedance at the enclosure walls cannot be assumed to approach infinity, the walls cannot be assumed to be rigid. The interaction between the non-rigid walls and the enclosed fluid will result in an acoustic response that is different than that predicted using the model for a rigid wall enclosure. The acoustic natural frequencies of the enclosure will be shifted away from those predicted using the rigid wall model. This section formulates the model for a rectangular enclosure which has walls that cannot be assumed to be rigid.

The formulation of the acoustic response in an enclosure with finite acoustic impedance boundary conditions can be approached similarly to that of the infinite impedance boundary case, but with a few very important differences. The eigenvalues and eigenfunctions may be complex depending on the nature of the finite acoustic impedance value associated with the walls. Also, due to the complex nature of the finite acoustic impedance eigenfunctions, they are not normalized with respect to the volume of the enclosure in the formulation that will be presented below. Therefore, the value of the normalization factor corresponding to each of the non-rigid-wall modes may be different.

The finite impedance that is associated with the boundary determines the amount of damping and frequency shift that will occur in the acoustic response, by determining the form of the eigenvalue. If the eigenvalue is a complex number, then it can be represented by the following equation.

$$k_n = \frac{\omega_n}{c} + \frac{\delta_n}{c}i \quad (3.2.1)$$

where ω_n determines the real part of the eigenvalue and δ_n determines the imaginary part of the eigenvalue.

A transfer function can then be written for the non-rigid-wall case corresponding to that given for the rigid-wall case in Eq. (3.1.16), which comes from the inhomogeneous wave equation, assuming that there is one harmonic source which acts at a point.

$$\frac{a_n}{q_0 \omega i} = \frac{\Psi_n(\mathbf{r}_0) \rho c^2}{V[\omega_n^2 - \omega^2 - \delta_n^2 + 2\delta_n \omega_n i]} \quad (3.2.2)$$

Comparison of Eq. (3.2.2) and Eq. (3.1.16) shows that the imaginary part of the complex eigenvalue can be related to a viscous damping term, and determines the amount of damping associated with the mode.

$$\delta_n = \zeta_n \omega \quad (3.2.3)$$

As a result, for purely real eigenvalues there will be no damping in the mode. The natural frequency associated with the mode is determined by ω_n when $\omega_n \gg \delta_n$, which is most often the case. The actual solutions for the non-rigid-wall eigenvalues and eigenfunctions are presented in the following section.

3.2.1 Solution for Non-rigid-wall Eigenvalues and Eigenfunctions

The boundary condition formulation presented in this section follows that presented by Kuttruff in his book entitled Room Acoustics, although many additional relationships and insights are developed here. The interaction between the acoustic

response in the enclosure and the vibration of the walls is accounted for through a finite acoustic impedance value. The acoustic particle velocity normal to the surface of a wall can be described as in Eq. (3.2.4).

$$v_n = \frac{i}{\omega\rho} \frac{\partial p}{\partial n} \quad (3.2.4)$$

where v_n particle velocity normal to wall
 p acoustic pressure at wall.

The air particle velocity, v_n , can be replaced by the pressure divided by the specific acoustic impedance, Z .

$$\frac{p}{Z} = \frac{i}{\omega\rho} \frac{\partial p}{\partial n}$$

This equation can be simplified further:

$$\frac{p}{Z} - \frac{i}{\omega\rho} \frac{\partial p}{\partial n} = 0$$

$$\frac{p}{Z} + \frac{1}{i\omega\rho} \frac{\partial p}{\partial n} = 0$$

$$pi\omega\rho + Z \frac{\partial p}{\partial n} = 0$$

$$\frac{pi\rho\omega}{\rho c} + \frac{Z}{\rho c} \frac{\partial p}{\partial n} = 0$$

$$pik + \zeta \frac{\partial p}{\partial n} = 0 \quad (3.2.5)$$

where

$$\zeta = Z/(\rho c).$$

If Eq. 3.2.5 is multiplied through by $\rho c/Z$, and Z is increased to infinity, then the boundary condition corresponding to a rigid wall will be obtained.

For simplification, we will focus on the x direction only for now. Similar formulations exist for the y and z directions. Assume a general harmonic solution is valid, which is given in by:

$$X(x) = C_x e^{-ik_x x} + D_x e^{ik_x x} \quad (3.2.6).$$

The boundary conditions for the x -direction are presented below.

$$\zeta_x \frac{dX(x)}{dx} = ikX(x) \quad \text{for } x = 0 \quad (3.2.7 \text{ a})$$

$$\zeta_x \frac{dX(x)}{dx} = -ikX(x) \quad \text{for } x = L_x \quad (3.2.7 \text{ b})$$

Substitute the expression for $X(x)$ of Eq. (3.2.6) into the boundary equations to get:

At $x = 0$,

$$\begin{aligned} -\zeta_x ik_x C_x e^{-ik_x x} + \zeta_x ik_x D_x e^{ik_x x} &= ik C_x e^{-ik_x x} + ik D_x e^{ik_x x} \\ -\zeta_x ik_x C_x + \zeta_x ik_x D_x &= ik C_x + ik D_x \\ C_x (k + \zeta_x k_x) + D_x (k - \zeta_x k_x) &= 0 \end{aligned} \quad (3.2.8)$$

At $x = L_x$,

$$\begin{aligned} -\zeta_x ik_x C_x e^{-ik_x L_x} + \zeta_x ik_x D_x e^{ik_x L_x} &= -ik C_x e^{-ik_x L_x} - ik D_x e^{ik_x L_x} \\ -\zeta_x ik_x C_x e^{-ik_x L_x} + \zeta_x ik_x D_x e^{ik_x L_x} &= -ik C_x e^{-ik_x L_x} - ik D_x e^{ik_x L_x} \\ C_x (k - \zeta_x k_x) e^{-ik_x L_x} + D_x (k + \zeta_x k_x) e^{ik_x L_x} &= 0 \end{aligned} \quad (3.2.9)$$

Combine Eq. (3.2.8) and Eq. (3.2.9) to get:

$$\begin{aligned}
 C_x &= -D_x \frac{(k - k_x \zeta_x)}{(k + k_x \zeta_x)} \\
 -D_x \frac{(k - k_x \zeta_x)}{(k + k_x \zeta_x)} (k - k_x \zeta_x) e^{-ik_x L_x} + D_x (k + k_x \zeta_x) e^{ik_x L_x} &= 0 \\
 -\frac{(k - k_x \zeta_x)^2}{(k + k_x \zeta_x) e^{ik_x L_x}} + (k + k_x \zeta_x) e^{ik_x L_x} &= 0 \\
 (e^{ik_x L_x})^2 &= \frac{(k - k_x \zeta_x)^2}{(k + k_x \zeta_x)^2} \\
 e^{ik_x L_x} &= \pm \frac{(k - k_x \zeta_x)}{(k + k_x \zeta_x)} \tag{3.2.10}
 \end{aligned}$$

An equivalent expression to Eq. (3.2.10) can be found from the following:

$$\cos(k_x L_x) + i \sin(k_x L_x) = \pm \frac{(k - k_x \zeta_x)}{(k + k_x \zeta_x)}$$

For a positive right hand side in Eq. (3.2.11):

$$\begin{aligned}
 \cos(k_x L_x) + i \sin(k_x L_x) &= \frac{(k - k_x \zeta_x)}{(k + k_x \zeta_x)} \\
 1 + \cos(k_x L_x) + i \sin(k_x L_x) &= \frac{(k - k_x \zeta_x)}{(k + k_x \zeta_x)} + \frac{(k + k_x \zeta_x)}{(k + k_x \zeta_x)} \\
 1 + \cos(k_x L_x) + i \sin(k_x L_x) &= \frac{2k}{(k + k_x \zeta_x)} \\
 \frac{(k + k_x \zeta_x)}{2k} &= \frac{1}{1 + \cos(k_x L_x) + i \sin(k_x L_x)}
 \end{aligned}$$

$$\frac{(k + k_x \zeta_x)}{2k} = \frac{1}{1 + \cos(k_x L_x) + i \sin(k_x L_x)}$$

$$\frac{1}{2} + \frac{k_x \zeta_x}{2k} = \frac{1}{1 + \cos(k_x L_x) + i \sin(k_x L_x)}$$

$$1 + \frac{k_x \zeta_x}{k} = \frac{2}{1 + \cos(k_x L_x) + i \sin(k_x L_x)}$$

$$\frac{k_x \zeta_x}{k} = \frac{2}{1 + \cos(k_x L_x) + i \sin(k_x L_x)} - \frac{1 + \cos(k_x L_x) + i \sin(k_x L_x)}{1 + \cos(k_x L_x) + i \sin(k_x L_x)}$$

$$\frac{ik_x L_x}{k} = \frac{\sin^2(k_x L_x) + 1 - 2 \cos(k_x L_x) + \cos^2(k_x L_x)}{2 \sin(k_x L_x)}$$

$$\frac{ik_x \zeta_x}{k} = \frac{\sin(k_x L_x) + i(1 - \cos(k_x L_x))}{1 + \cos(k_x L_x) + i \sin(k_x L_x)} = \frac{\sin(k_x L_x) + i(1 - \cos(k_x L_x))}{1 + \cos(k_x L_x) + i \sin(k_x L_x)} \frac{\sin(k_x L_x) - i(1 - \cos(k_x L_x))}{\sin(k_x L_x) - i(1 - \cos(k_x L_x))}$$

$$\frac{ik_x \zeta_x}{k} = \frac{\sin^2(k_x L_x) + (1 - \cos(k_x L_x))^2}{\sin(k_x L_x) + \cos(k_x L_x) \sin(k_x L_x) + i \sin^2(k_x L_x) - i(1 - \cos^2(k_x L_x)) + \sin(k_x L_x) - \sin(k_x L_x) \cos(k_x L_x)}$$

$$\frac{k_x \zeta_x}{k} = \frac{1 - \cos(k_x L_x) - i \sin(k_x L_x)}{1 + \cos(k_x L_x) + i \sin(k_x L_x)}$$

$$\frac{ik_x L_x}{k} = \frac{1 - \cos(k_x L_x)}{\sin(k_x L_x)}$$

$$\frac{ik_x \zeta_x}{k} - \tan\left(\frac{1}{2} k_x L_x\right) = 0 \quad (3.2.11 \text{ a})$$

For a negative right hand side in Eq. (3.2.10):

$$\cos(k_x L_x) + i \sin(k_x L_x) = -\frac{(k - k_x \zeta_x)}{(k + k_x \zeta_x)}$$

$$1 + \cos(k_x L_x) + i \sin(k_x L_x) = \frac{(-k + k_x \zeta_x)}{(k + k_x \zeta_x)} + \frac{(k + k_x \zeta_x)}{(k + k_x \zeta_x)}$$

$$1 + \cos(k_x L_x) + i \sin(k_x L_x) = \frac{2k_x \zeta_x}{(k + k_x \zeta_x)}$$

$$\frac{k + k_x \zeta_x}{2k_x \zeta_x} = \frac{1}{1 + \cos(k_x L_x) + i \sin(k_x L_x)}$$

$$\frac{k}{2k_x \zeta_x} + \frac{1}{2} = \frac{1}{1 + \cos(k_x L_x) + i \sin(k_x L_x)}$$

$$\frac{k}{k_x \zeta_x} + 1 = \frac{2}{1 + \cos(k_x L_x) + i \sin(k_x L_x)}$$

$$\frac{k}{k_x \zeta_x} = \frac{2}{1 + \cos(k_x L_x) + i \sin(k_x L_x)} - \frac{1 + \cos(k_x L_x) + i \sin(k_x L_x)}{1 + \cos(k_x L_x) + i \sin(k_x L_x)}$$

$$\frac{k}{k_x \zeta_x} = \frac{2 - \cos(k_x L_x) - i \sin(k_x L_x)}{1 + \cos(k_x L_x) + i \sin(k_x L_x)}$$

$$\frac{ik}{k_x \zeta_x} = \frac{\sin(k_x L_x) + i(1 - \cos(k_x L_x))}{1 + \cos(k_x L_x) + i \sin(k_x L_x)}$$

$$\frac{ik}{k_x \zeta_x} - \tan\left(\frac{1}{2} k_x L_x\right) = 0 \quad (3.2.11 \text{ b})$$

Therefore, Eq. (3.2.10) is equivalent to Eq. (3.2.11 a) and Eq. (3.2.11 b). The Newton-Raphson iteration method can be used to find the roots of these two equations. For specified k , L_x and ζ_x values, the root corresponds to the distinct complex eigenvalue, k_x . Due to the nature of the tangent function, there will be an infinite number of distinct solutions for k_x . The following equations can be used to solve for the eigenvalues.

For $n_x = 1, 3, 5, \dots$

$$n = (n_x + 1)/2$$

$$f_1(k_x(m)) = -\frac{1}{2}L_x k_x(m) + \tan^{-1}\left(\frac{ik_x(m)\zeta_x}{k}\right) + n\pi \quad (3.2.12)$$

$$\frac{\partial f_1(k_x(m))}{\partial k_x} = -\frac{1}{2}L_x + \frac{\left(\frac{i\zeta_x}{k}\right)}{\left(1 + \left(\frac{ik_x(m)\zeta_x}{k}\right)^2\right)} \quad (3.2.13)$$

and for $n_x = 0, 2, 4, \dots$

$$n = n_x/2$$

$$f_2(k_x(m)) = -\frac{1}{2}L_x k_x(m) + \tan^{-1}\left(\frac{ik}{k_x(m)\zeta_x}\right) + n\pi \quad (3.2.14)$$

$$\frac{\partial f_2(k_x(m))}{\partial k_x} = -\frac{1}{2}L_x - \frac{\left(\frac{ik}{\zeta_x}\right)}{\left(k_x(m)\right)^2 + \left(\frac{ik}{\zeta_x}\right)^2} \quad (3.2.15)$$

$$k_x(m+1) = k_x(m) - \frac{f(k_x(m))}{\left(\frac{\partial f(k_x(m))}{\partial k_x}\right)} \quad (3.2.16)$$

Eq. (3.2.12) and Eq. (3.2.13) are used to find the roots of Eq. (3.2.11 a). Eq. (3.2.14) and Eq. (3.2.15) are used to find the roots of Eq. (3.2.11 b). The eigenvalue can be found from Eq. (3.2.16). The $n\pi$ terms in Eq. (3.2.12) and Eq. (3.2.14) are used to converge on higher order eigenvalues, by increasing the value of the integer n_x .

A similar process can be used to find the eigenvalues in the y and z directions of the enclosure. As given for the rigid wall case in Eq. (3.1.30), the overall value for the three dimensional non-rigid wall eigenvalue is a combination of the eigenvalues found for

each individual direction. Once the eigenvalues are found which satisfy Eq. (3.2.10), their corresponding eigenfunctions can be found.

From Eq. (3.2.8) the ratio of the coefficients C_x and D_x can be formulated.

$$\frac{C_x}{D_x} = -\frac{(k - k_x \zeta_x)}{(k + k_x \zeta_x)} = \pm e^{ik_x L_x} \quad (3.2.17)$$

This ratio can be substituted into Eq. (3.2.6) to find the eigenfunction in the x direction.

$$X(x) = \pm D_x (e^{ik_x L_x} e^{-ik_x x} + e^{ik_x x}) \quad (3.2.18)$$

Due to the \pm sign in the expression for the eigenfunction, there are two expressions that can be developed. One expression is the eigenfunction corresponding to an even valued mode, and the other expression corresponds to an odd valued mode.

For an even valued mode ($n_x = 0, 2, 4, \dots$), the positive sign is valid.

$$X(x) = D_x (e^{ik_x L_x} e^{-ik_x x} + e^{ik_x x})$$

$$X(x) = D_x (e^{i(k_x L_x - k_x x)} + e^{ik_x x})$$

$$X(x) = D_x [\cos(k_x L_x - k_x x) + i \sin(k_x L_x - k_x x) + \cos(k_x x) + i \sin(k_x x)]$$

$$X(x) = D_x [\cos(k_x x) + \cos(k_x L_x - k_x x) + i(\sin(k_x x) + \sin(k_x L_x - k_x x))]$$

$$X(x) = 2D_x [\cos(\frac{k_x x - k_x L_x - k_x x}{2}) \cos(\frac{k_x x - k_x L_x + k_x x}{2}) + \dots \\ i \sin(\frac{k_x x - k_x L_x - k_x x}{2}) \cos(\frac{k_x x - k_x L_x + k_x x}{2})]$$

$$X(x) = 2D_x [\cos(\frac{k_x L_x}{2}) \cos(k_x (x - \frac{L_x}{2})) + i \sin(\frac{k_x L_x}{2}) \cos(k_x (x - \frac{L_x}{2}))]$$

$$X(x) = 2D_x \cos(k_x (x - \frac{L_x}{2})) (\cos(\frac{k_x L_x}{2}) + i \sin(\frac{k_x L_x}{2})) \quad (3.2.19 a)$$

For an odd valued mode ($n_x = 1, 3, 5, \dots$), the negative sign is valid.

$$X(x) = D_x (-e^{ik_x L_x} e^{-ik_x x} + e^{ik_x x})$$

$$X(x) = D_x (-e^{i(k_x L_x - k_x x)} + e^{ik_x x})$$

$$X(x) = D_x [-\cos(k_x L_x - k_x x) - i \sin(k_x L_x - k_x x) + \cos(k_x x) + i \sin(k_x x)]$$

$$X(x) = D_x [\cos(k_x x) - \cos(k_x L_x - k_x x) + i(\sin(k_x x) - \sin(k_x L_x - k_x x))]$$

$$X(x) = 2D_x [-\sin(\frac{k_x x + k_x L_x - k_x x}{2}) \sin(\frac{k_x x - k_x L_x + k_x x}{2}) + \dots \\ i \cos(\frac{k_x x + k_x L_x - k_x x}{2}) \sin(\frac{k_x x - k_x L_x + k_x x}{2})]$$

$$X(x) = 2D_x [-\sin(\frac{k_x L_x}{2}) \sin(k_x (x - \frac{L_x}{2})) + i \cos(\frac{k_x L_x}{2}) \sin(k_x (x - \frac{L_x}{2}))]$$

$$X(x) = 2D_x \sin(k_x (x - \frac{L_x}{2})) (i \cos(\frac{k_x L_x}{2}) - \sin(\frac{k_x L_x}{2})) \quad (3.2.19 \text{ b})$$

The eigenfunctions that Kuttruff presents in his book Room Acoustics are slightly different than the ones developed in Eq. (3.2.19 a,b). The functions that he presents are given below.

For the even mode case:

$$X(x) = \cos(k_x (x - \frac{L_x}{2})) \quad (3.2.20 \text{ a})$$

and for the odd mode case:

$$X(x) = \sin(k_x (x - \frac{L_x}{2})) \quad (3.2.20 \text{ b}).$$

These functions are only portions of the fully developed eigenfunctions. It is believed that Kuttruff presents only portions of the fully developed eigenfunctions in order

to simplify the expressions. A comparison between the eigenfunctions which he presents and the full eigenfunctions was performed, and it was found that his simplified forms do not give accurate phase values. For active controls purposes, the simplified eigenfunctions will not work, because accurate gain and phase relationships are required.

Similar eigenfunctions can be found for the y and z directions. The three dimensional eigenfunction is found by multiplying the eigenfunctions found for each individual direction. As for the rigid wall case, the eigenfunctions are orthogonal.

For the x direction:

For $n_x = 0, 2, 4, \dots$

$$\int_{L_x} X^2(x)dx = D_x^2 e^{ik_x L_x} [2L_x + 2\sin(k_x L_x)]$$

and for $n_x = 1, 3, 5, \dots$

$$\int_{L_x} X^2(x)dx = D_x^2 e^{ik_x L_x} [-2L_x + 2\sin(k_x L_x)].$$

Similar equations exist for the y and z directions.

The volume integral of the three dimensional eigenfunction squared is then equal to:

$$\Lambda_n = \int_{L_x} X^2(x)dx \int_{L_y} Y^2(y)dy \int_{L_z} Z^2(z)dz$$

Numerical results using the finite acoustic impedance approach for the acoustic response in a non-rigid-wall enclosure will be presented in Chapter 4. Another modeling approach for the acoustic response in a non-rigid-wall enclosure is the coupled modal approach. This is discussed in the next section.

3.3 Coupled Modal Approach

Another approach which can be used to model the acoustic response in an enclosure is to treat the vibration of the enclosure walls as additional sources, as discussed by Fahy in his book Sound and Structural Vibration. This structural vibration can be expressed in terms of the *in vacuo* structural modes of the enclosure walls. The acoustic pressure is expressed in terms of the rigid wall acoustic modes. In general the modes of the combined structural acoustic system are different than the modes found for each system separately. How different they are depends on the degree of coupling between the two systems.

As in the uncoupled formulation, the inhomogeneous wave equation, Eq. (3.1.1), governs the acoustic response in the enclosure. The vibrations of the walls can be represented by:

$$q_b(\mathbf{r}) = -2 \frac{\partial w(\mathbf{r}_s)}{\partial t} \delta(\xi - \xi_0) \quad (3.3.1)$$

where w normal displacement of wall directed outward from the fluid volume

\mathbf{r}_s surface location

$\delta(\xi - \xi_0)$ delta function used to confine the vibration source to an infinitesimally thin layer situated on a surface S_0 just inside a rigid boundary.

The expression given in Eq. (3.3.1) can be inserted into the inhomogeneous wave equation:

$$\nabla^2 p - \frac{1}{c^2} \frac{\partial^2 p}{\partial t^2} = 2\rho \frac{\partial^2 w(\mathbf{r}_s)}{\partial t^2} \delta(\xi - \xi_0) - \rho \frac{\partial q(\mathbf{r}_0)}{\partial t} \quad (3.3.2)$$

The pressure is expressed as the sum of the acoustic modal contributions by use of Eq. (3.1.2), leading to the following equation.

$$\nabla^2 \sum_{n=0}^{\infty} a_n(t) \Psi_n(\mathbf{r}) - \frac{1}{c^2} \sum_{n=0}^{\infty} \frac{\partial^2 \sum_{n=0}^{\infty} a_n(t) \Psi_n(\mathbf{r})}{\partial t^2} = \dots \quad (3.3.3)$$

$$2\rho \frac{\partial^2 w(\mathbf{r}_s)}{\partial t^2} \delta(\xi - \xi_0) - \rho \frac{\partial q(\mathbf{r}_0)}{\partial t}$$

Use the homogeneous Helmholtz equation, Eq. (3.1.6), and substitute in for $\nabla^2 \Psi_n$:

$$\sum_{n=0}^{\infty} -k_n^2 a_n(t) \Psi_n(\mathbf{r}) - \frac{1}{c^2} \sum_{n=0}^{\infty} \ddot{a}_n(t) \Psi_n(\mathbf{r}) = 2\rho \frac{\partial^2 w(\mathbf{r}_s)}{\partial t^2} \delta(\xi - \xi_0) - \rho \frac{\partial q(\mathbf{r}_0)}{\partial t} \quad (3.3.4).$$

Multiply by $\Psi_m(\mathbf{r})$ and integrate over the enclosure volume:

$$\int_V \sum_{n=0}^{\infty} k_n^2 a_n(t) \Psi_n(\mathbf{r}) \Psi_m(\mathbf{r}) dV - \int_V \frac{1}{c^2} \sum_{n=0}^{\infty} \ddot{a}_n(t) \Psi_n(\mathbf{r}) \Psi_m(\mathbf{r}) dV = \dots \quad (3.3.5).$$

$$\int_V 2\rho \frac{\partial^2 w(\mathbf{r}_s)}{\partial t^2} \delta(\xi - \xi_0) \Psi_m(\mathbf{r}) dV - \int_V \rho \frac{\partial q(\mathbf{r}_0)}{\partial t} \Psi_m(\mathbf{r}) dV$$

Use Eq. (3.1.9) and the orthogonality condition of the eigenfunctions to simplify the expression in Eq. (3.3.6):

$$-k_m^2 a_m(t)V - \frac{1}{c^2} \ddot{a}_m(t)V = \dots \quad (3.3.6).$$

$$\rho \int_V 2 \frac{\partial^2 w(\mathbf{r}_s)}{\partial t^2} \delta(\xi - \xi_0) \Psi_m(\mathbf{r}) dV - \rho \int_V \frac{\partial q(\mathbf{r}_0)}{\partial t} \Psi_m(\mathbf{r}) dV$$

The first volume integral on the right hand side of Eq. (3.3.6) becomes a surface integral due to dirac delta function inside the integral.

$$-k_m^2 a_m(t)V - \frac{1}{c^2} \ddot{a}_m(t)V = \rho \int_S \frac{\partial^2 w(\mathbf{r}_s)}{\partial t^2} \Psi_m(\mathbf{r}) dS - \rho \int_V \frac{\partial q(\mathbf{r}_0)}{\partial t} \Psi_m(\mathbf{r}) dV \quad (3.3.7)$$

Multiply Eq. (3.3.7) by $-c^2/V$ to find:

$$\ddot{a}_m(t) + \omega_m^2 a_m(t) = -\frac{\rho c^2}{V} \int_S \frac{\partial^2 w(\mathbf{r}_s)}{\partial t^2} \Psi_m(\mathbf{r}) dS + \frac{\rho c^2}{V} \int_V \frac{\partial q(\mathbf{r}_0)}{\partial t} \Psi_m(\mathbf{r}) dV \quad (3.3.8).$$

Replace m with n to get:

$$\ddot{a}_n(t) + \omega_n^2 a_n(t) = -\frac{\rho c^2}{V} \int_S \frac{\partial^2 w(\mathbf{r}_s)}{\partial t^2} \Psi_n(\mathbf{r}) dS + \frac{\rho c^2}{V} \int_V \frac{\partial q(\mathbf{r}_0)}{\partial t} \Psi_n(\mathbf{r}) dV \quad (3.3.9).$$

It should be noted that the summation of the rigid wall acoustic modes does not converge to the correct boundary normal velocity, but does converge to the correct surface pressure, which is all that we're concerned with for this formulation.

Coupled differential equations governing the acoustic modal pressure amplitudes and structural modal displacements can be formulated from Eq. (3.3.9). In order to find the differential equations for the acoustic modal pressure amplitudes, first the vibration of the structure can be expressed as a sum of its characteristic structural eigenfunctions:

$$w(\mathbf{r}_s, t) = \sum_{p=1}^{\infty} w_p(t) \Phi_p(\mathbf{r}_s) \quad (3.3.10)$$

where

$w(\mathbf{r}_s, t)$	normal displacement of structure at point \mathbf{r}_s
$w_p(t)$	structural modal amplitude
$\Phi_p(\mathbf{r}_s)$	structural modal eigenfunction.

The second derivative with respect to time is given by:

$$\frac{\partial^2 \sum_{p=1}^{\infty} w_p(t) \Phi_p(\mathbf{r}_s)}{\partial t^2} = \sum_{p=1}^{\infty} \ddot{w}_p(t) \Phi_p(\mathbf{r}_s) \quad (3.3.11)$$

Substitute the expression for the second derivative into Eq. (3.3.9).

$$\ddot{a}_n(t) + \omega_n^2 a_n(t) = \frac{\rho c^2}{V} \int_S \Psi_n(\mathbf{r}_s) \sum_{p=1}^{\infty} \ddot{w}_p(t) \Phi_p(\mathbf{r}_s) dS + \frac{\rho c^2}{V} \int_V \frac{\partial q(\mathbf{r}_o)}{\partial t} \Psi_n(\mathbf{r}) dV \quad (3.3.12)$$

$$\begin{aligned} \ddot{a}_n(t) + \omega_n^2 a_n(t) = & \dots \\ & - \frac{\rho c^2}{V} \sum_{p=1}^{\infty} \ddot{w}_p(t) \int_S \Psi_n(\mathbf{r}_s) \Phi_p(\mathbf{r}_s) dS + \frac{\rho c^2}{V} \int_V \frac{\partial q(\mathbf{r}_o)}{\partial t} \Psi_n(\mathbf{r}) dV \end{aligned} \quad (3.3.13)$$

Damping in the enclosed fluid can be added to the differential equation governing the acoustic modal amplitude through the use of a viscous damping coefficient, which is added to the left hand side of the equation.

$$\begin{aligned} \ddot{a}_n(t) + 2\zeta_n \omega_n \dot{a}_n(t) + \omega_n^2 a_n(t) = & \dots \\ & - \frac{\rho c^2}{V} \sum_{p=1}^{\infty} \ddot{w}_p(t) \int_S \Psi_n(\mathbf{r}_s) \Phi_p(\mathbf{r}_s) dS + \frac{\rho c^2}{V} \int_V \frac{\partial q(\mathbf{r}_o)}{\partial t} \Psi_n(\mathbf{r}) dV \end{aligned} \quad (3.3.14)$$

Now, a differential equation governing the structural modal amplitude will be developed. First, the equation of motion of the structure can be written.

$$L[w(\mathbf{r}_s)] + m(\mathbf{r}_s) \frac{\partial^2 w(\mathbf{r}_s)}{\partial t^2} = f(\mathbf{r}_s) + p(\mathbf{r}_s) \quad (3.3.15)$$

- where
- $L[w(\mathbf{r}_s)]$ the operator governing the elastic forces in the structure
 - $w(\mathbf{r}_s)$ the normal vibration displacement of the structure (directed outward from the fluid volume)
 - $m(\mathbf{r}_s)$ the mass per unit area of the wall with surface area corresponding to the structural mode
 - $f(\mathbf{r}_s)$ the distribution of mechanically applied force per unit area (directed outward from fluid volume)

$p(\mathbf{r}_s)$ the distribution of surface pressures

The operator governing the elastic forces in the structure can be found assuming a homogeneous case.

$$L[\Phi_p(\mathbf{r}_s)] - \omega_p^2 m(\mathbf{r}_s) \Phi_p(\mathbf{r}_s) = 0 \quad (3.3.16)$$

$$L\left[\sum_{p=1}^{\infty} w_p(t) \Phi_p(\mathbf{r}_s)\right] + m(\mathbf{r}_s) \frac{\partial^2 \sum_{p=1}^{\infty} w_p(t) \Phi_p(\mathbf{r}_s)}{\partial t^2} = f(\mathbf{r}_s) + p(\mathbf{r}_s) \quad (3.3.17)$$

$$\sum_{p=1}^{\infty} w_p(t) \omega_p^2 m(\mathbf{r}_s) \Phi_p(\mathbf{r}_s) + m(\mathbf{r}_s) \sum_{p=0}^{\infty} \ddot{w}_p(t) \Phi_p(\mathbf{r}_s) = f(\mathbf{r}_s) + p(\mathbf{r}_s) \quad (3.3.18)$$

Multiply Eq. (3.3.18) by $\Phi_q(\mathbf{r}_s)$ and integrate over the surface corresponding to the structural mode.

$$\int_S \sum_{p=1}^{\infty} w_p(t) \omega_p^2 m(\mathbf{r}_s) \Phi_p(\mathbf{r}_s) \Phi_q(\mathbf{r}_s) dS + \int_S m(\mathbf{r}_s) \sum_{p=1}^{\infty} \ddot{w}_p(t) \Phi_p(\mathbf{r}_s) \Phi_q(\mathbf{r}_s) dS = \dots \quad (3.3.19)$$

$$\int_S f(\mathbf{r}_s) \Phi_q(\mathbf{r}_s) dS + \int_S p(\mathbf{r}_s) \Phi_q(\mathbf{r}_s) dS$$

Use the orthogonality relationship of the structural modes to find:

$$\int_S m(\mathbf{r}_s) \Phi_p(\mathbf{r}_s) \Phi_q(\mathbf{r}_s) dS = \begin{cases} \Lambda_q, p = q \\ 0, p \neq q \end{cases} \quad (3.3.20)$$

where $\Lambda_q = m(\mathbf{r}_s) S$ (mass units).

$$w_q(t) \omega_q^2 \Lambda_q + \ddot{w}_q(t) \Lambda_q = \int_S f(\mathbf{r}_s) \Phi_q(\mathbf{r}_s) dS + \int_S p(\mathbf{r}_s) \Phi_q(\mathbf{r}_s) dS \quad (3.3.21)$$

Express $p(\mathbf{r}_s, t)$ in terms of the acoustic modes:

$$w_q(t)\omega_q^2\Lambda_q + \ddot{w}_q(t)\Lambda_q = \int_S f(\mathbf{r}_s)\Phi_q(\mathbf{r}_s)dS + \int_S \sum_{n=0}^{\infty} a_n(t)\Psi_n(\mathbf{r}_s)\Phi_q(\mathbf{r}_s)dS \quad (3.3.22)$$

$$\ddot{w}_q(t) + \omega_q^2 w_q(t) = \frac{1}{\Lambda_q} \int_S f(\mathbf{r}_s)\Phi_q(\mathbf{r}_s)dS + \frac{1}{\Lambda_q} \sum_{n=0}^{\infty} a_n(t) \int_S \Psi_n(\mathbf{r}_s)\Phi_q(\mathbf{r}_s)dS \quad (3.3.23)$$

Replace q with p to get:

$$\ddot{w}_p(t) + \omega_p^2 w_p(t) = \frac{1}{\Lambda_p} \int_S f(\mathbf{r}_s)\Phi_p(\mathbf{r}_s)dS + \frac{1}{\Lambda_p} \sum_{n=0}^{\infty} a_n(t) \int_S \Psi_n(\mathbf{r}_s)\Phi_p(\mathbf{r}_s)dS \quad (3.3.24).$$

Damping in the structure can be added to the differential equation governing the structural modal amplitude through the use of a viscous damping coefficient, which is added to the left hand side of the equation.

$$\begin{aligned} \ddot{w}_p(t) + 2\zeta_p\omega_p\dot{w}_p(t) + \omega_p^2 w_p(t) = & \dots \\ \frac{1}{\Lambda_p} \int_S f(\mathbf{r}_s)\Phi_p(\mathbf{r}_s)dS + \frac{1}{\Lambda_p} \sum_{n=0}^{\infty} a_n(t) \int_S \Psi_n(\mathbf{r}_s)\Phi_p(\mathbf{r}_s)dS & \quad (3.3.25) \end{aligned}$$

The coupling integral

$$\int_S \Psi_n(\mathbf{r}_s)\Phi_p(\mathbf{r}_s)dS,$$

which appears in Eq. (3.3.14) and Eq. (3.3.25), determines how well energy is transferred between the structure and the enclosed fluid. Fahy (1985) presents an analysis of how the acoustic and structural resonances are shifted as a result of the coupling between the enclosed fluid and the structure. When the two systems are coupled together the resonant frequencies associated with each individual system may shift. This shift can be attributed to the well-known frequency splitting phenomenon. When an uncoupled acoustic resonant frequency is approximately equal to an uncoupled structural resonant frequency, one of

the coupled resonant frequencies will be shifted up in magnitude, and the other will be shifted down in magnitude. In order to model this shift accurately, the *in vacuo* structural modes of the enclosure, as well as the rigid-wall acoustic modes of the enclosed fluid must be modeled accurately. The rigid-wall acoustic modes were developed in Sec. 3.1. In order to complete the coupled model, the structural modes of the enclosure must be developed.

Several methods can be used to estimate the structural modes of the enclosure. The accuracy of the *in vacuo* structural modal functions is important in determining the accuracy of the acoustic response that is found using the coupled approach. One of the simplest approaches assumes that each of the walls of the enclosure is simply supported. Thus, the equations for the structural eigenfunctions of the walls are sinusoidal functions. This approach, however, does not account for coupling between the walls of the structure at coincident edges.

The simply supported structural eigenfunctions are given by Eq. (3.3.26).

$$\Phi_p(x, y) = \sin\left(\frac{p_x \pi x}{L_x}\right) \sin\left(\frac{p_y \pi y}{L_y}\right) \quad (3.3.26)$$

The simply supported structural eigenfrequencies are given by Eq. (3.3.27).

$$\omega_p = \left(\frac{D}{\rho_m h L_x L_y}\right)^{\frac{1}{2}} \left[\left(\frac{p_x \pi}{L_x}\right)^2 + \left(\frac{p_y \pi}{L_y}\right)^2 \right] \quad (3.3.27)$$

Similar functions exist for the *yz* and *xz* surfaces of the enclosure.

$$D = \frac{Eh^3}{12(1-\nu^2)} \quad (3.3.28)$$

E	Young's modulus of wall material
h	thickness of wall
L_x	length of enclosure in x direction
L_y	length of enclosure in y direction
p	structural mode number
p_x	modal integer corresponding to x direction
p_y	modal integer corresponding to y direction
ν	Poisson's ratio of wall material
ρ_m	wall material density

If the walls of the enclosure are assumed to be clamped, then the analysis for the structural eigenfunctions and eigenfrequencies becomes more difficult, due to the more complex nature of the clamped modal equations. Another possible method to find the structural eigenfunctions and eigenfrequencies is to use a finite element analysis to solve for them numerically.

The coupled modal equations, Eq. (3.3.14) and Eq. (3.3.25), can be implemented in a state space model to find the acoustic response of the system. Numerical results for the acoustic response in an enclosure using the coupled approach will be presented in Chapter 4.

3.4 Transducer Dynamics Model

The three models presented in the previous sections relate acoustic pressure to the volume acceleration of the source. In order to directly compare the frequency responses given by the models to the actual frequency responses found experimentally for a plexiglass enclosure, the dynamics of the source loudspeaker need to be known. Specifically, the relationship between the volume acceleration of the speaker and the input voltage to the speaker is needed. Small (1972) presents a simplified transfer function for the dynamics of a direct-radiator loudspeaker placed in an infinite baffle, which is presented below.

$$\frac{\dot{q}}{V_{in}} = \left(\frac{Bl}{(R_g + R_E)S_D} \right) \frac{sC_{AS}}{s^2M_{AS}C_{AS} + sR_{AT}C_{AS} + 1} \quad (3.4.1)$$

$$R_{AT} = R_{AS} + \frac{B^2l^2}{(R_g + R_E)S_D^2} \quad (3.4.2)$$

- B magnetic flux density in driver air gap
- C_{AS} acoustic compliance of driver suspension
- l length of the voice-coil conductor in magnetic field of air gap
- M_{AS} acoustic mass of driver diaphragm assembly including voice coil and air load
- R_{AS} acoustic resistance of driver suspension losses
- R_{AT} total acoustic resistance

R_E	dc resistance of driver voice coil
R_g	output resistance of source
\dot{q}	volume acceleration of the source (speaker)
S_D	effective projected surface area of driver diaphragm
V_{in}	input voltage to the speaker

An attempt was made to use this model to generate the frequency response of the source speaker. The resulting frequency response was four orders of magnitude greater than that found experimentally with the use of an accelerometer. This was attributed to not having the correct values for the speaker parameters. Therefore, it was decided to use the experimental frequency response for the speaker dynamics, when comparing the overall acoustic frequency responses given by the models to the experimental acoustic frequency responses found for the enclosure. In addition to the dynamics associated with the loudspeaker, there are also dynamics associated with the sensor microphone. These dynamics are discussed in Chapter 4, as well as the comparisons of the acoustic responses predicted by the models to the actual acoustic responses found for the experimental enclosure.

Chapter 4. Comparison of Numerical Results for Acoustic

Models and Experimental Results

Development of an accurate simulation for the acoustic response in a non-rigid-wall enclosure has been shown to depend on accurate knowledge of the structural boundary conditions or the acoustic impedance values at every boundary. Different models of the acoustic response in an enclosure were presented in Chapter 3. The models that were presented produce different acoustic responses. These differences will be compared to actual acoustic frequency responses that were found experimentally. A discussion of the experimental set-up and measurements is presented in the next section.

4.1 Experimental Set-up and Results

Experimental acoustic frequency responses were obtained for an enclosure that is 1.7145 m x .4826 m x .6223 m (See Figures A.1-A.6 in Appendix A). These dimensions were chosen in order to ensure certain rigid wall eigenvalues, based on simulation. The acoustic pressure at several different response points in the enclosure were measured with a ½" B & K microphone. A 6" loudspeaker was used as an acoustic source and was located at the boundary of the enclosure. The walls of the enclosure were built from .25" plexiglass, which vibrated when the loudspeaker was excited through a hole in the side of the enclosure.

In order to get a modeled frequency response that could be compared to an experimental frequency response (acoustic pressure/voltage into loudspeaker), the

frequency response function relating the volume acceleration of the loudspeaker to the input voltage to the loudspeaker was needed. This was approximated experimentally using an accelerometer that was placed on the center of the loudspeaker cone. The mass of the accelerometer was roughly 10% the mass of the diaphragm. Based on this fact, it is assumed that there is a slight mass loading effect present in the experimentally measured frequency response for the speaker. This response is shown in Fig. 4.1.

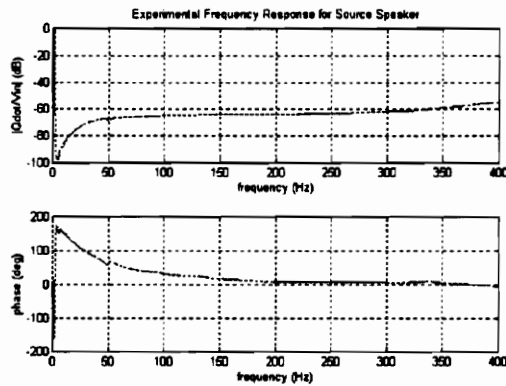


Figure 4.1 Experimentally Measured Speaker Frequency Response

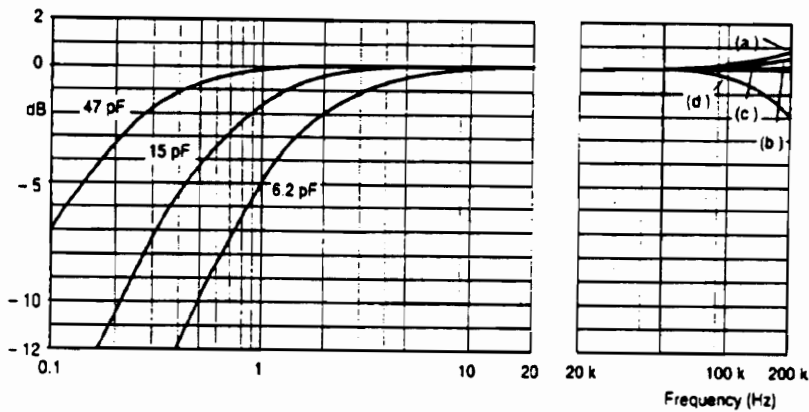
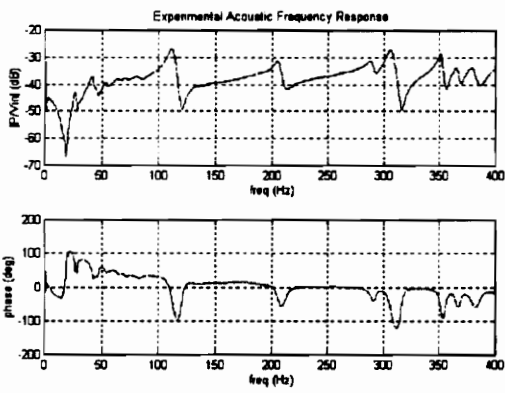


Figure 4.2 Frequency Response of Sensor Microphone

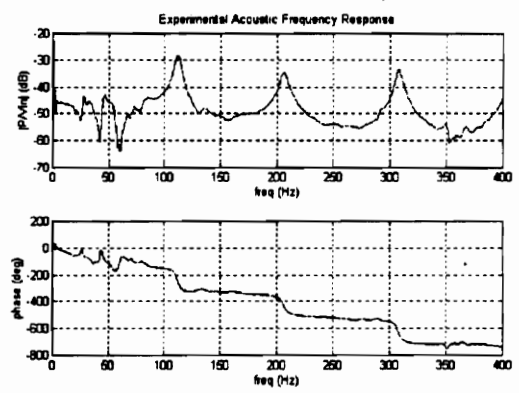
Figure 4.2 shows a plot of the frequency response function associated with the dynamics of the microphone and its amplifier. The response associated with the

microphone can be modeled with a zero at the origin, and a pole at 3 Hz. These dynamics of the microphone occur at such a low frequency that they are not seen in the experimentally measured acoustic responses, and the microphone response is essentially flat for the frequency range excited by the loudspeaker.

The actual acoustic frequency response functions relating pressure in Pascals to the input voltage into the loudspeaker are shown in Figure 4.3 for two different cases. Case (a) is for when the response and source points are collocated, and case (b) is for when they are non-collocated. For the collocated case, the source loudspeaker was located at speaker location 1 (see Appendix A.), and the microphone was located directly in front of it. For the non-collocated case, the loudspeaker was located at speaker location 2, and the microphone was located directly in front of speaker location 1. The frequency range for the plots is 0 to 400 Hz, where the acoustic response is dominated by distinct identifiable modes.



(a) Collocated



(b) Non-collocated

Figure 4.3 Experimental Acoustic Frequency Response

Additional experimentally obtained frequency response plots for various source and response locations for a frequency range of 0 to 800 Hz are presented in Appendix A. The influence of the structural vibration of the enclosure on the enclosed acoustic response was greater than originally anticipated. This was the motivation for formulating a model for the acoustic response in an enclosure which had walls that vibrated.

4.2 Infinite Impedance Model (Rigid Wall)

If the walls of an enclosure are approximately rigid, then the acoustic model for a rigid-wall enclosure should give a response that matches that found experimentally. How great the acoustic impedance at the walls has to be for this assumption to be valid is not known. An investigation of the influence of the acoustic wall impedance on the acoustic eigenvalues that are obtained for an enclosure is discussed in Sec. 4.3.

The differential equation presented in the last chapter for the rigid-wall acoustic modal contribution factors, Eq. (3.1.15), can be implemented in a state-space model configuration. The states of the model correspond to the acoustic modal contribution amplitudes (a_n) and their derivatives. The volume velocity input is assumed to act as a point source. The state space model is presented below.

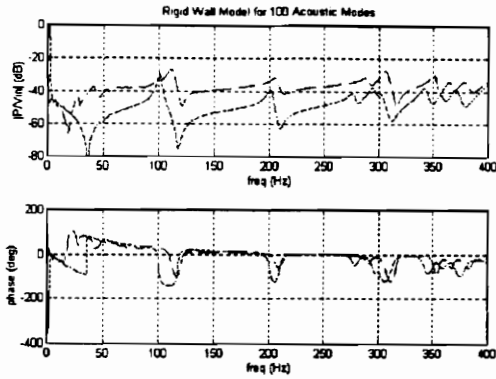
$$\begin{bmatrix} [\dot{a}_n]_{nx1} \\ [\ddot{a}_n]_{nx1} \end{bmatrix}_{2nx1} = \begin{bmatrix} [0]_{nxn} & [I]_{nxn} \\ \begin{bmatrix} -\omega_1^2 & 0 & 0 \\ 0 & \cdot & 0 \\ 0 & 0 & -\omega_n^2 \end{bmatrix}_{nxn} & \begin{bmatrix} -2\zeta_1\omega_1 & 0 & 0 \\ 0 & \cdot & 0 \\ 0 & 0 & -2\zeta_n\omega_n \end{bmatrix}_{nxn} \end{bmatrix}_{2nx2n} \begin{bmatrix} [a_n]_{nx1} \\ [\dot{a}_n]_{nx1} \end{bmatrix}_{2nx1} \dots \quad (4.2.1)$$

$$+ \begin{bmatrix} [0]_{nx1} \\ \left[\frac{\rho c^2}{V} \Psi_n(\mathbf{r}_0) \right]_{nx1} \end{bmatrix}_{2nx1} \dot{q}(t)$$

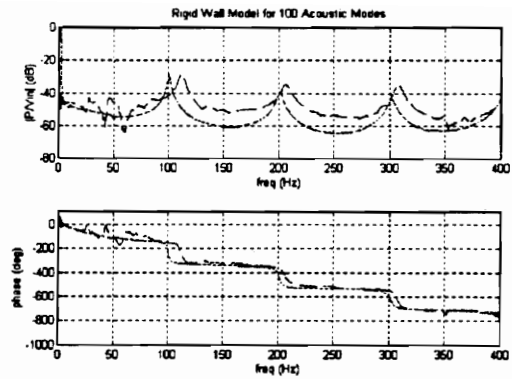
$$p(\mathbf{r}, t) = \left[[\Psi_n(\mathbf{r})]_{1xn} \quad [0]_{1xn} \right]_{1x2n} \begin{bmatrix} [a_n] \\ [\dot{a}_n] \end{bmatrix}_{2nx1} + [0]_{1x1} \dot{q}(t) \quad (4.2.2)$$

This state space model was used to generate an acoustic frequency response (acoustic pressure/volume acceleration of source) for both a collocated and non-collocated case corresponding to the same source and response points used in Figure 4.3.

The viscous damping ratio for each of the acoustic modes was assumed to be .01. The predicted acoustic frequency responses are shown in Fig. 4.4, along with the actual frequency responses found experimentally. It is easily seen from Fig. 4.4 that the responses given by the model do not match the actual responses. The difference in the zero locations between the frequency responses can be attributed to the limited number of modes which were used in the rigid wall model. This number was limited to 100, due to the increasing amount of computation needed for an increasing number of contributing acoustic modes. As more modes are added to the model, the zero locations approach those of the actual frequency response.



(a) Collocated



(b) Non-collocated

(Dashed line is actual frequency response)

Figure 4.4 Comparison of Experiment to Rigid Wall Model Acoustic Frequency Response

The peak frequencies given by the model do not match those of the actual response. The actual collocated frequency response has peaks at 112, 207, 288, 306, 352, 362, and 376 Hz, for the frequency range of interest. The collocated frequency response generated using the rigid wall model has peaks at 100, 201, 277, 295, 302, 342, 357, and 371 Hz, which are all less than the corresponding peak frequencies of the actual frequency response. Similar results were obtained for the non-collocated case. There are also additional peaks in the experimental responses below 100 Hz that do not appear in the simulated responses. These peaks are a result of the structural resonances of the enclosure, and cannot be generated with the rigid wall acoustic model.

Due to the fact that the modeled acoustic peak frequencies did not match those found experimentally, it was decided that this model did not represent the dynamics of the acoustic system accurately enough for stability analyses. Another model was needed,

which accounted for the non-rigid walls of the enclosure. The finite impedance model was investigated as a possibility.

4.3 Finite Impedance Model (Non-rigid Wall)

When the walls of an enclosure are not approximately rigid, it is no longer valid to assume that the acoustic response can be estimated with the model for a rigid-wall enclosure. The boundary conditions can be formulated from a finite complex acoustic impedance value. In general, the impedance at the walls of the enclosure varies with both position and frequency. The model used here assumes that the impedance for each pair of opposite walls is uniform over the surface area of the walls and increases linearly with frequency for each characteristic mode.

4.3.1 Influence of Impedance Value and Frequency on Eigenvalue

As discussed in Sec. 3.2, the real part of the complex eigenvalue determines the natural frequency, and the imaginary part determines the damping in the system. Using Eq. (3.2.12 - 3.2.16), an analysis was performed in order to gain a better understanding of the influence of both the impedance ratio, ζ_x , and the frequency value in k , on the eigenvalue, k_x . It was found that Eq. (3.2.12) and Eq. (3.2.13) generate eigenvalues corresponding to odd numbered modes. Eq. (3.2.14) and Eq. (3.2.15) correspond to even numbered modes.

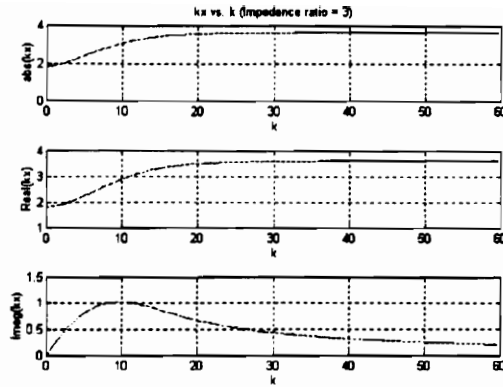


Figure 4.5 k_x vs. k

When the value for the impedance ratio was very large, the eigenvalue obtained was essentially the same as the eigenvalue for a rigid-wall boundary condition. For large impedance ratio values, the eigenvalue was not very sensitive to the value of k . When the magnitude of the impedance ratio and k were of the same order, the influence of k on the value obtained for k_x was greater, as seen in Fig. 4.5. This was true for real, imaginary, or complex values for the impedance ratio.

In order for the magnitude of each of the eigenvalues to remain constant over a specified frequency range, the value for the impedance associated with each mode must increase linearly with frequency. This comes from the steady-state assumption inherent in this modeling approach, and has not been validated experimentally. Mathematically, this ensures that the ratio between k and ζ_x remains constant, and therefore the value for k_x does as well.

The value obtained for the eigenvalue is determined by both the imaginary and real parts of the complex impedance ratio. Fig. 4.6 and Fig 4.7, were generated using the iteration technique previously described and allowing the real and imaginary parts of the

impedance ratio to vary from -5 to 5. The magnitude of the eigenvalue obtained is shown in the plot labeled (a), while the corresponding real and imaginary parts of the eigenvalue are labeled (b) and (c), respectively. The value of k was kept at a constant value corresponding to a frequency of 100 Hz. As shown in Fig. 4.6 for the case of an odd eigenvalue, there is a discontinuity in the magnitude of the real part of the eigenvalue for opposite signs on the imaginary part of the impedance. This is explained physically, by the appearance of an additional wavelength in the direction corresponding to the eigenvalue.

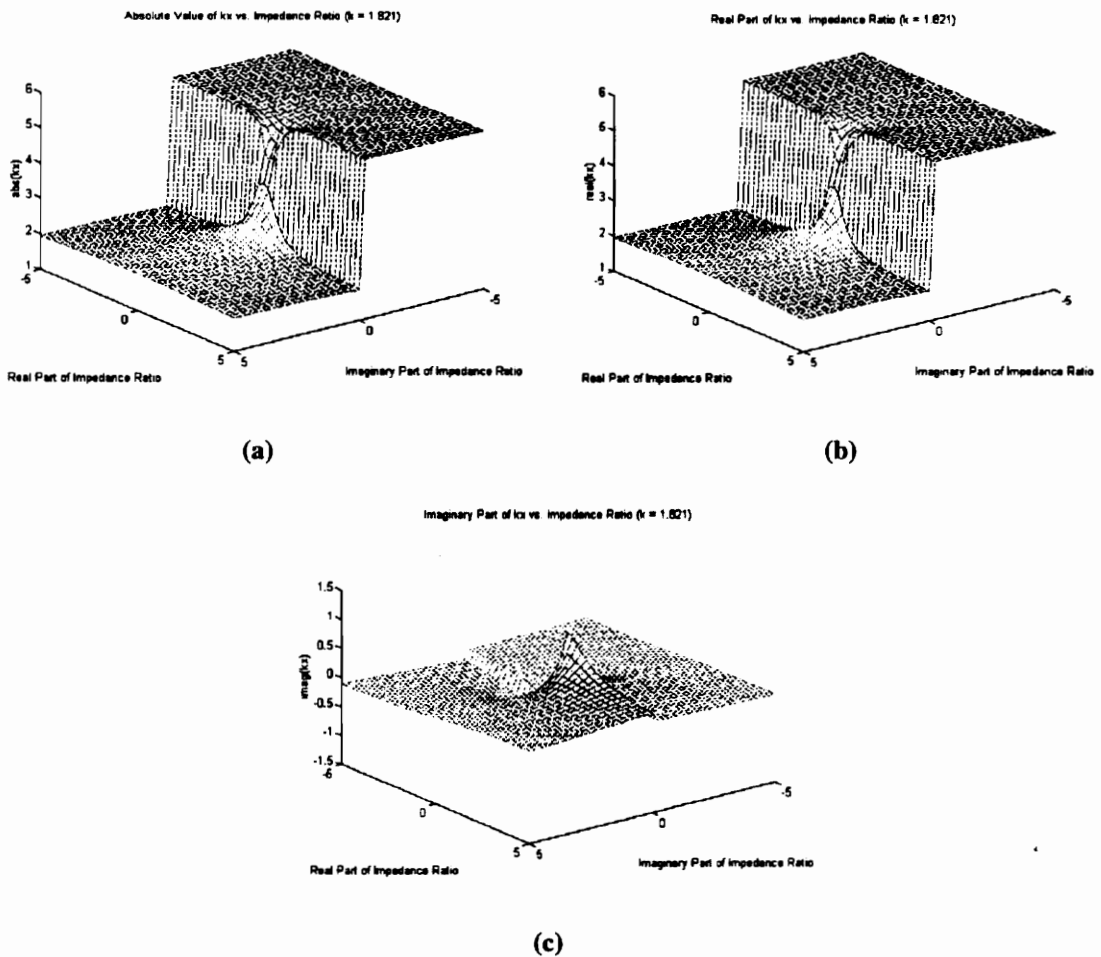
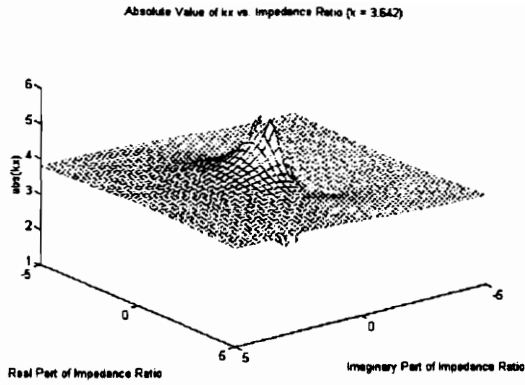
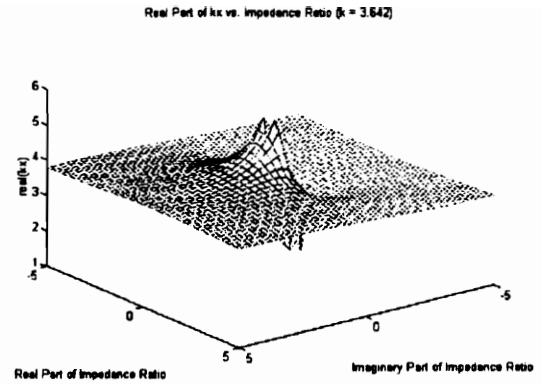


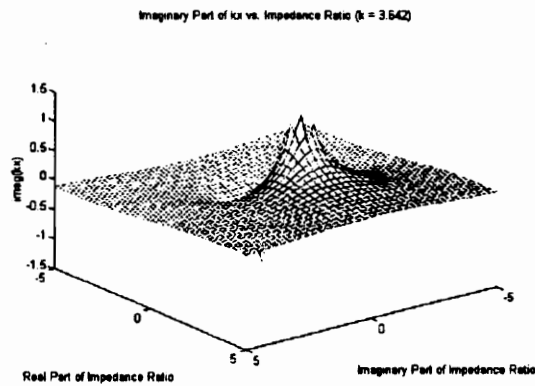
Figure 4.6 k_x (odd) vs. Impedance Ratio



(a)



(b)



(c)

Figure 4.7 k_x (even) vs. Impedance Ratio

For purely real impedance ratio values, the eigenvalue obtained had a large real part and a small imaginary part. As shown in Fig. 4.8, the imaginary part was negative for negative values of the impedance ratio, and positive for positive values of the impedance ratio.

As shown in Fig. 4.9, for purely imaginary impedance ratio values, the value obtained for k_x was purely real. For positive imaginary values for the impedance ratio, as the magnitude was decreased, the magnitude of k_x increased. For negative imaginary values for the impedance ratio, as the magnitude was decreased, the magnitude of k_x

decreased.

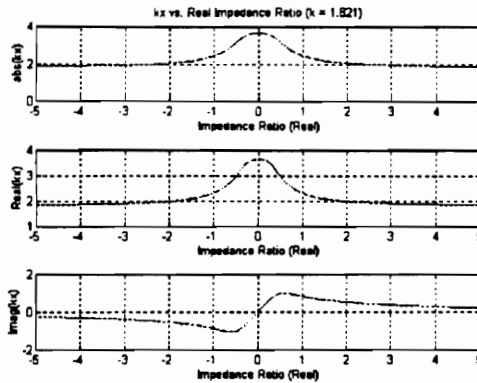


Figure 4.8 k_x (odd) vs. Real Impedance Ratio

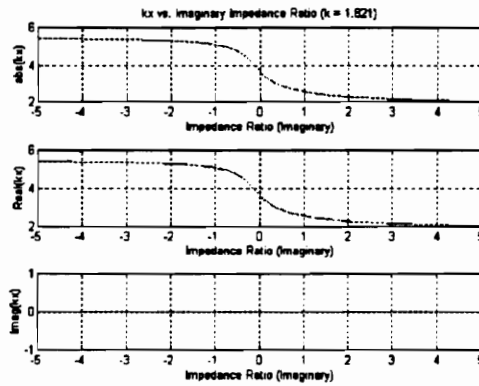


Figure 4.9 k_x (odd) vs. Imaginary Impedance Ratio

From the analysis described above, it was concluded that the impedance of the walls of the actual enclosure must have a real part, due to the fact that there was some damping in the system. A purely imaginary impedance would not allow for any damping in the system.

With an understanding of how the eigenvalue is effected by the value of the impedance, an attempt was made to estimate the values of the modal acoustic impedances needed to obtain the resonances corresponding to the actual acoustic system, which were

found experimentally. As stated previously, the resonant frequencies that were found experimentally were greater in magnitude than the ones that were predicted assuming that the walls of the enclosure were rigid.

The eigenfunctions for a finite impedance model were given in Chapter 3., Eq. (3.2.19 a) and Eq. (3.2.19 b). In order to get a visual picture of how the eigenfunctions are affected by the value of the wall impedance, the eigenfunction corresponding to the third x-directed axial mode was plotted for different values of impedance.

As shown in Fig. 4.10, when the impedance ratio, $Z/(\rho c)$, is essentially infinite, the eigenfunction has distinct nodal points, much like that of the rigid-wall eigenfunction. When the impedance ratio is purely real, the nodal lines begin to disappear as shown in Fig. 4.11. For a purely imaginary impedance ratio, the eigenfunction no longer has antinodes at the boundaries, as shown in Fig. 4.12.

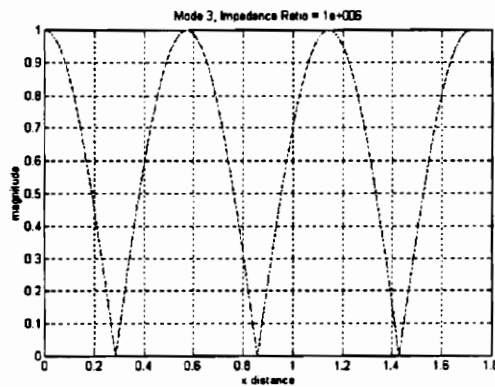


Figure 4.10 Magnitude of Eigenfunction For Infinite Impedance Ratio

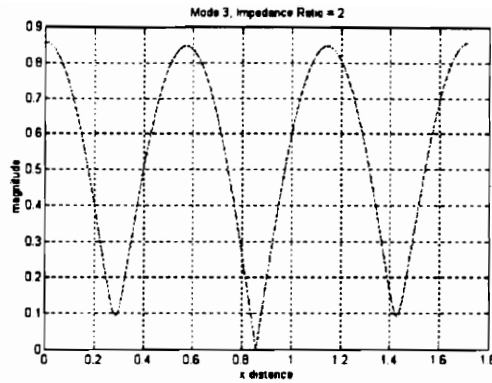


Figure 4.11 Magnitude of Eigenfunction When Impedance Ratio is Real

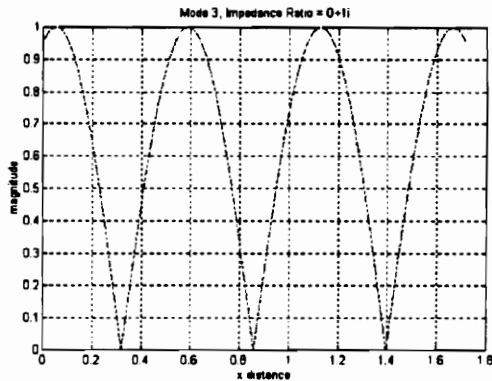
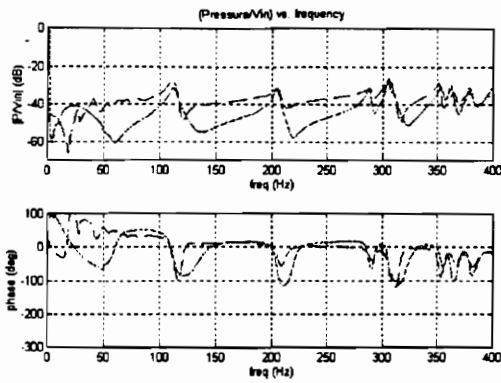
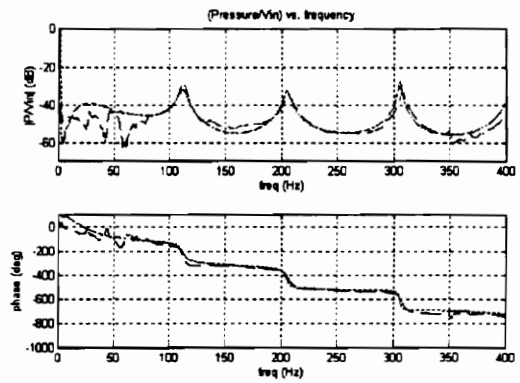


Figure 4.12 Magnitude of Eigenfunction When Impedance Ratio is Imaginary

The frequency response function given in Eq. (3.2.2) was used to generate the acoustic frequency responses shown in Fig. 4.13 for collocated and non-collocated source and response locations. The simulated acoustic frequency responses generated with the finite acoustic impedance modeling approach match their corresponding actual frequency responses much better than the responses obtained using the rigid-wall model. By choosing appropriate values for the acoustic impedance of the enclosure walls, the modeled resonant frequencies are shifted to those found for the actual response.



(a) Collocated



(b) Non-collocated

(Dashed line is actual frequency response)

Figure 4.13 Comparison of Experiment to Finite Impedance Model Acoustic Frequency Response

There is also good agreement between the phase plots found with the model and for the actual response. Acoustic impedance values were selected for the first 10 acoustic modes, which corresponded to acoustic resonance frequencies found for the experimental data. The impedance values which were chosen were based on a source frequency of 100 Hz. The actual acoustic impedance for one of the end walls of the enclosure was experimentally estimated by measuring the wall vibration and the acoustic pressure at the surface of the wall at a point. An example of this data is shown in Fig. 4.14. The estimated magnitudes of the impedance values that were used in the model for the first three axial modes perpendicular to the wall are shown with an asterisk, for a k value corresponding to 100 Hz.

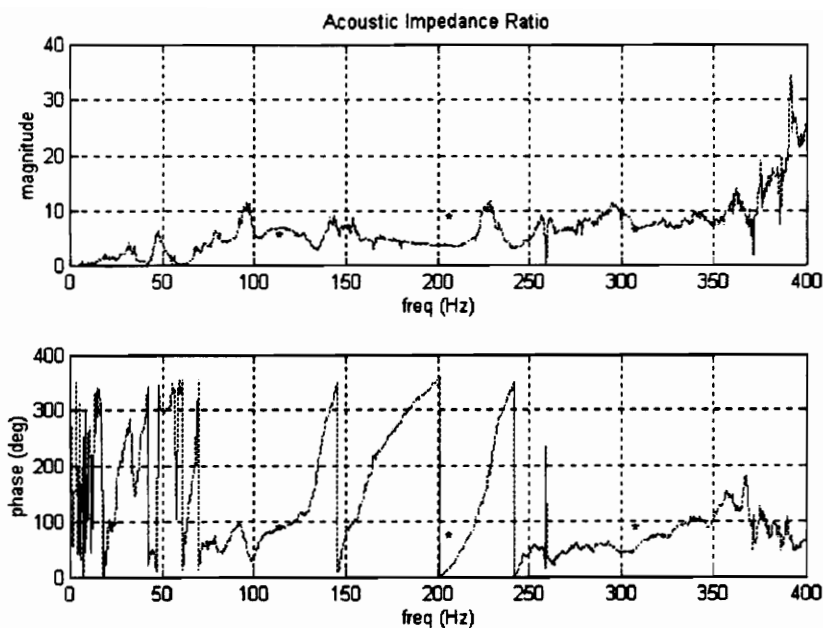


Figure 4.14 Experimentally Estimated Acoustic Impedance Ratio

Table 4.1 presents the impedance ratio values used for the first ten acoustic modes of the enclosure. The axial modes of the enclosure, corresponding to the modeled impedance ratio values shown in Fig. 4.14 with an asterisk, also have an asterisk by their mode numbers in the table. The modal integers for each direction are specified for each acoustic mode, as well as the impedance ratio values for each direction.

Table 4.1 Modeled Impedance Ratio Values

mode	nx	ny	nz	Zx/(pc)	Zy/(pc)	Zz/(pc)	frequency (Hz)
0	0	0	0	100	100	100	15
1*	1	0	0	.7128+4.8697i	100	100	112
2*	2	0	0	3.1401+7.4197i	100	100	205
3	0	0	1	100	100	.7944+5.5588i	288
4*	3	0	0	.7944+5.5588i	100	100	305.5
5	1	0	1	.7128+4.8697i	100	.7944+5.5588i	309
6	2	0	1	3.1401+7.4197i	100	.7944+5.5588	353.5
7	0	1	0	100	4.0845+12.4205i	100	362
8	1	1	0	.7128+4.8697i	4.0845+12.4205i	100	379
9	4	0	0	1.6010+3.7787i	100	100	406

For simplification, the acoustic impedance ratio values used to calculate the higher order modes corresponding to resonant frequencies greater than 400 Hz were all assumed to be a constant value of 100. This assumption effects the accuracy of the response found below 400 Hz, due to the fact that the higher order modes influence the response for this frequency range. Better accuracy in the predicted acoustic response may be obtained if the impedance values corresponding to the higher order modes are more precisely chosen. As with the rigid-wall modeling approach, the zeros of the simulated frequency response will approach those of the actual response with the addition of more modes.

4.4 Coupled Modal Approach

The two differential equations, Eq. (3.3.13) and Eq. (3.3.24), that were developed in Chapter 3 for the coupled modal simulation approach, were implemented in a state-space model. The state-space model that was formulated assumed that the only source present was an acoustic point source. The states were the acoustic modal amplitudes (a_n) and their time derivatives, as well as the structural modal amplitudes (w_p) and their time derivatives. The equation for the acoustic modal amplitude was modified, due to the fact that the structural modal accelerations were not state variables. A substitution in terms of the other states was performed to give Eq. (4.4.1).

$$\begin{aligned}
\ddot{a}_n(t) = & -2\zeta_n \omega_n \dot{a}_n(t) - \omega_n^2(t) + \frac{\rho c^2}{V} \sum_{p=1}^{\infty} 2\zeta_p \omega_p \dot{w}_p(t) \int_S \Psi_n(\mathbf{r}_s) \Phi_p(\mathbf{r}_s) dS + \dots \\
& \frac{\rho c^2}{V} \sum_{p=1}^{\infty} \omega_p^2 w_p(t) \int_S \Psi_n(\mathbf{r}_s) \Phi_p(\mathbf{r}_s) dS - \\
& \frac{\rho c^2}{V} \sum_{p=1}^{\infty} \left\{ \frac{1}{\Lambda_p} \left[\sum_{n=0}^{\infty} a_n(t) \int_S \Psi_n(\mathbf{r}_s) \Phi_p(\mathbf{r}_s) dS \right] \int_S \Psi_n(\mathbf{r}_s) \Phi_p(\mathbf{r}_s) \right\} + \dots \\
& \frac{\rho c^2}{V} \int_V \frac{\partial q(\mathbf{r}_o)}{\partial t} \Psi_n(\mathbf{r}) dV
\end{aligned} \tag{4.4.1}$$

The state-space model is presented below.

$$\begin{aligned}
\begin{bmatrix} \dot{a}_n \\ \ddot{a}_n \\ \dot{w}_p \\ \ddot{w}_p \end{bmatrix}_{(2n+2p) \times 1} &= \begin{bmatrix} [0]_{n \times n} & [I]_{n \times n} & [0]_{n \times p} & [0]_{n \times p} \\ [A_5]_{n \times n} & [A_6]_{n \times n} & [A_7]_{n \times p} & [A_8]_{n \times p} \\ [0]_{p \times n} & [0]_{p \times n} & [0]_{p \times p} & [I]_{p \times p} \\ [A_{13}]_{p \times n} & [0]_{p \times n} & [A_{15}]_{p \times p} & [A_{16}]_{p \times p} \end{bmatrix}_{(2n+2p) \times (2n+2p)} \begin{bmatrix} a_n \\ \dot{a}_n \\ w_p \\ \dot{w}_p \end{bmatrix}_{(2n+2p) \times 1} + \dots \\
\begin{bmatrix} [0]_{n \times 1} \\ [B_2]_{n \times 1} \\ [0]_{p \times 1} \\ [0]_{p \times 1} \end{bmatrix}_{(2n+2p) \times 1} & \dot{q}(t)
\end{aligned} \tag{4.4.2}$$

$$p(\mathbf{r}, t) = \begin{bmatrix} [\Psi_n(\mathbf{r})]_{1 \times n} & [0]_{1 \times n} & [0]_{1 \times p} & [0]_{1 \times p} \end{bmatrix}_{1 \times (2n+2p)} \begin{bmatrix} a_n \\ \dot{a}_n \\ w_p \\ \dot{w}_p \end{bmatrix}_{(2n+2p) \times 1} \tag{4.4.3}$$

The submatrices in the A and B matrices of the state-space model are given below.

$$A_5 = \begin{bmatrix} -\omega_1^2 - \frac{\rho c^2}{V} \sum_{p=1}^{\infty} \frac{1}{\Lambda_p} \int_S \Psi_1(\mathbf{r}_s) \Phi_p(\mathbf{r}_s) dS \int_S \Psi_1(\mathbf{r}_s) \Phi_p(\mathbf{r}_s) dS & \dots & -\frac{\rho c^2}{V} \sum_{p=1}^{\infty} \frac{1}{\Lambda_p} \int_S \Psi_n(\mathbf{r}_s) \Phi_p(\mathbf{r}_s) dS \int_S \Psi_1(\mathbf{r}_s) \Phi_p(\mathbf{r}_s) dS \\ \dots & \dots & \dots \\ -\frac{\rho c^2}{V} \sum_{p=1}^{\infty} \frac{1}{\Lambda_p} \int_S \Psi_1(\mathbf{r}_s) \Phi_p(\mathbf{r}_s) dS \int_S \Psi_n(\mathbf{r}_s) \Phi_p(\mathbf{r}_s) dS & \dots & -\omega_n^2 - \frac{\rho c^2}{V} \sum_{p=1}^{\infty} \frac{1}{\Lambda_p} \int_S \Psi_n(\mathbf{r}_s) \Phi_p(\mathbf{r}_s) dS \int_S \Psi_n(\mathbf{r}_s) \Phi_p(\mathbf{r}_s) dS \end{bmatrix}_{n \times n}$$

$$A_6 = \begin{bmatrix} -2\zeta_1\omega_1 & 0 & 0 \\ 0 & \cdot & 0 \\ 0 & 0 & -2\zeta_n\omega_n \end{bmatrix}$$

$$A_7 = \begin{bmatrix} \frac{\rho c^2}{V} \omega_1^2 \int_S \Psi_1(\mathbf{r}_s) \Phi_1(\mathbf{r}_s) dS & \dots & \frac{\rho c^2}{V} \omega_p^2 \int_S \Psi_1(\mathbf{r}_s) \Phi_p(\mathbf{r}_s) dS \\ \frac{\rho c^2}{V} \omega_1^2 \int_S \Psi_n(\mathbf{r}_s) \Phi_1(\mathbf{r}_s) dS & \dots & \frac{\rho c^2}{V} \omega_p^2 \int_S \Psi_n(\mathbf{r}_s) \Phi_p(\mathbf{r}_s) dS \end{bmatrix}_{n \times p}$$

$$A_8 = \begin{bmatrix} 2 \frac{\rho c^2}{V} \zeta_1 \omega_1 \int_S \Psi_1(\mathbf{r}_s) \Phi_1(\mathbf{r}_s) dS & \dots & 2 \frac{\rho c^2}{V} \zeta_p \omega_p \int_S \Psi_1(\mathbf{r}_s) \Phi_p(\mathbf{r}_s) dS \\ 2 \frac{\rho c^2}{V} \zeta_p \omega_p \int_S \Psi_n(\mathbf{r}_s) \Phi_1(\mathbf{r}_s) dS & \dots & 2 \frac{\rho c^2}{V} \zeta_p \omega_p \int_S \Psi_n(\mathbf{r}_s) \Phi_p(\mathbf{r}_s) dS \end{bmatrix}_{n \times p}$$

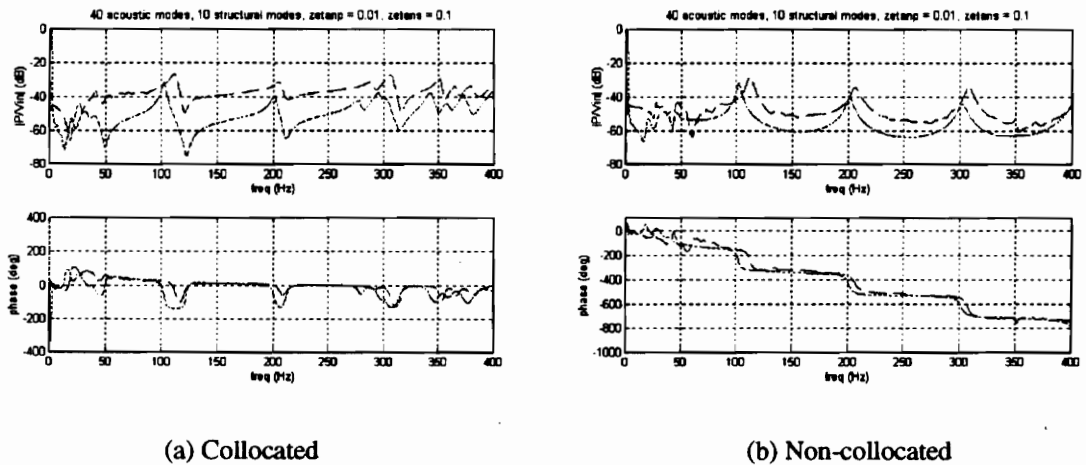
$$A_{13} = \begin{bmatrix} \frac{1}{\Lambda_1} \int_S \Psi_1(\mathbf{r}_s) \Phi_1(\mathbf{r}_s) dS & \dots & \frac{1}{\Lambda_1} \int_S \Psi_n(\mathbf{r}_s) \Phi_1(\mathbf{r}_s) dS \\ \frac{1}{\Lambda_p} \int_S \Psi_n(\mathbf{r}_s) \Phi_p(\mathbf{r}_s) dS & \dots & \frac{1}{\Lambda_p} \int_S \Psi_n(\mathbf{r}_s) \Phi_p(\mathbf{r}_s) dS \end{bmatrix}_{p \times n}$$

$$A_{15} = \begin{bmatrix} -\omega_1^2 & 0 & 0 \\ 0 & \cdot & 0 \\ 0 & 0 & -\omega_p^2 \end{bmatrix}$$

$$A_{16} = \begin{bmatrix} -2\zeta_1\omega_1 & 0 & 0 \\ 0 & \cdot & 0 \\ 0 & 0 & -2\zeta_p\omega_p \end{bmatrix}$$

$$B_2 = \begin{bmatrix} \frac{\rho c^2}{V} \Psi_1(\mathbf{r}_0) \\ \cdot \\ \frac{\rho c^2}{V} \Psi_n(\mathbf{r}_0) \end{bmatrix}_{n \times 1}$$

In general, the coupled eigenvalues are different than the individual rigid wall eigenvalues and the *in vacuo* structural eigenvalues. The characteristic frequencies corresponding to the acoustic modes will shift away from those found assuming that the walls of the enclosure are rigid. How great this shift is depends on the degree of coupling between the structure and the enclosed fluid, and is discussed in Chapter 3. The coupled modes will be either fluid dominated or structure dominated, depending on whether the majority of the energy of the mode resides in the fluid or in the structure.



(a) Collocated

(b) Non-collocated

(Dashed line is actual frequency response)

Figure 4.15 Comparison of Experiment to Coupled Model Acoustic Frequency Response

The coupled modeling approach was used to generate the frequency responses shown in Fig. 4.15 for collocated and non-collocated source and response locations.

The viscous damping values associated with each of the acoustic modes was set at .01. The viscous damping values associated with each of the structural modes was set at .1, based on experimental measurements of a plexiglass plate. The other parameters used

to determine the *in vacuo* structural modes of the enclosure are presented below.

Young's Modulus, $E = 3.73e9 \text{ N/m}^2$

Poisson's ratio, $\nu = .3$

density, $\rho_m = 1150 \text{ kg/m}^3$

wall thickness, $h = .00635 \text{ m}$

The frequency responses obtained with the coupled modeling approach do not match the experimental frequency responses, primarily due to the fact that the calculated structural modes do not match the actual structural modes accurately. The structural modes were found assuming that each of the enclosure walls was simply supported. It was known that these were not the actual structural boundary conditions, but the calculations were performed in order to obtain a representative coupled model frequency response. The peaks corresponding to the acoustic resonant frequencies generated with the coupled model shifted 1 to 2 Hz from those given by the rigid wall model. This shift was not enough for the modeled peak frequencies to match those of the actual response.

The relatively small peaks which are seen below 100 Hz in the actual frequency response appear in the frequency response generated with the coupled modeling approach, although they are at different frequencies, due to the inaccurate boundary conditions that were assumed when calculating the structural modes of the enclosure walls. If the *in vacuo* structural modes of the enclosure were more accurately modeled, then the peaks corresponding to the fluid loaded structural modes should match those found experimentally. This task is left for future work.

Chapter 5. Conclusions and Future Work

The simulation of an active acoustic control system, specifically a feedback control system, requires an accurate model of the dynamics of the system to be controlled. The stability of the system can be evaluated by obtaining the gain and phase margins from a frequency response plot, or by examining a pole-zero plot. The work presented in this thesis was motivated by the need for an accurate modeling approach for the acoustic response in a non-rigid-wall enclosure. The acoustic response in any enclosure is determined by the boundary conditions at the interior surface of the enclosure walls, and the types of sources present. The analyses presented in this thesis assumed that the sources were either at the surface of the enclosure, or interior to the enclosure walls.

Three different analytical modeling approaches were investigated and presented in this thesis paper for the acoustic response in a rectangular enclosure. A reference model assumed that the walls of the enclosure were rigid, corresponding to an infinite acoustic impedance boundary condition. The pressure response was expressed in terms of the characteristic rigid-wall acoustic modes of the enclosure. The second modeling approach used a finite acoustic impedance boundary condition to model the influence of non-rigid walls on the acoustic response. The resultant acoustic eigenvalues which were found are complex. The pressure was again expressed in terms of these characteristic modes. The third modeling approach treated the vibration of the enclosure walls as additional sources which were constructed from the *in vacuo* structural modes of the enclosure. The pressure is expressed in terms of the rigid-wall acoustic modes. The frequency responses

generated using these three models were compared to the actual acoustic frequency response obtained experimentally for a non-rigid wall, plexiglass enclosure.

5.1 Assessment of Acoustic Models

An assessment is presented in this section regarding the accuracy of the acoustic frequency responses generated using each of the modeling approaches investigated in this thesis. All of the modeling approaches presented in this thesis are based on modal summations. The number of modes used in the summation has a very strong influence on the zero locations of the simulated frequency response functions. As more modes are used in the modal summation, the zeros of the predicted frequency response approach those of the actual response, but the computational requirements increase. As the response and source locations approach a collocated case, the number of modes needed to accurately predict the acoustic response can be in the thousands. The number of modes used in the predicted frequency responses was limited to 100, in order to decrease the required amount of computational time. This effected the accuracy of the responses generated by the models. Specific parameters related to the accuracy of each individual acoustic model are discussed below.

5.1.1 Rigid-wall Model

As anticipated, the rigid-wall model did not produce a frequency response that accurately represented the actual frequency response found experimentally. This was due

to the fact that there was no mechanism to account for the influence of the flexibility of the walls on the acoustic response. The peaks of the simulated frequency response corresponding to the acoustic resonances of the enclosure were at frequencies which were less than those of the actual response. This indicated that a model which accounted for the effects of non-rigid walls on the acoustic response in an enclosure was needed.

5.1.2 Finite Acoustic Impedance Model

The finite impedance modeling approach produced an acoustic frequency response that best matched the actual frequency response for a non-rigid wall enclosure. The peak frequencies of the predicted acoustic frequency response could be made to match those of the experimental response by calculating the necessary modal impedance values. Additional accuracy in the simulated response may be obtained with further refinement of the impedance values corresponding to the higher order modes. There is no mechanism in this modeling approach to produce the acoustic peaks which correspond to the structural resonances of the enclosure.

5.1.3 Coupled Model

The frequency response generated using the coupled modeling approach did not match the experimental frequency response, due to the inaccuracy of the *in vacuo* structural modes that were calculated assuming simply supported boundary conditions. The frequency response peaks corresponding to the characteristic acoustic modes of the enclosure did show a shift from the rigid-wall values, but it was not significant. If a more

accurate model for the structural modes of the enclosure were used, then the accuracy of the predicted acoustic frequency response would increase. This would be achieved by modeling the structural boundary conditions more accurately.

5.2 Future Work

The intent of this work was to provide a single document presenting different analytical modeling approaches for the acoustic response in a non-rigid-wall enclosure. A feedback controller design can be used to add damping to the acoustic resonances of an enclosure in order to reduce the overall sound pressure level in the enclosure due to an acoustic source disturbance. An analysis of the stability of the controller design should be performed. Before this can be accomplished the models presented in this thesis must be further investigated. A more accurate analysis of the structural vibration of the enclosure should be performed. This may include developing a finite element model of the enclosure structure. Additional modeling approaches for the acoustic response in a non-rigid-wall enclosure may be investigated, such as a complete structural-acoustic finite element model analysis.

The finite impedance model, as it was developed in this thesis, assumed that the acoustic impedance increased linearly with frequency for each acoustic mode. This assumption should be validated with experimental data. Laser velocimetry could be a means to obtain the structural response of the enclosure, which could be used in

conjunction with a sensor microphone to obtain experimental values for the acoustic impedance at the wall surfaces.

Accurate analytical models for the transducer dynamics associated with both the source loudspeaker and the sensor microphone used in the actual controller design should be developed. In addition, a distributed source may be used to model the source loudspeaker instead of a point source. These could be incorporated into the model of the controlled acoustic system.

Bibliography

Articles

Alves, G.S., Shoureshi, R., Knurek, T., Novotony, D., and Ogundipe, L., "Feedback Control Techniques for Active Noise Control," ASME Paper 95-WA/NCA-14.

Balas, M.J., "Active Control of Flexible Systems," *Journal of Optimization Theory and Application*, Vol. 25, No. 3, July 1978.

Balas, M.J., "Direct Velocity Feedback Control of Large Space Structures," *Journal of Guidance and Control*, Vol. 2, No. 3, May/June 1979.

Batta, G.R. and Shoureshi, R., "Three-Dimensional Active Noise Control Using a Direct Feedback Approach," American Control Conference, Vol. 3, 1990.

Bleazey, J.C., "Electronic Sound Absorber," *Journal of the Audio Engineering Society*, April 1962, Vol. 10, No. 2.

Boone, M. M. and Janssen, G., "Modal Superposition in the Time Domain: Theory and Experimental Results," *Journal of the Acoustic Society of America* 97(1), January 1995.

Bullmore, A.J., Nelson, P.A., Curtis, A.R.D., and Elliott, S.J. "The Active Minimization of Harmonic Enclosed Sound Fields, Part II: A Computer Simulation", *Journal of Sound and Vibration* (1987), 117(1), pp. 15-33.

Chaplin, B., "Anti-noise -- The Essex Breakthrough," *Chartered Mechanical Engineer*, 30 1983.

Clark, R.L. and Cole, D.G., "Active Damping of Enclosed Sound Fields Through Direct Rate Feedback Control," *Journal of the Acoustical Society of America* 97(3), March 1995.

Costin, M.H. and Elzinga, D.R., "Active Reduction of Low-Frequency Tire Impact Noise Using Digital Feedback Control," *IEEE Control Systems Magazine*, August 1989.

Curtis, A.R.D., Nelson, P.A., Elliott, S.J. and Bullmore, A.J., "The Active Suppression of Acoustic Resonance," *Journal of the Acoustic Society of America* 81(3), March 1987.

Dohner, J.L. and Shoureshi, R., "A Method for Active Noise Control Using a Source-Point Model," *Journal of the Acoustic Society of America* 86(3), September 1989 I.

Dohner, J.L. and Shoureshi, R., "Modal Control of Acoustic Plants," Transactions of the ASME, Vol. 111, July 1989 II.

Dowell, E.H., "Reverberation Time, Absorption, and Impedance," *Journal of the Acoustic Society of America* 64(1), July 1978.

Dowell, E.H., Gorman III, G.F., and Smith D.A., "Acoustoelasticity: General Theory, Acoustic Natural Modes and Forced Response to Sinusoidal Excitation, Including Comparisons With Experiment," *Journal of Sound and Vibration* (1977) 52(4), pp. 519-542.

Dowling, E.M. and Turi, J., "On Some Practical Aspects of Single Sensor Active Noise Control," Proceedings of the IEEE Conference on Decision and Control, Vol. 1, 1995.

Elliott, S.J., Curtis, A.R.D., Bullmore, A.J., and Nelson, P.A., "The Active Minimization of Harmonic Enclosed Sound Fields, Part III: Experimental Verification", *Journal of Sound and Vibration* (1987), 117(1), pp. 35-58.

Elliott, S.J., Stothers, I.M., Nelson, P.A., McDonald, A.M., Quinn, D.C., and Saunders, T., "The Active Control of Engine Noise Inside Cars," *Inter-Noise* 88, pp. 987-990.

Elliott, S.J. and Nelson, P.A., "The Active Control of Sound," *Electronics & Communication Engineering Journal*, August 1990.

Elliott, S.J., Joseph, P., Nelson, P.A. and Johnson, M.E., "Power Output Minimization and Power Absorption in the Active Control of Sound," *Journal of the Acoustical Society of America* 90(5), November 1991.

Elliott, S.J., "Active Control of Structure-Borne Noise," *Journal of Sound and Vibration* (1994) 177(5), pp. 651-673.

Eriksson, L.J., "Recent Trends in The Development of Active Sound and Vibration Control Systems," *Noise-Con* 94, pp. 271-278.

Fuller, C.R. and von Flotow, A.H., "Active Control of Sound and Vibration," *IEEE Control Systems*, December 1995.

Guicking, D. and Rollwage, M., "Active Systems in Room Acoustics - Solved and Unsolved Problems," *Inter-Noise* 84, pp. 457-462.

Guicking, D., Karcher, K. and Rollwage, M., "Active Control of the Acoustic Reflection Coefficient at Low Frequencies," *Inter-Noise* 83, pp. 419-422.

Hong, J., Akers, J.C., Venugopal, R., Miin-Nan, L., Sparks, A.G., Washabaugh, P.D., and Bernstein, D.S., "Modeling, Identification, and Feedback Control of Noise in an Acoustic Duct," *IEEE Transactions on Control Systems Technology*, Vol. 4, No. 3, May 1996.

Hull, A.J., Radcliffe, C.J. and Southward, S.C., "Global Active Noise Control of a One-Dimensional Acoustic Duct Using a Feedback Controller," ASME Paper 91-WA-DSC-10.

Jie, P. and Bies, D. A., "An Experimental Investigation Into the Interaction Between a Sound Field and its Boundaries," *Journal of the Acoustical Society of America* 83(4), April 1988.

Johnson, M.E. and Elliott, S.J., "Measurement of Acoustic Power in the Active Control of Sound," *Journal of the Acoustical Society of America* 93(3), March 1993.

Joseph, P., Elliott, S.J. and Nelson, P.A., "Near Field Zones of Quiet," *Journal of Sound and Vibration* (1994 I) 172(5), pp. 605-627.

Joseph, P., Elliott, S.J. and Nelson, P.A., "Statistical Aspects of Active Control in Harmonic Enclosed Sound Fields," *Journal of Sound and Vibration* (1994 II) 172(5), pp. 629-655.

Leitch, R.R. and Tokhi, M.O., "Active Noise Control Systems," IEE Proceedings, Vol. 134, Pt. A, No. 6, June 1987.

Lueg, P., "Process of Silencing Sound Oscillations", U.S. Patent No. 2,043,416, 1936.

Morse, P.M., "Some Aspects of the Theory of Room Acoustics," *Journal of the Acoustical Society of America*, Vol. 11, July 1939.

Nelson, P.A., Curtis, A.R.D., Elliott, S.J. and Bullmore, A.J., "The Minimum Power Output of Free Field Point Sources and the Active Control of Sound," *Journal of Sound and Vibration* (1987 I) 116(3), pp. 397-414.

Nelson, P.A., Hammond, J.K., Joseph, P. and Elliott, S.J., "Active Control of Stationary Random Sound Fields," *Journal of the Acoustic Society of America* 87(3), March 1990.

Nelson, P.A., Hammond, J.K. and Elliott, S.J., "Analytical Approaches to the Active Control of Stationary Random Enclosed Sound Fields," *Inter-Noise* 88, pp. 959-962.

Nelson, P.A., Curtis, A.R.D., Elliott, S.J. and Bullmore, A.J., "The Active Minimization of Harmonic Enclosed Sound Fields, Part I: Theory", *Journal of Sound and Vibration* (1987 II), 117(1), pp. 1-13.

Olson, H.F. and May, E. G., "Electronic Sound Absorber," *Journal of the Acoustical Society of America*, Vol. 25, No. 6, November 1953.

Olson, H.F., "Electronic Control of Noise, Vibration, and Reverberation," *Journal of the Acoustical Society of America*, Vol. 28, Number 5, 1956.

Ross, C.F., "A Demonstration of Active Control of Broadband Sound," *Journal of Sound and Vibration* (1981) 74(3), pp. 411-417.

Ross, C.F., "An Algorithm for Designing a Broadband Active Sound Control System," *Journal of Sound and Vibration* (1982 I) 80(3), pp. 373-380.

Ross, C.F., "An Adaptive Digital Filter for Broadband Active Sound Control," *Journal of Sound and Vibration* (1982 II) 80(3), pp. 381-388.

Short, W.R., "Global Low Frequency Active Noise Attenuation," *Inter-Noise 80*, pp. 695-698.

Schroeder, M.R., "Frequency-Correlation Functions of Frequency Responses in Rooms," *Journal of the Acoustical Society of America*, Vol. 34, No. 12, December 1962.

Small, R.H., "Direct-Radiator Loudspeaker System Analysis," *Journal of the Audio Engineering Society*, Vol. 20, No. 5, June 1972.

Swinbanks, M.A., "The Active Control of Sound Propagation in Long Ducts," *Journal of Sound and Vibration* (1973) 27(3), pp. 411-436.

Tichy, J., "Achievements and Tasks for Active Noise Control," *Noise-Con 94*, pp. 309-314.

Tohyama, M. and Suzuki, A., "Active Power Minimization of a Sound Source in a Closed Space," *Journal of Sound and Vibration* (1987) 119(3), pp. 562-564.

Warnaka, G.E., "Active Attenuation of Noise -- The State of the Art," *Noise Control Engineering*, May/June 1982.

Wu, Z., Varadan, V.K. and Varadan, V.V., "Active Absorption of Acoustic Waves Using State-Space Model and Optimal Control Theory," *Journal of the Acoustical Society of America* 97(2), February 1995.

Yang, X.H., Niekerk, J.V., Parwani, K.S., Packard, A. and Tongue, B., "Attenuation of Structurally Generated Interior Noise Through Active Control," *Proceedings of the American Control Conference*, June 1993 WA1-9:15.

Textbooks

Beranek, L. and Ver, I.L., Noise and Vibration Control Engineering, John Wiley & Sons, Inc., New York, 1992.

Kuttruff, H., Room Acoustics, Elsevier Science Publishers Ltd., New York, 1991.

Fahy, F., Sound and Structural Vibration, Academic Press, Inc., Orlando, FL. 1985.

Morse, P.M., Vibration and Sound, McGraw-Hill Book Company, Inc, New York, 1936.

Morse, P.M. and Ingard, K.U., Theoretical Acoustics, McGraw-Hill Book Company, Inc., New York, 1968.

Nelson, P.A. and Elliott, S.J., Active Control of Sound, Academic Press, Inc., San Diego, CA. 1993.

Pierce, A.D., Acoustics, Acoustical Society of America, New York, 1989.

Appendix A. Experimental Enclosure Characteristics

This appendix includes plots of experimentally obtained open-loop frequency response functions for the enclosure discussed in Chapter 4. All speaker and microphone locations are numbered as shown in figures A.1-A.6. The plots are labeled according to this numbering system. A 6 “ loudspeaker was located flush against the enclosure wall, while a microphone protruded 2 inches into the enclosure. A microphone location specified as ‘c’ means that the microphone was located directly in front of the speaker. For each speaker and microphone combination, four plots are shown. These include the frequency response function relating pressure in Pascals to input voltage to the speaker, wrapped phase, unwrapped phase, and coherence. These plots were generated from data which was taken relating microphone output voltage to the input voltage to the amplifier. The amplifier frequency response, shown as Figure A.7, was divided out in order to get the frequency response relating output voltage from the microphone to input voltage to the speaker. A calibration factor was then used in order to convert the microphone voltage to pressure in Pascals. All plots are for the frequency range 0 to 800 Hz.

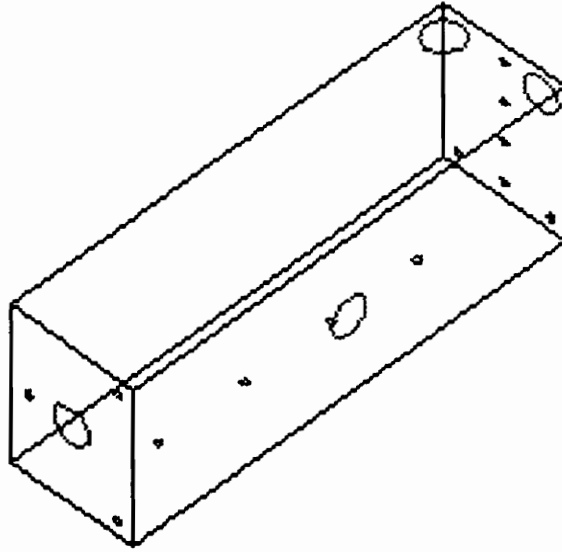


Figure A.1 Enclosure (Note: Holes Sealed When Not in Use)

Left End

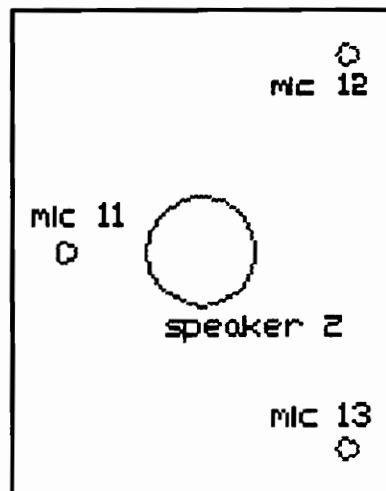


Figure A.2 Left End of Enclosure

Right End

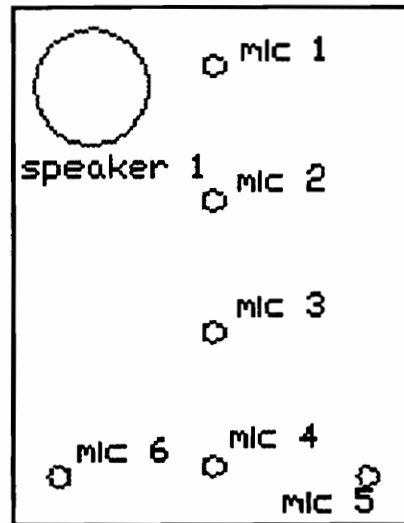


Figure A.3 Right End of Enclosure

Front

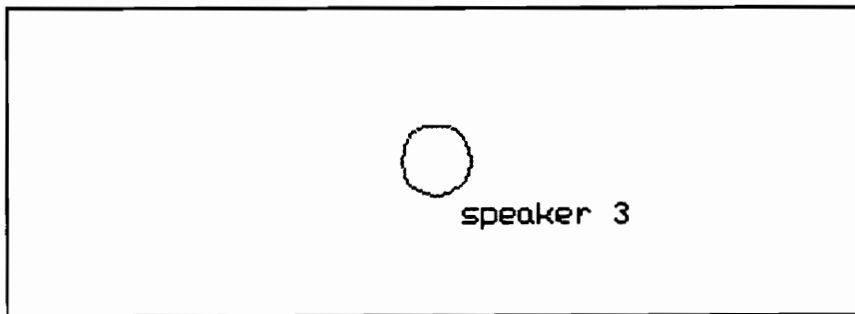


Figure A.4 Front of Enclosure

Top

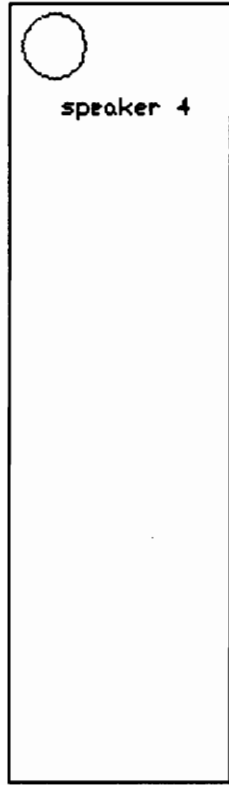


Figure A.5 Top of enclosure

Bottom

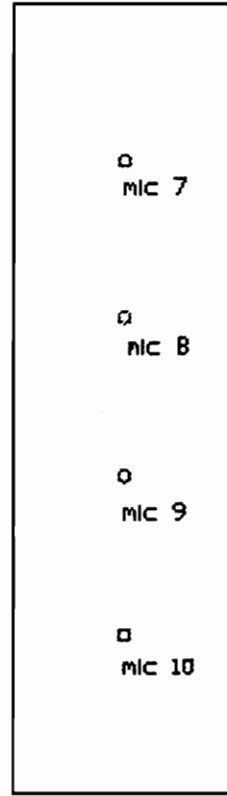


Figure A.6 Bottom of Enclosure

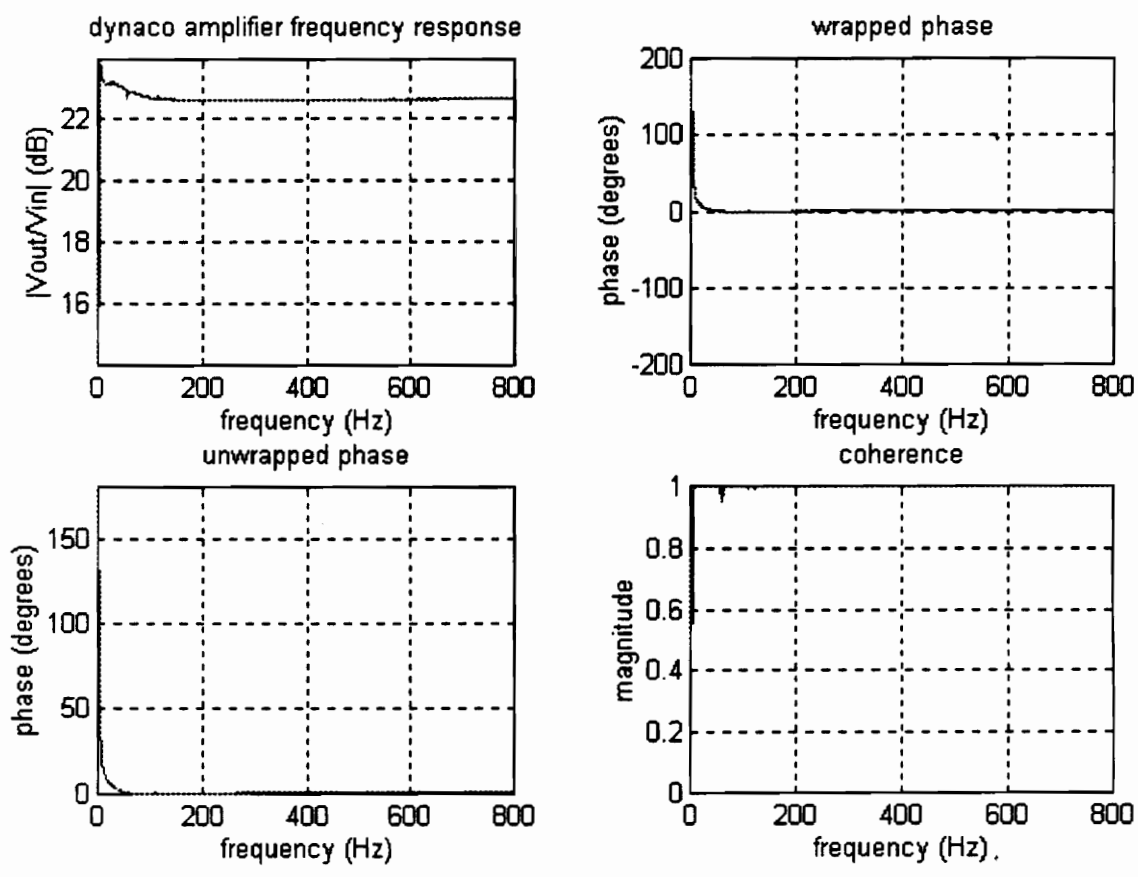


Figure A.7 Dynaco Amplifier Frequency Response

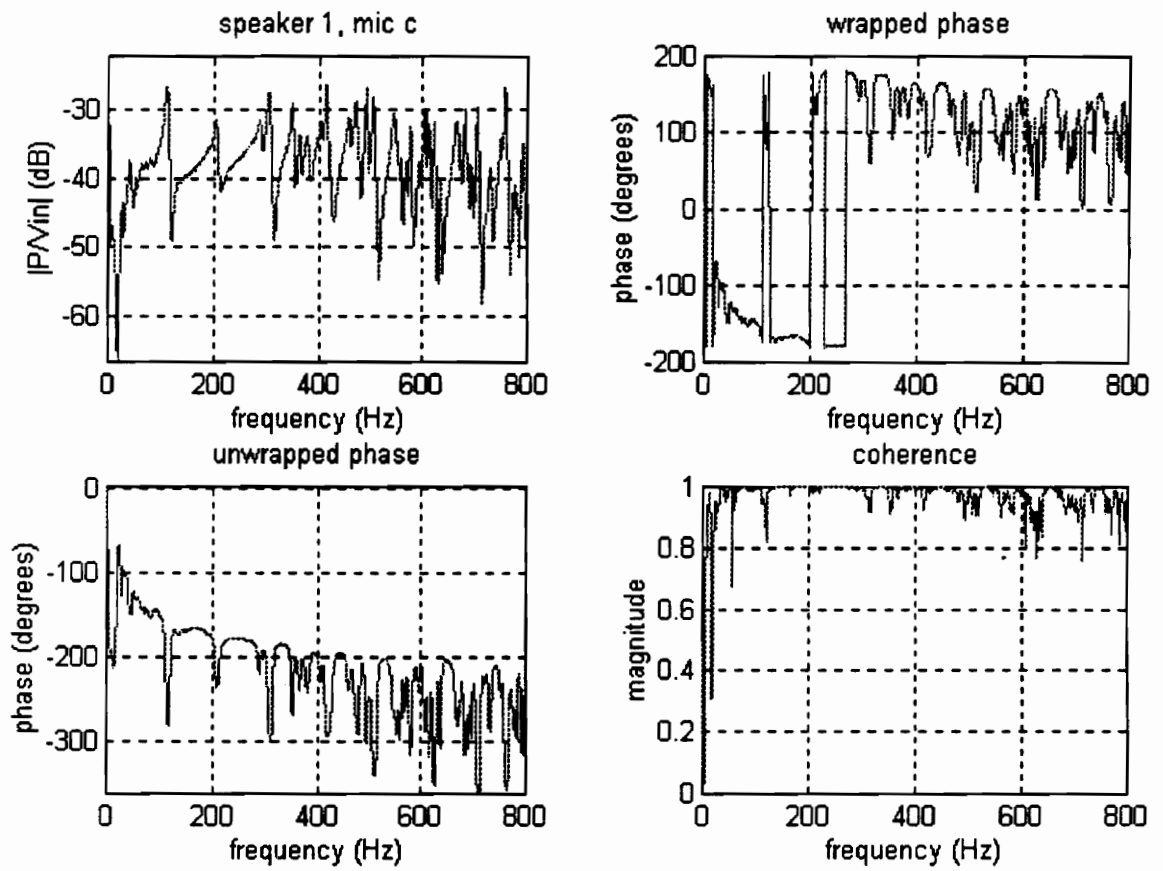


Figure A.8 Speaker 1, Collocated Microphone

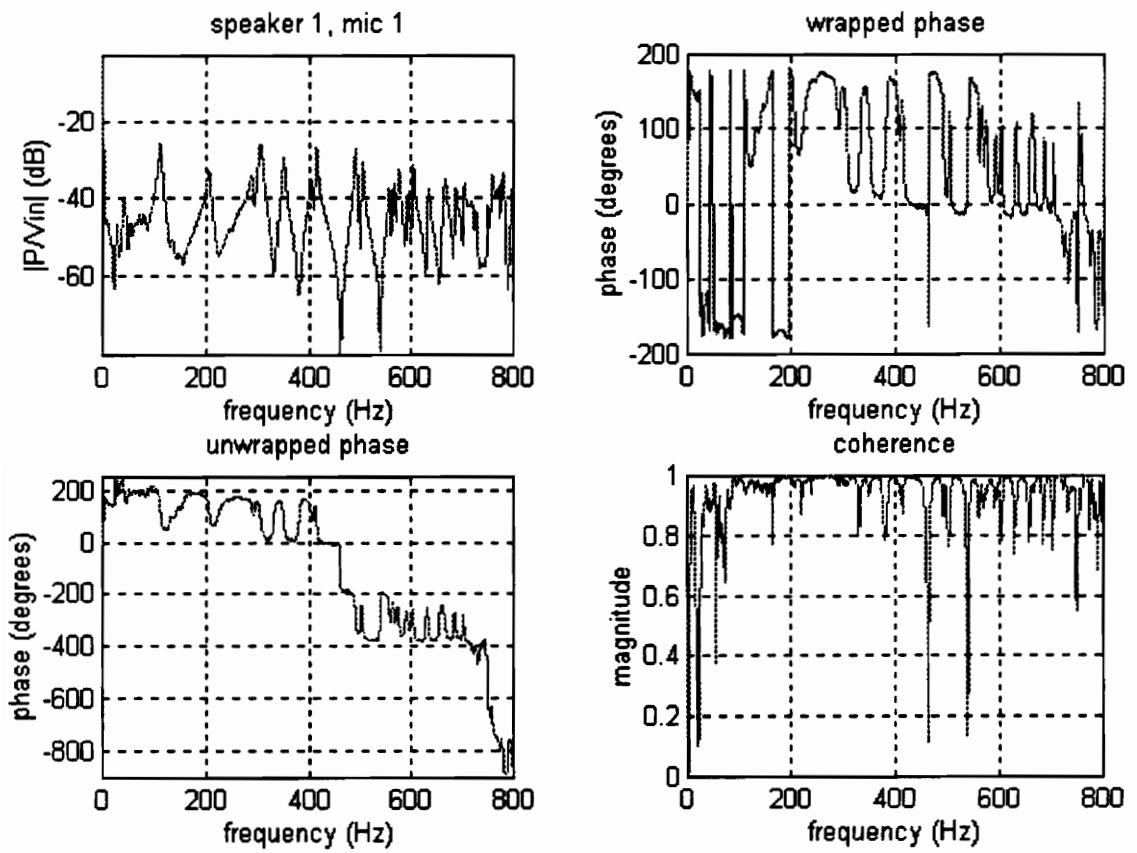


Figure A.9 Speaker 1, Microphone 1

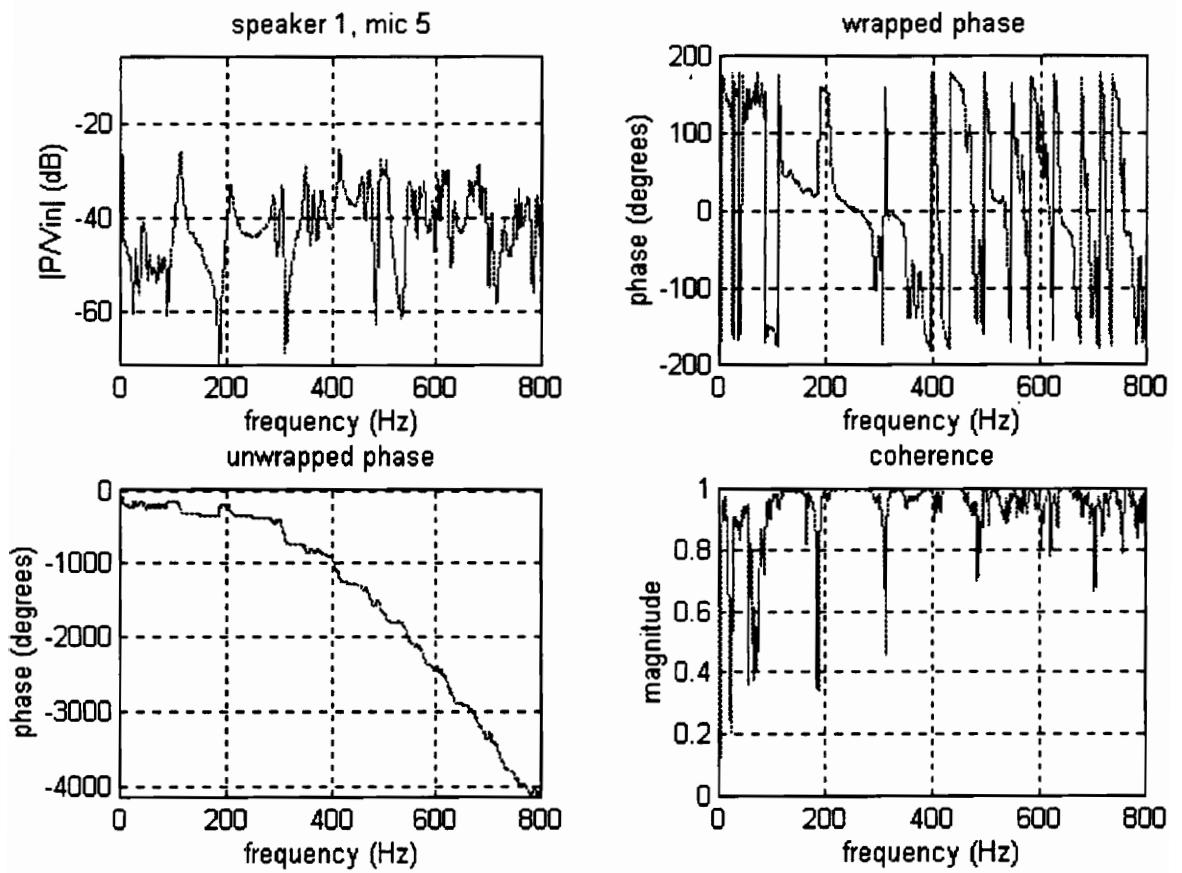


Figure A.10 Speaker 1, Microphone 5

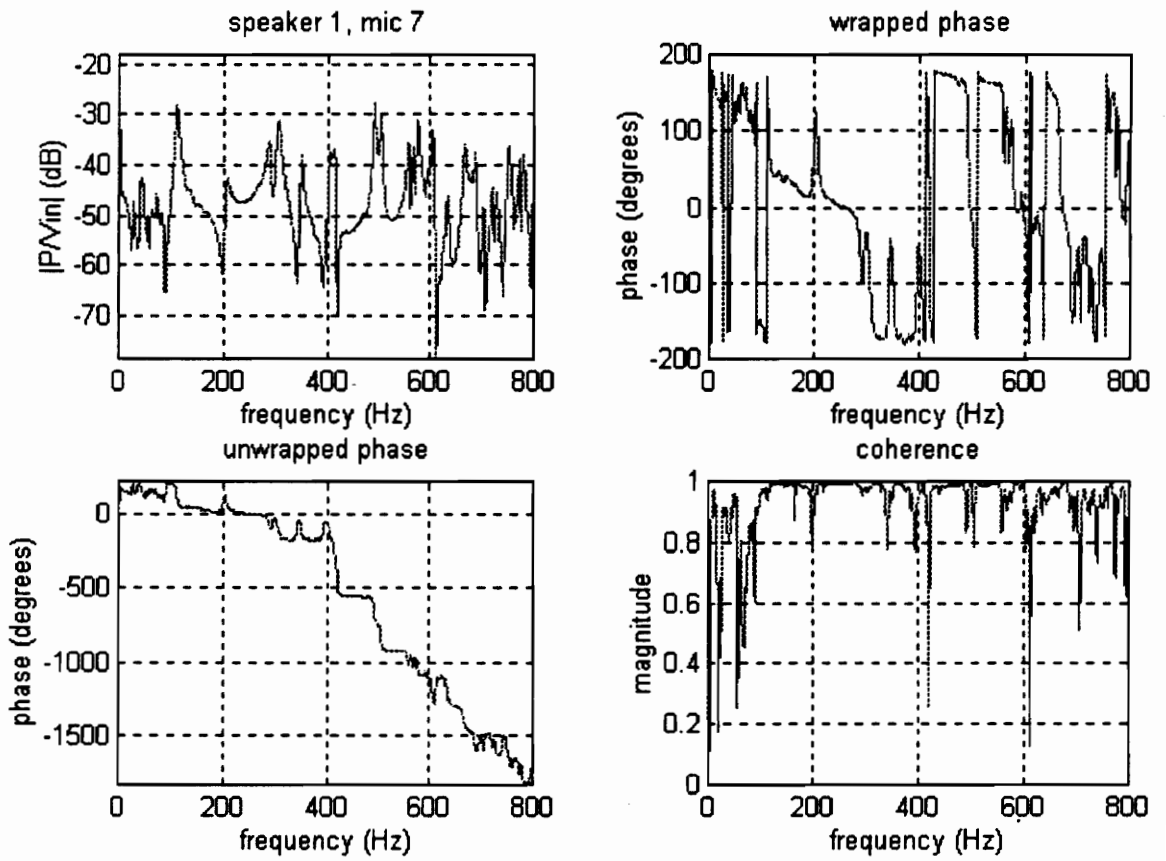


Figure A.11 Speaker 1, Microphone 7

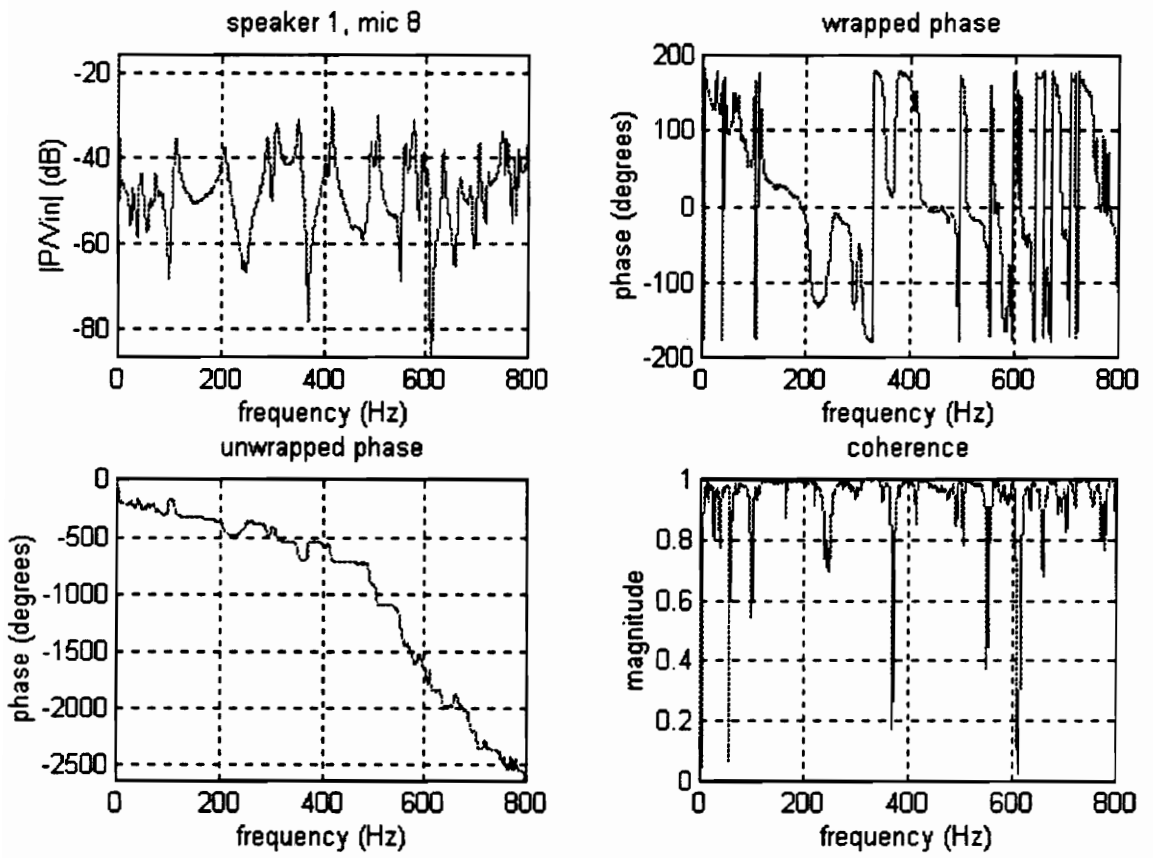


Figure A.12 Speaker 1, Microphone 8

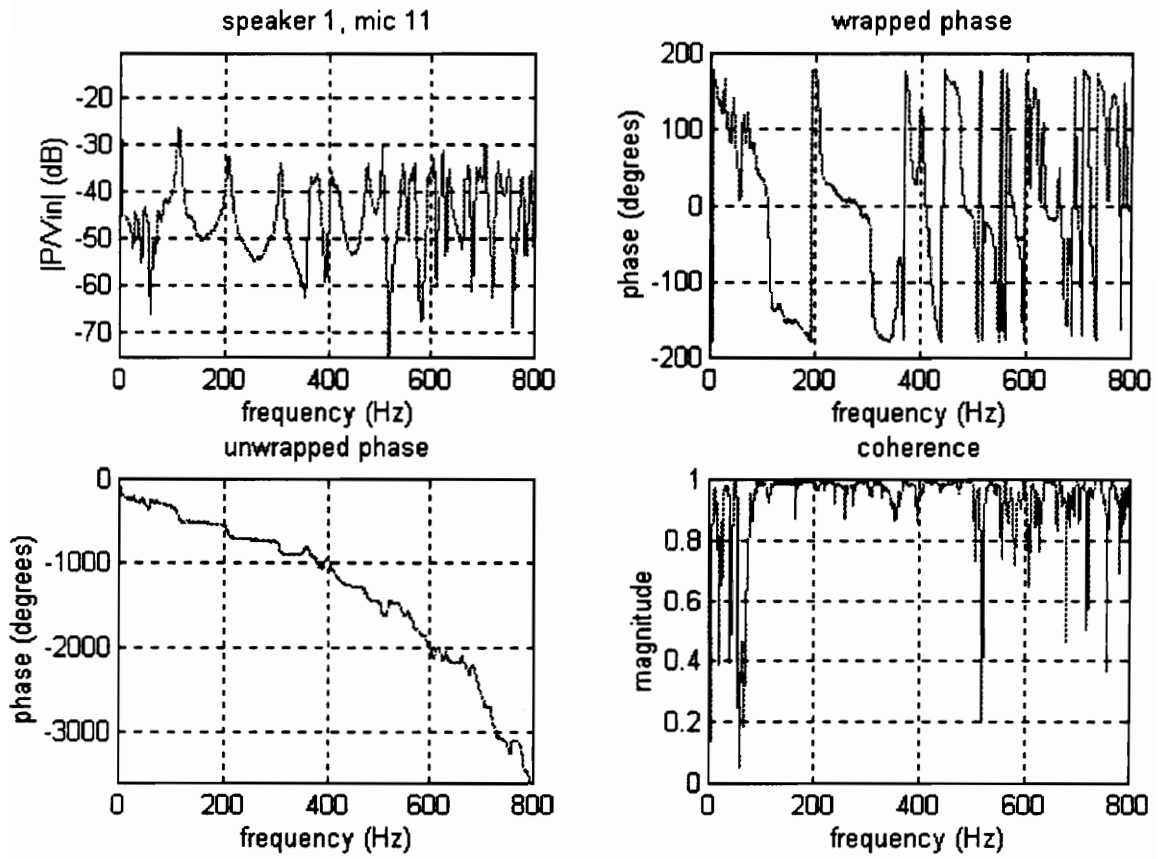


Figure A.13 Speaker 1, Microphone 11

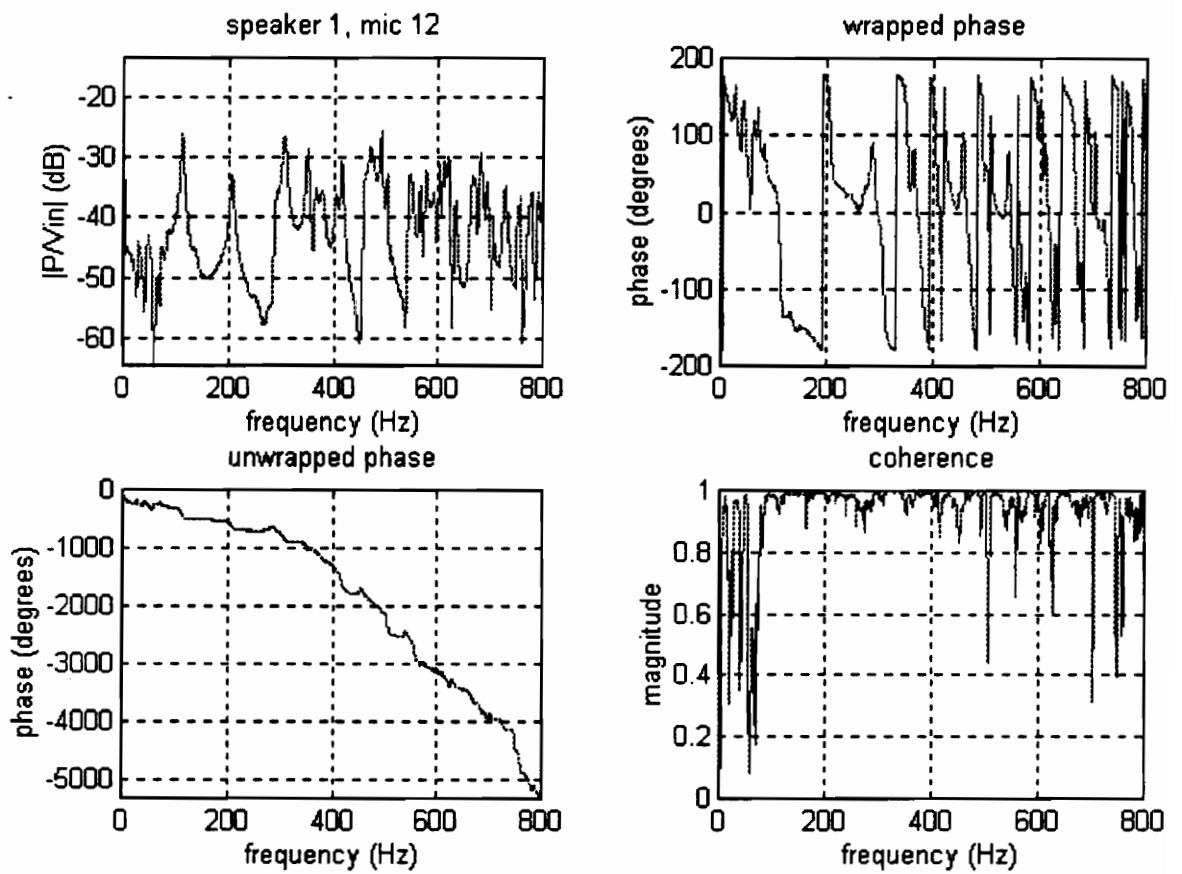


Figure A.14 Speaker 1, Microphone 12

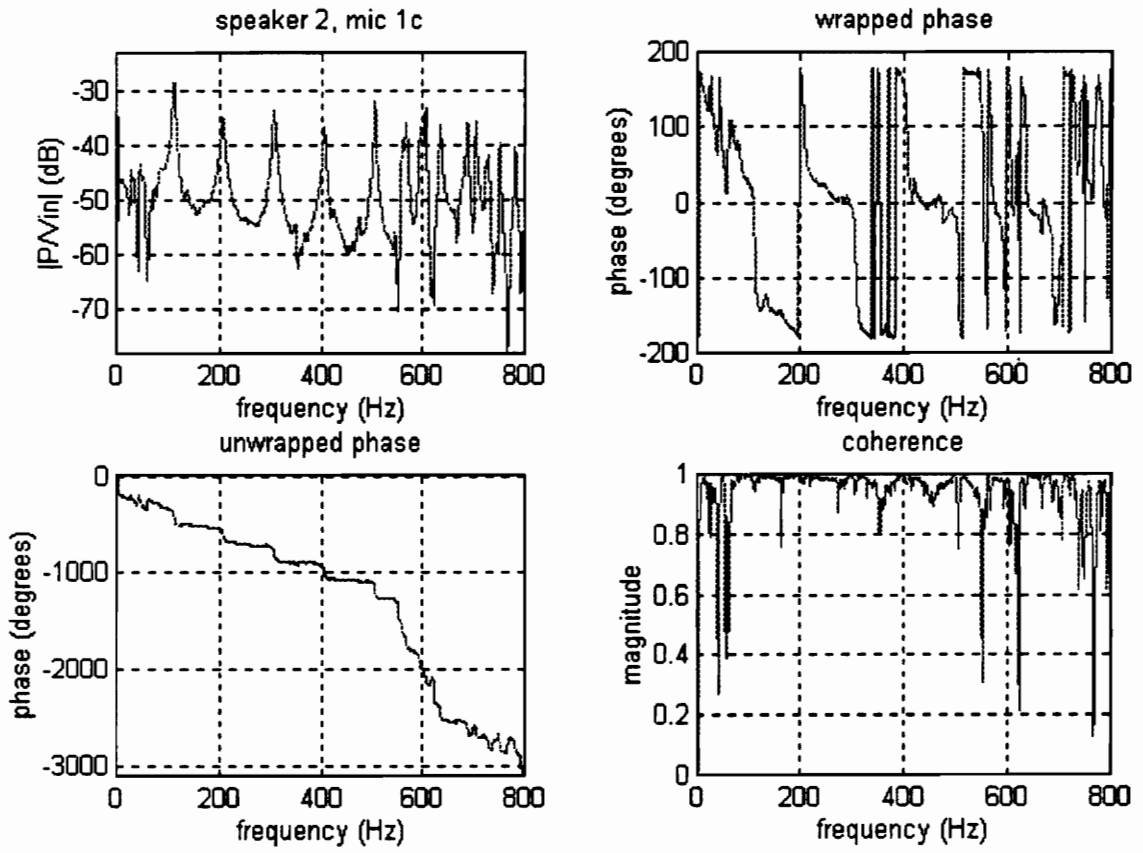


Figure A.15 Speaker 2, Microphone Collocated With Speaker 1

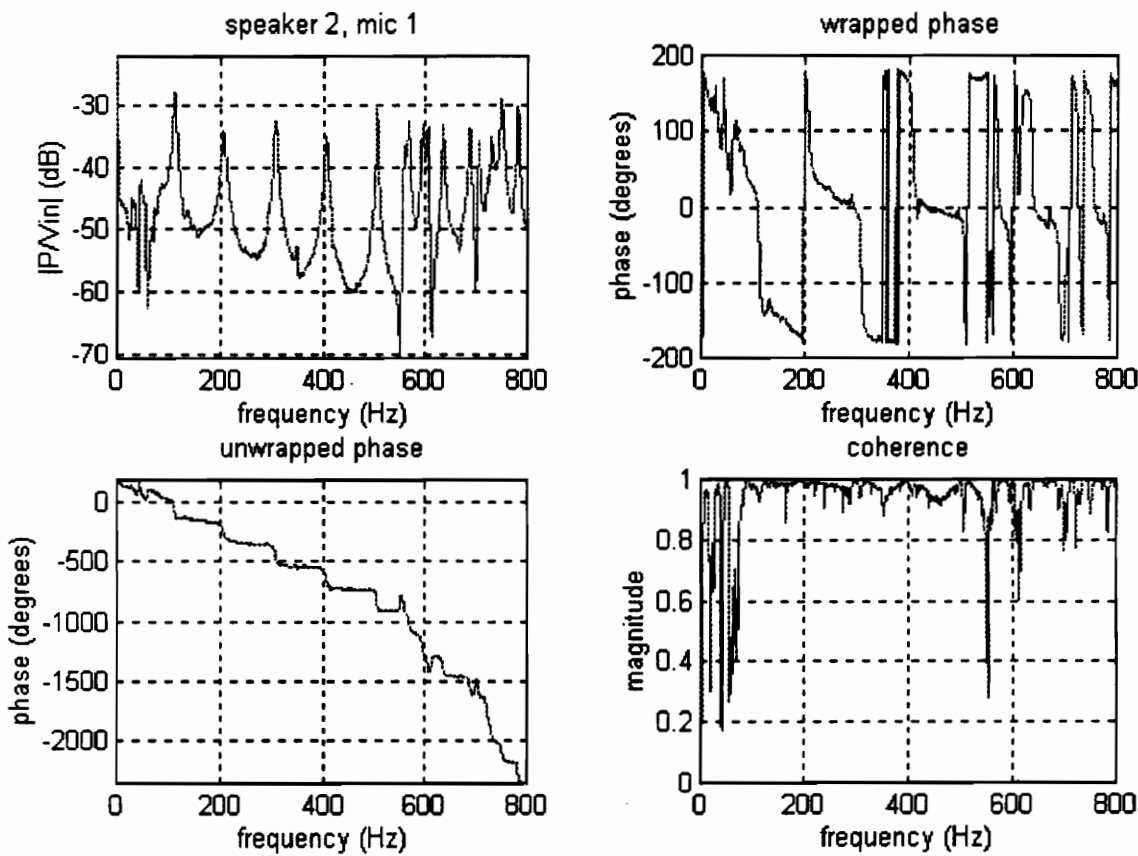


Figure A.16 Speaker 2, Microphone 1

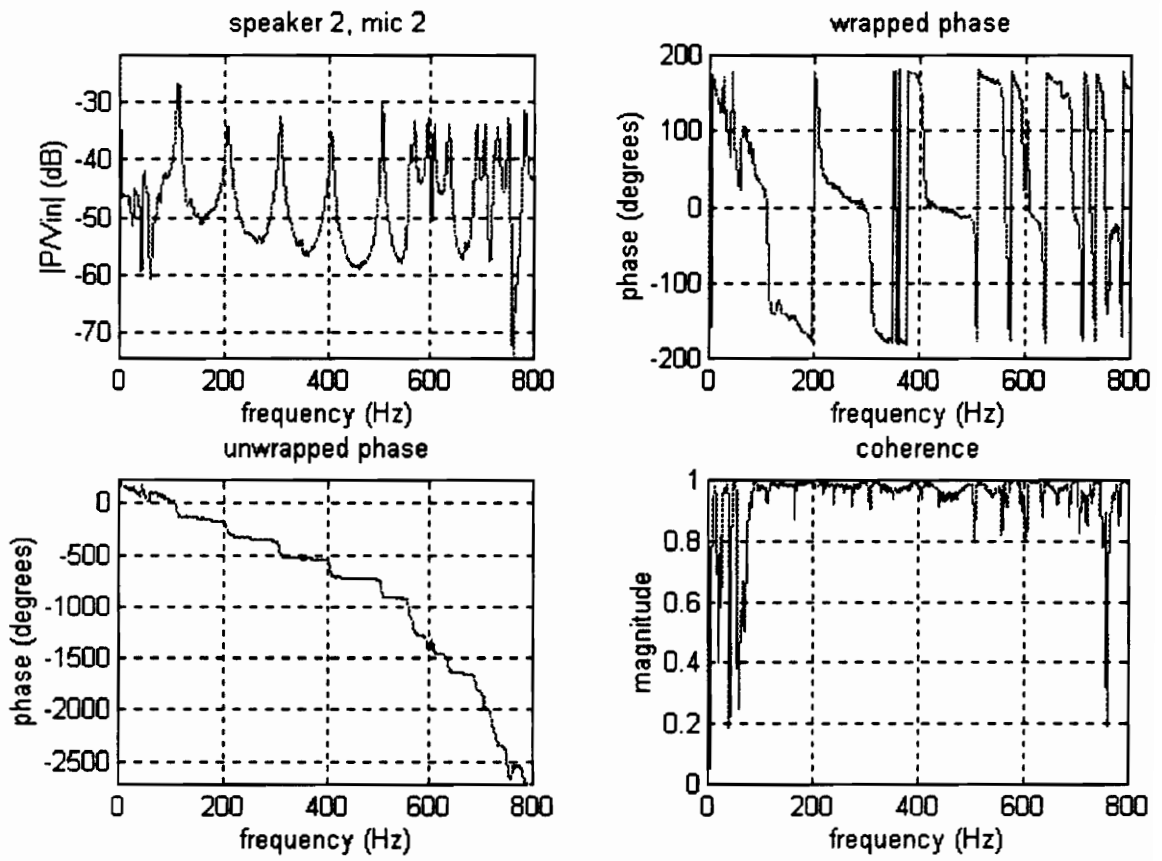


Figure A.17 Speaker 2, Microphone 2

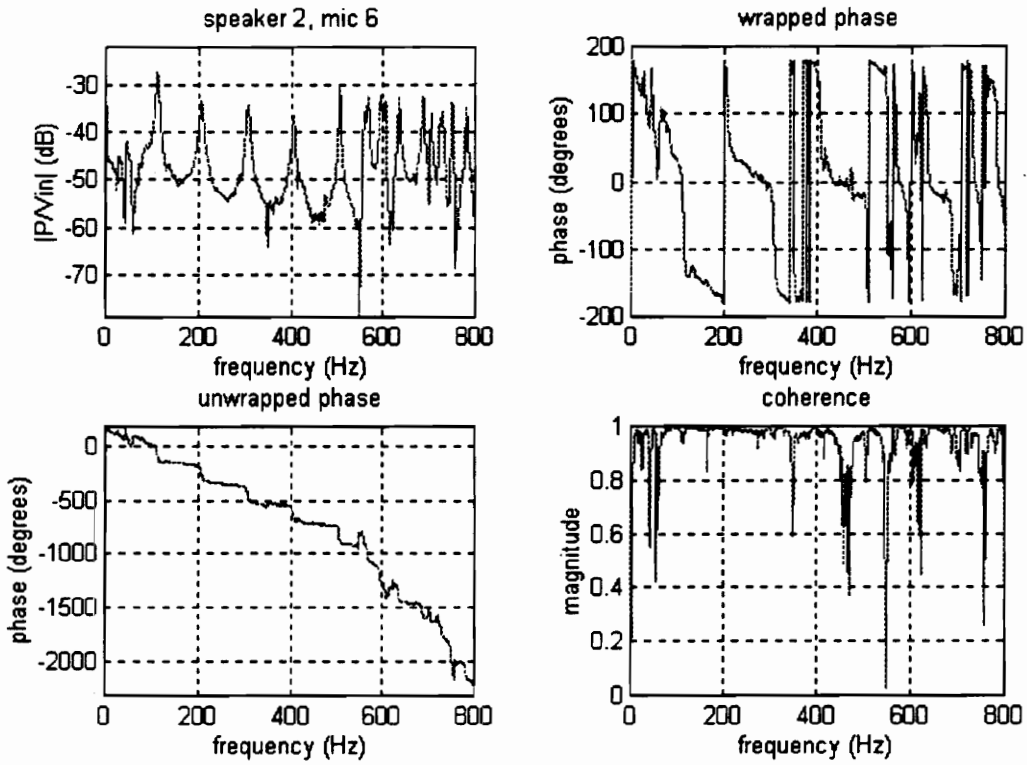


Figure A.18 Speaker 2, Microphone 6

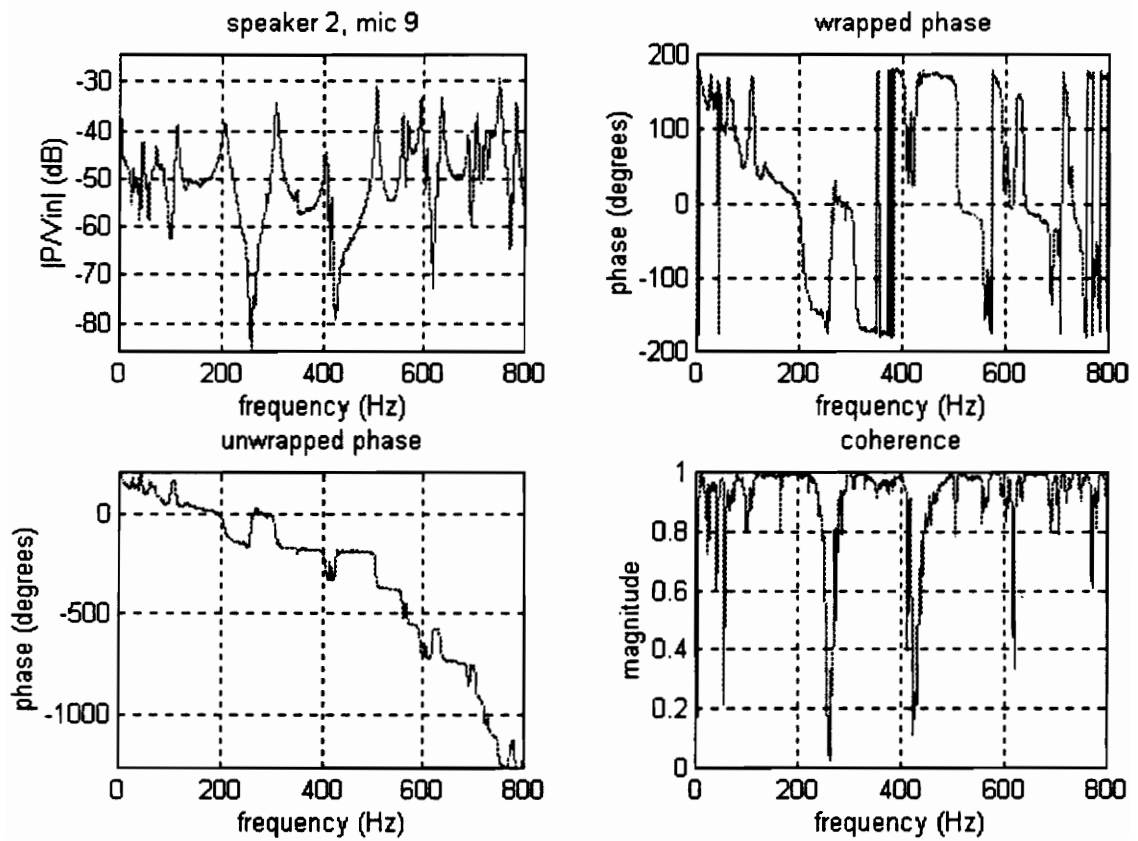


Figure A.19 Speaker 2, Microphone 9

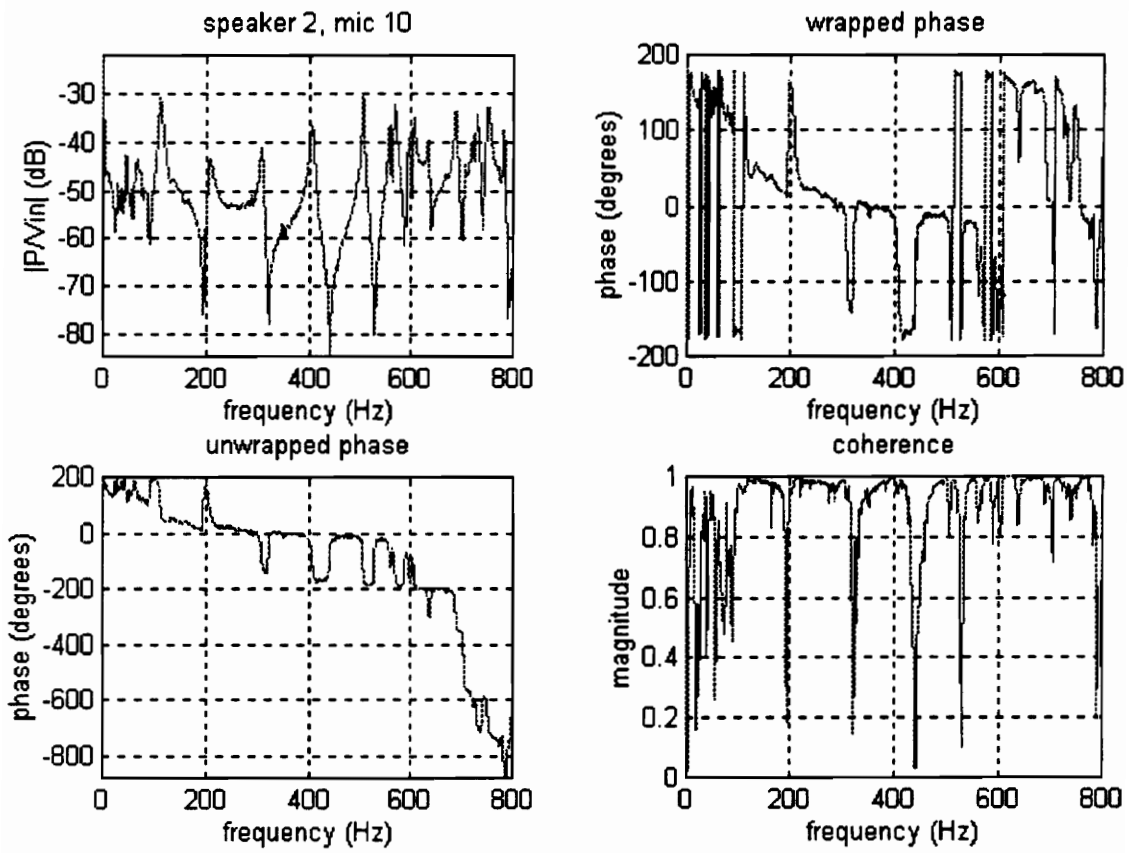


Figure A.20 Speaker 2, Microphone 10

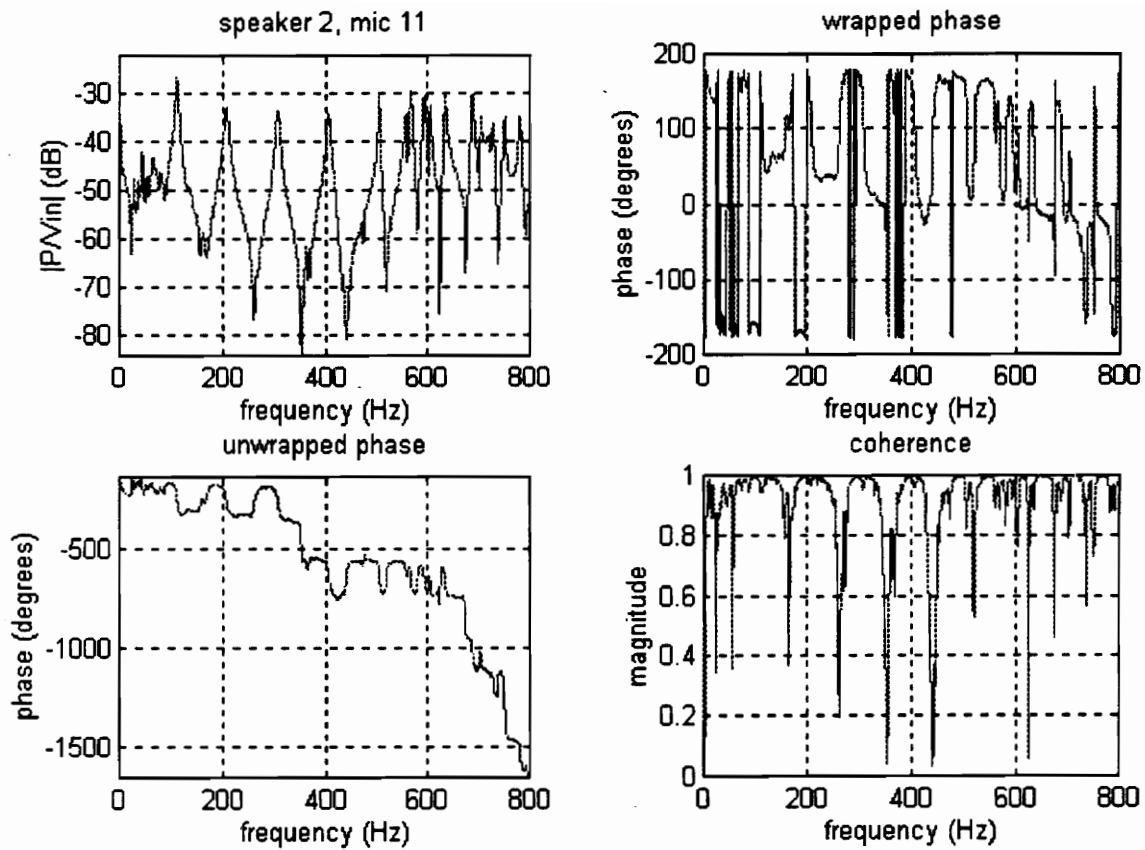


Figure A.21 Speaker 2, Microphone 11

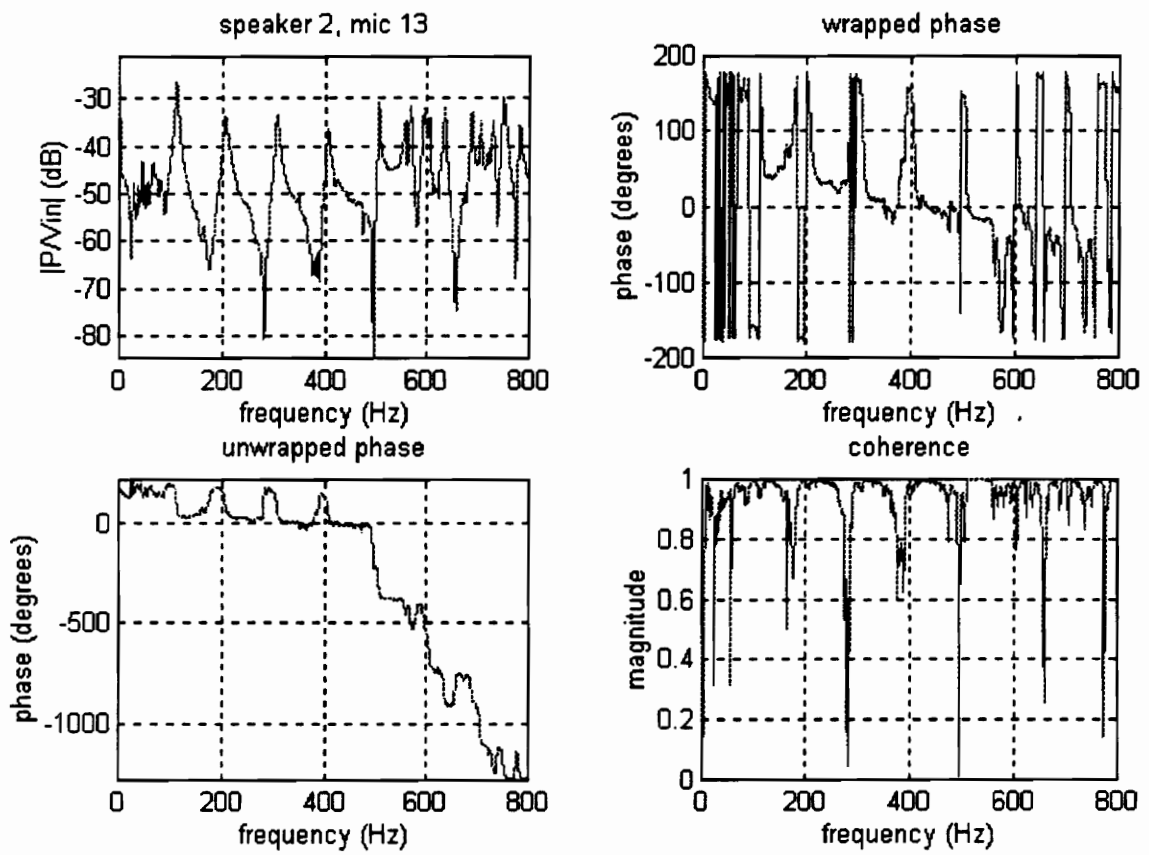


Figure A.22 Speaker 2, Microphone 13

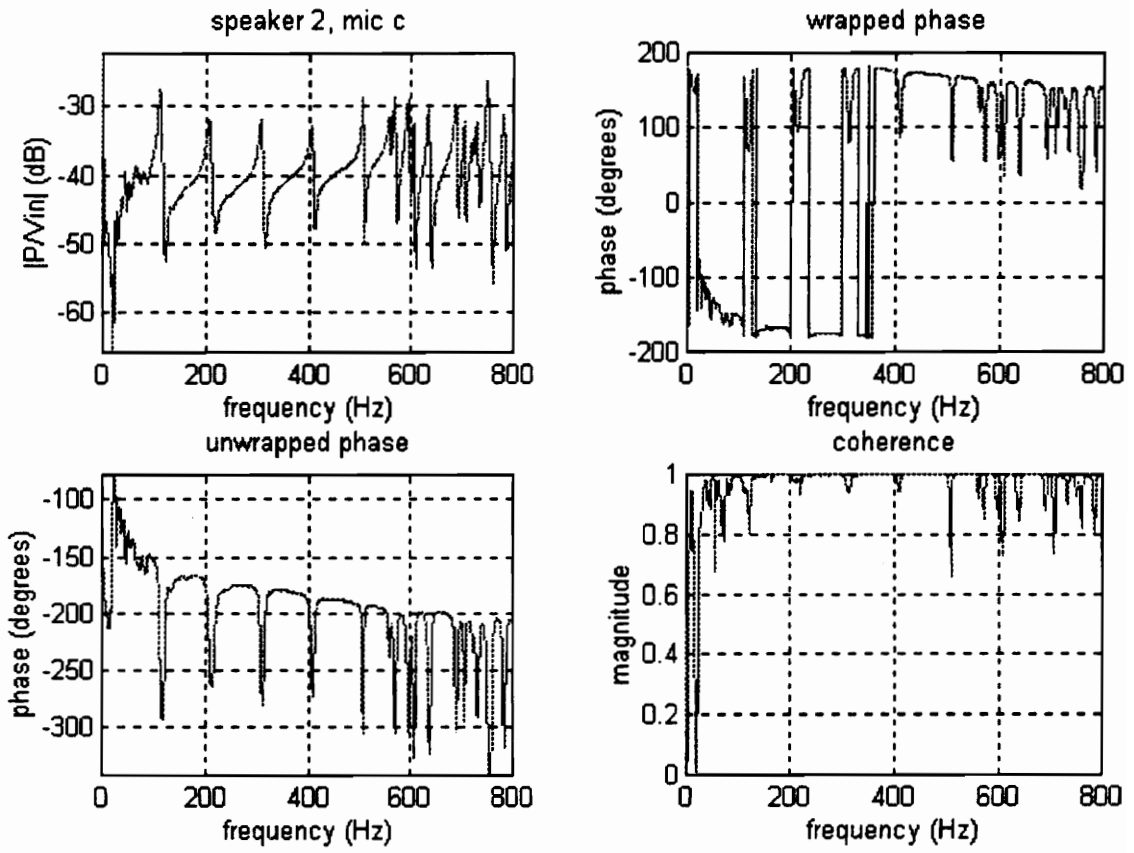


Figure A.23 Speaker 2, Microphone Collocated

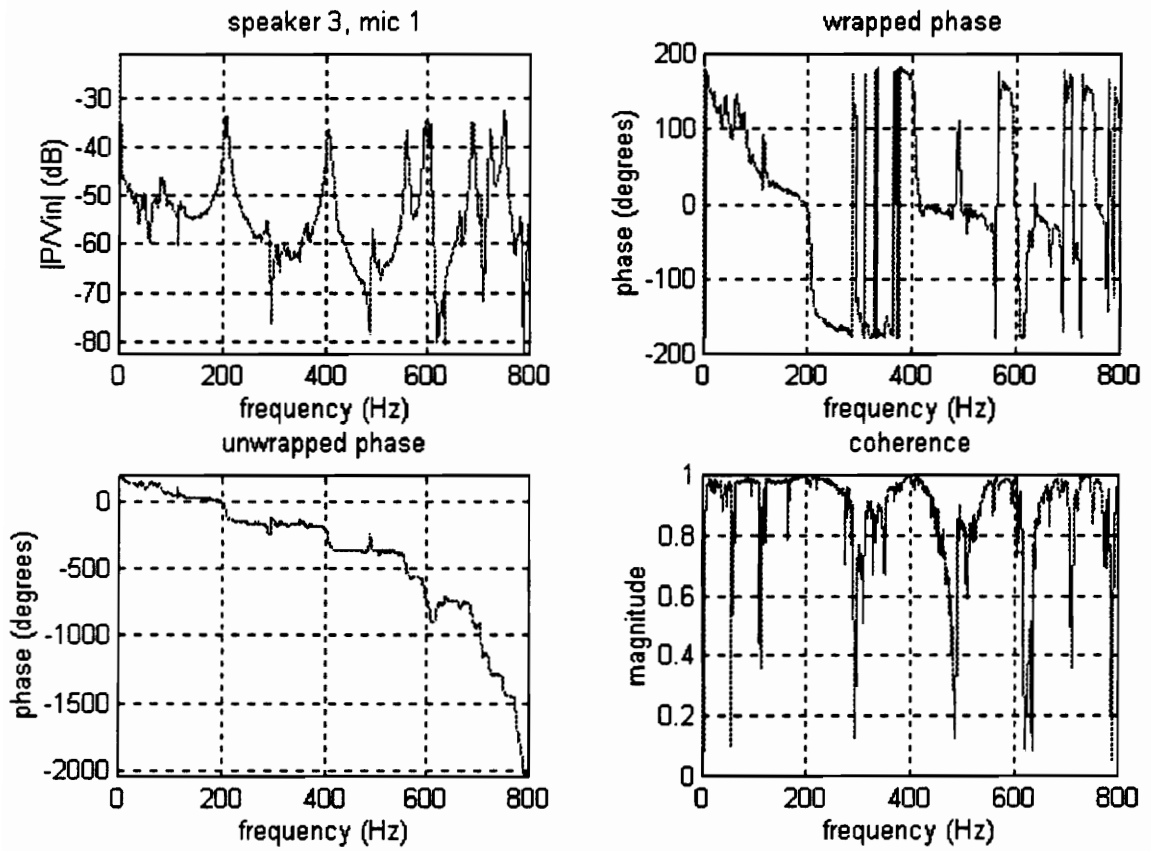


Figure A.24 Speaker 3, Microphone 1

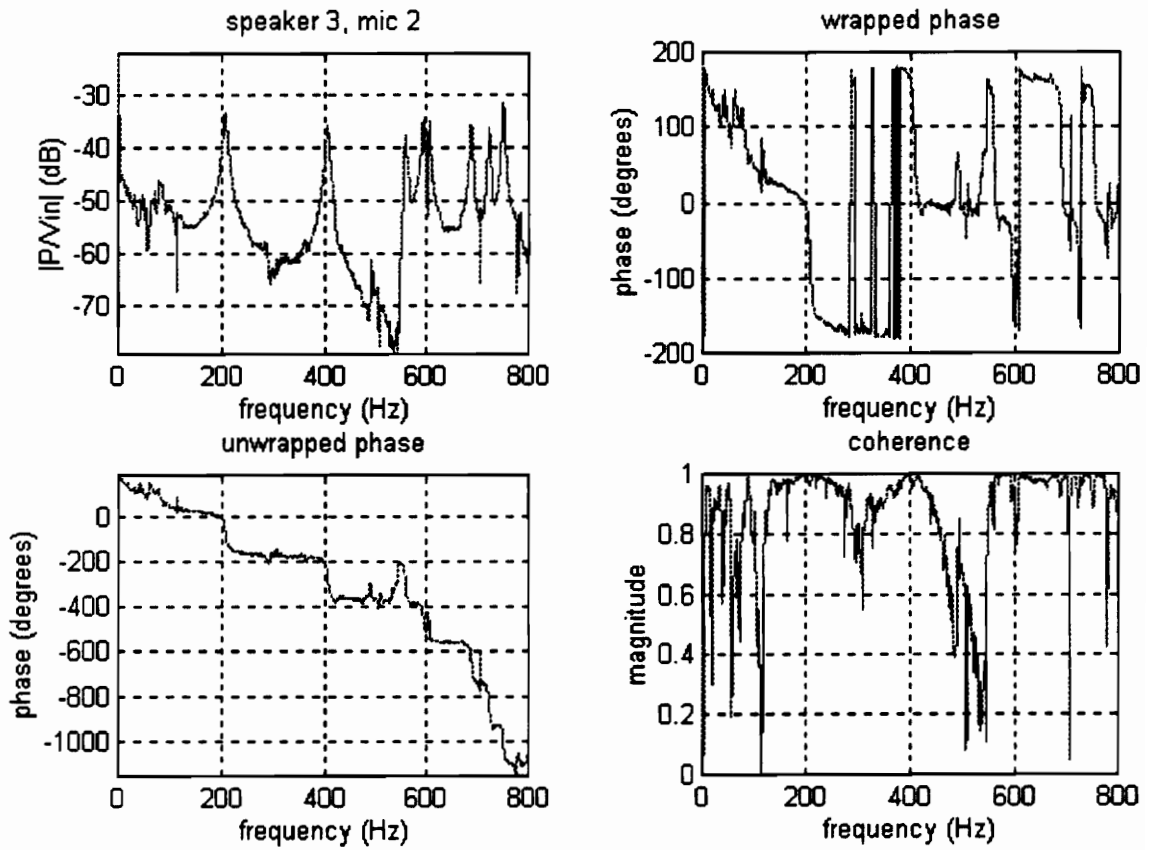


Figure A.25 Speaker 3, Microphone 2

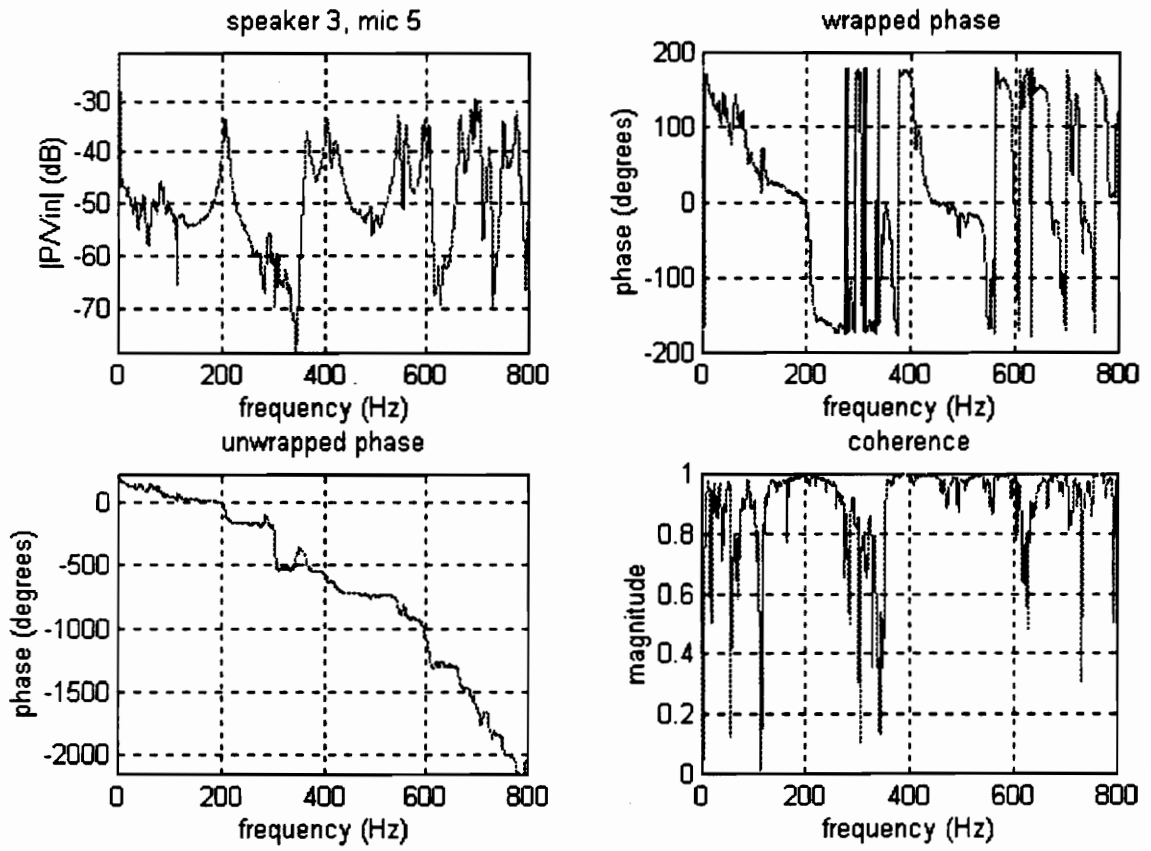


Figure A.26 Speaker 3, Microphone 5

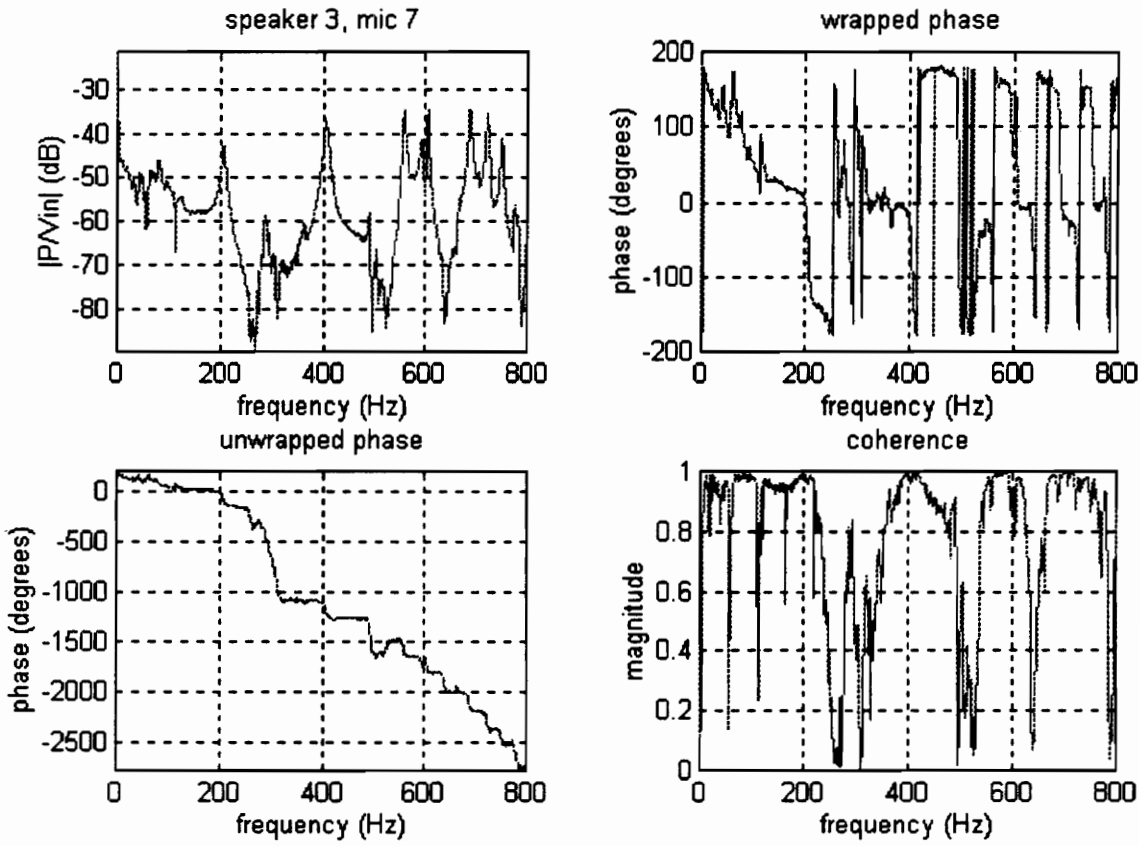


Figure A.27 Speaker 3, Microphone 7

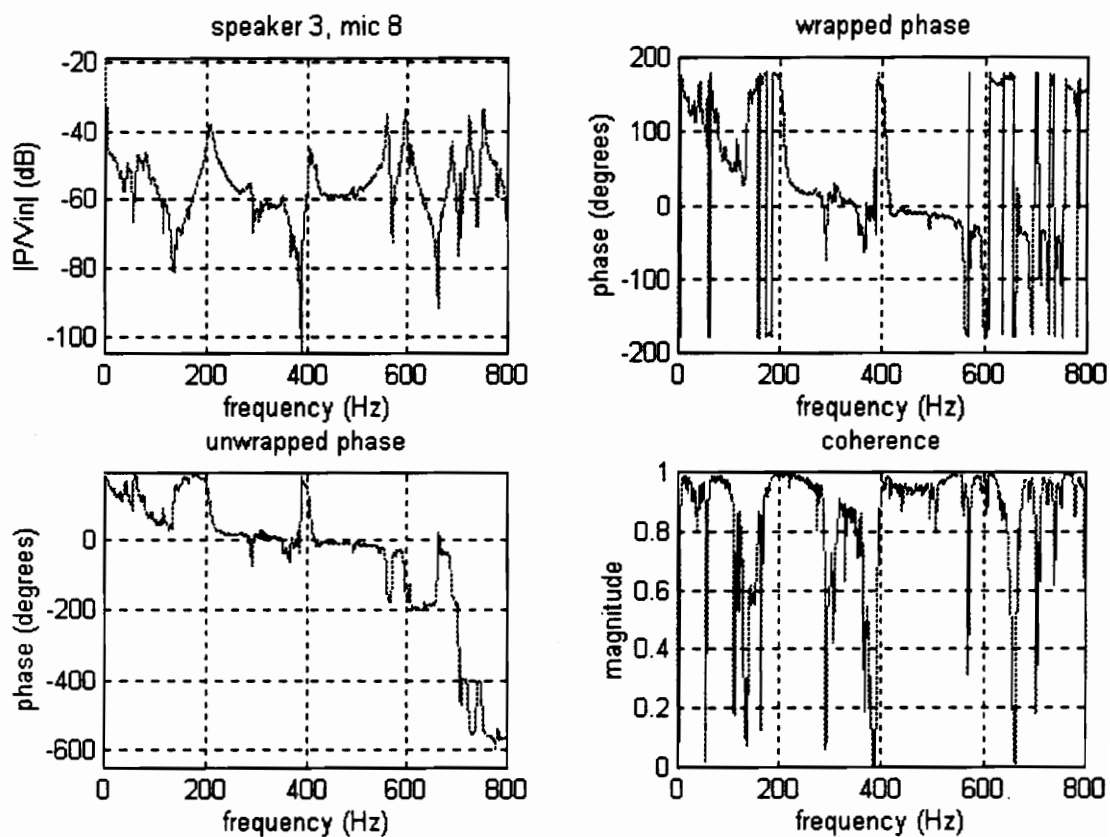


Figure A.28 Speaker 3, Microphone 8

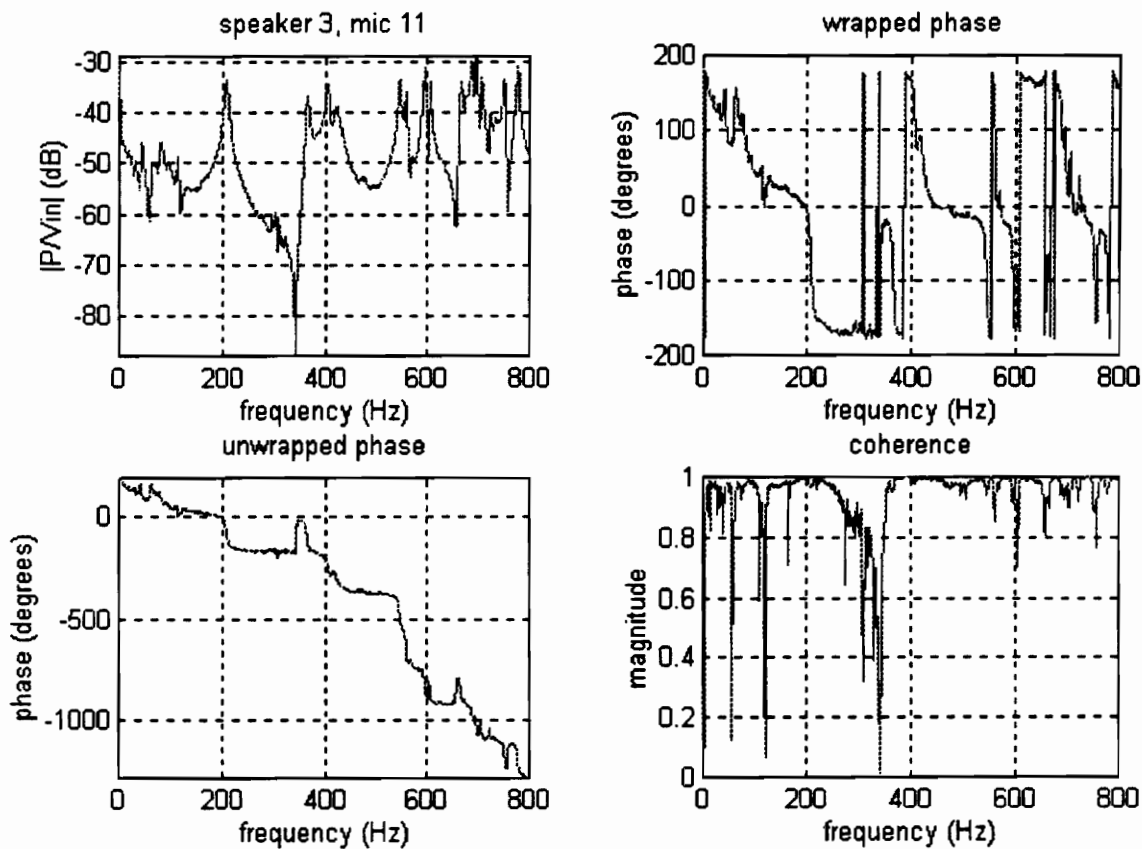


Figure A.29 Speaker 3, Microphone 11

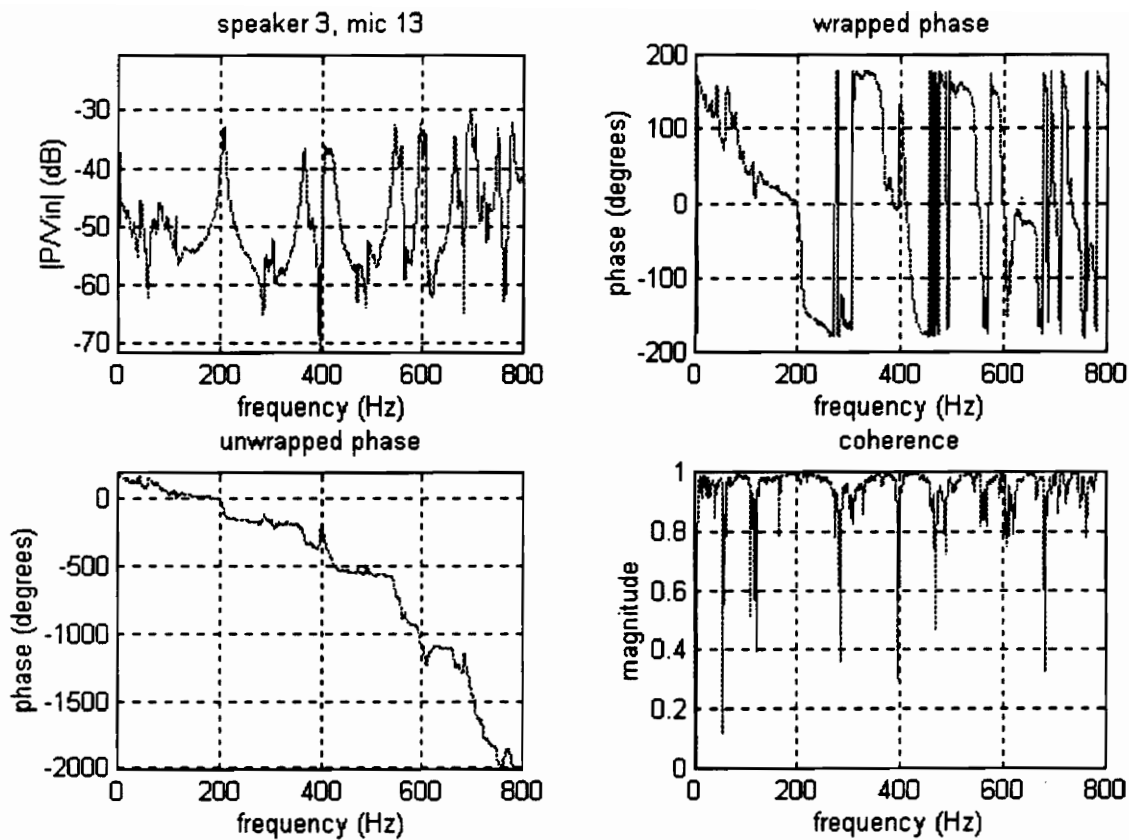


Figure A.30 Speaker 3, Microphone 13

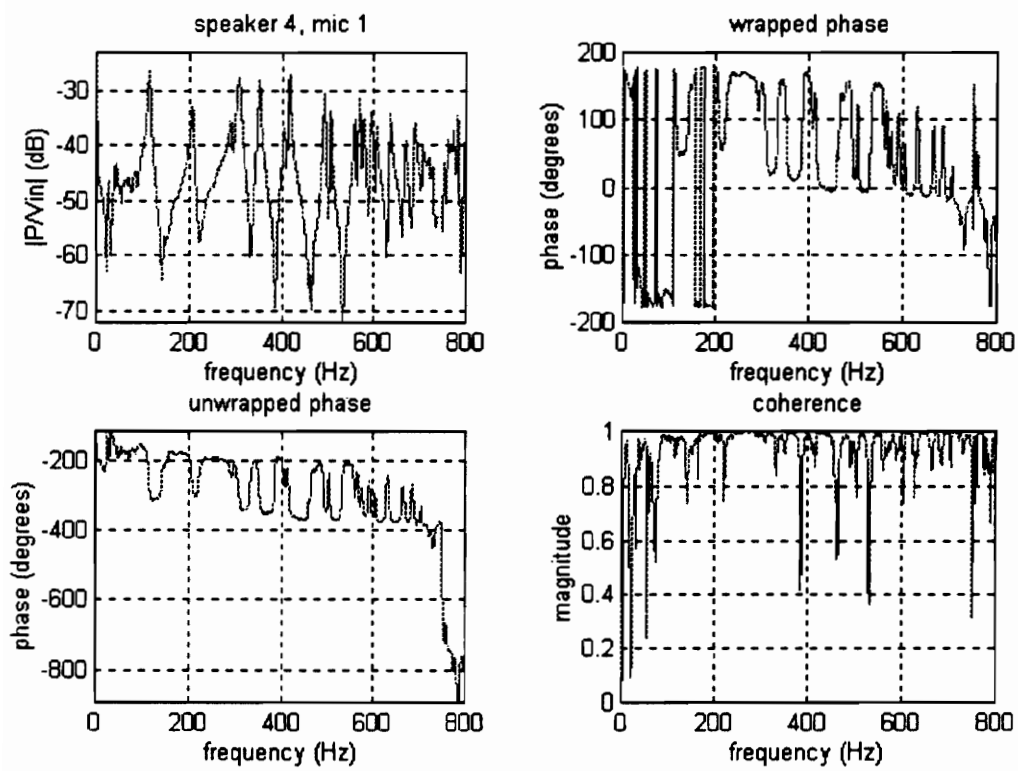


Figure A.31 Speaker 4, Microphone 1

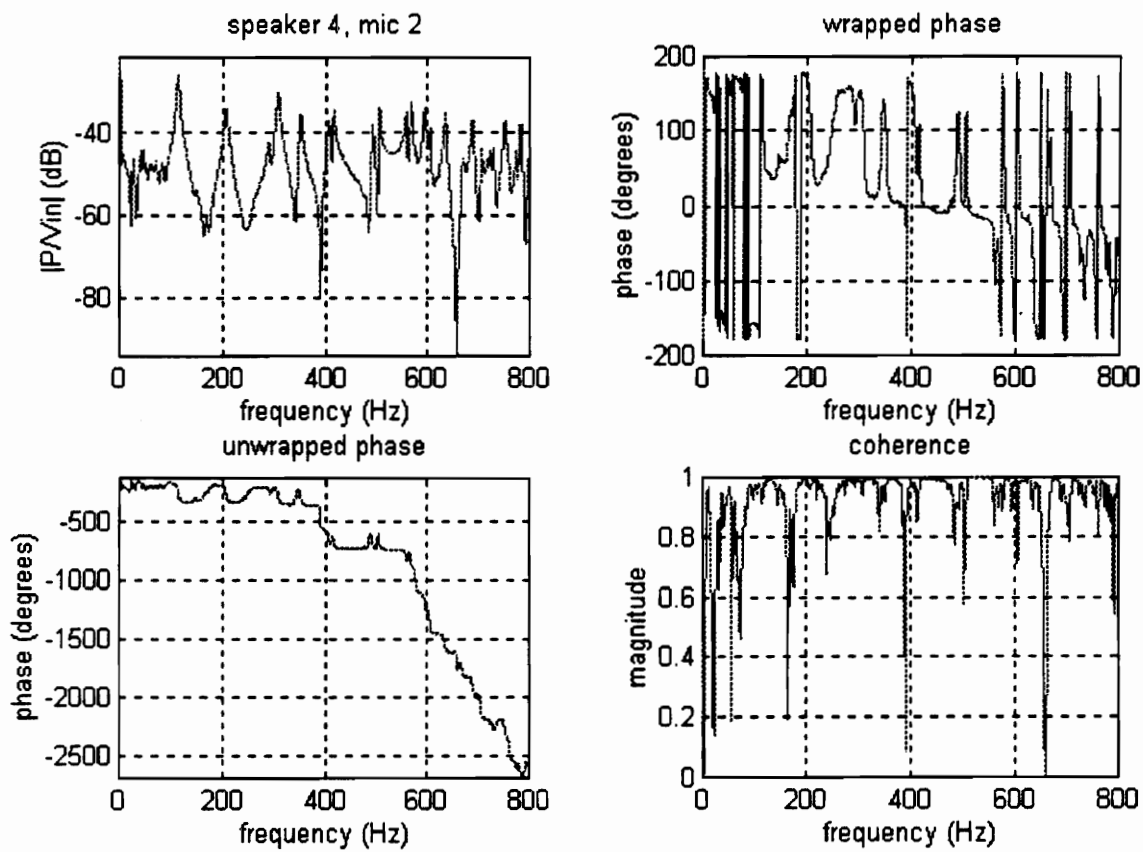


Figure A.32 Speaker 4, Microphone 2

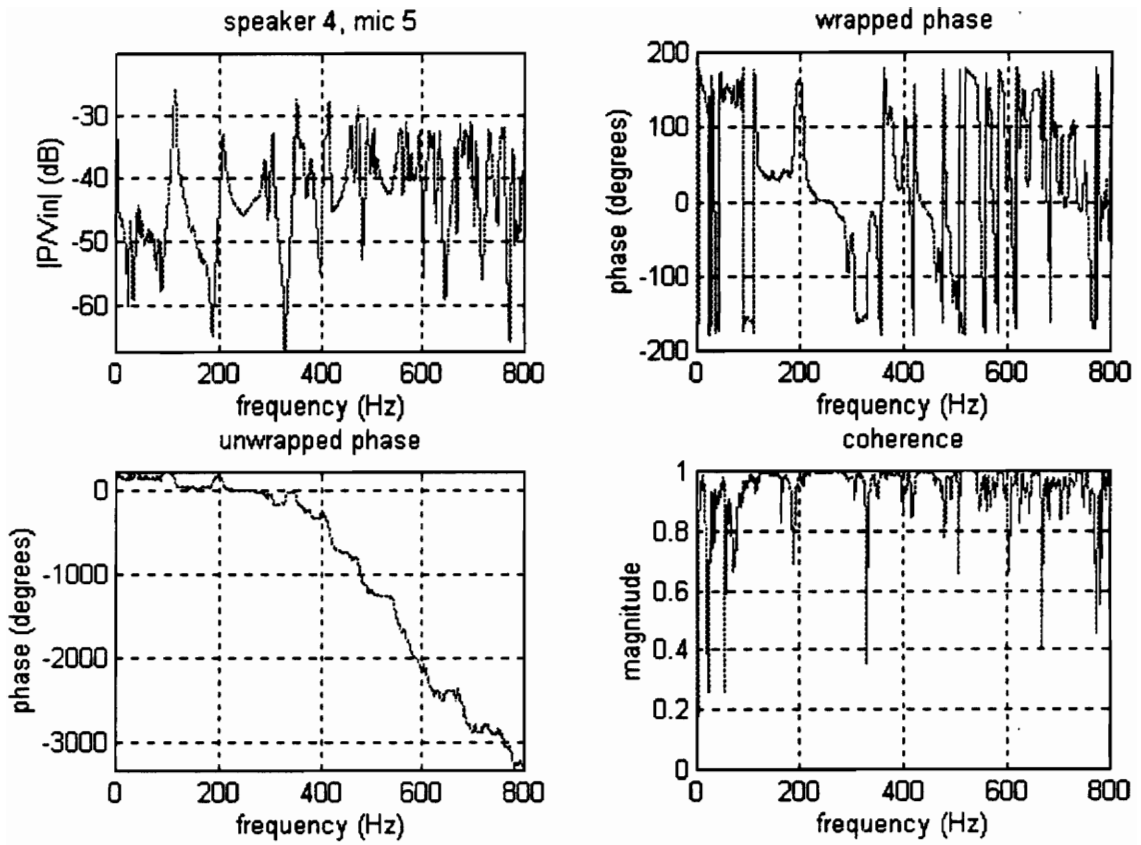


Figure A.33 Speaker 4, Microphone 5

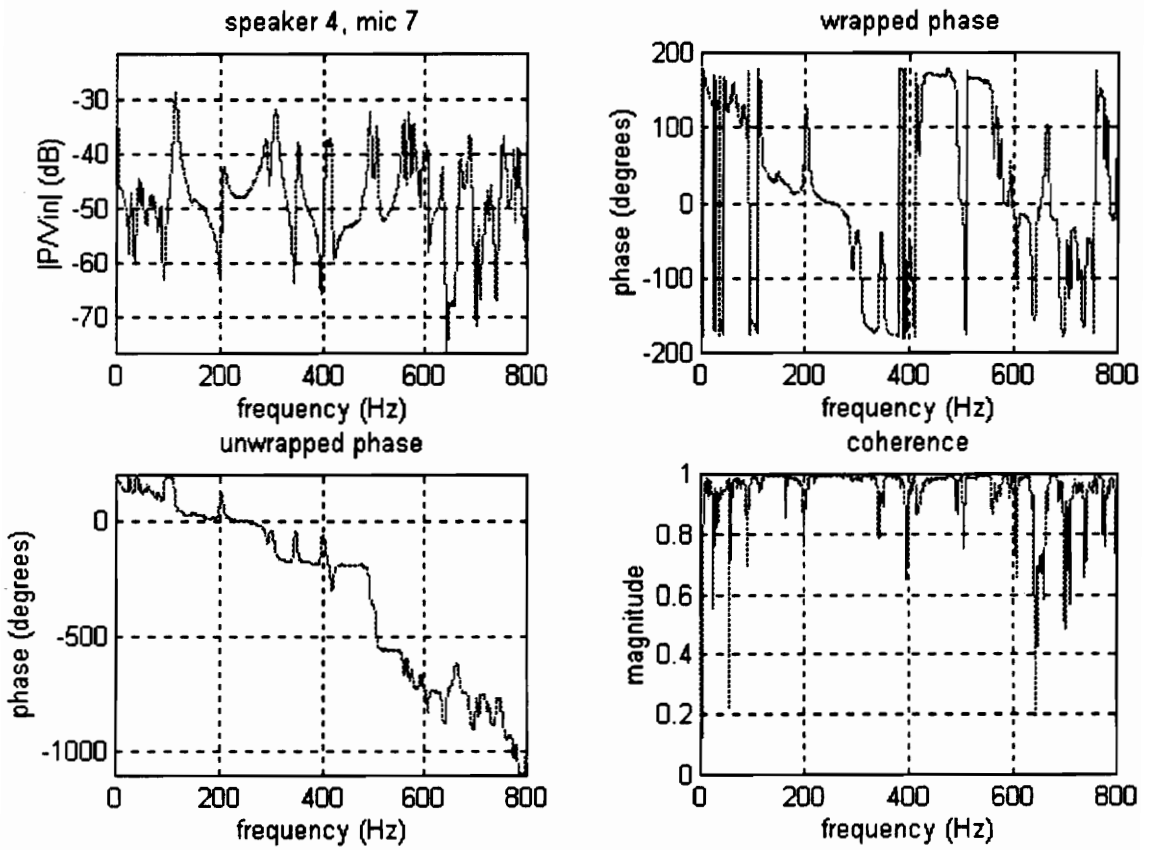


Figure A.34 Speaker 4, Microphone 7

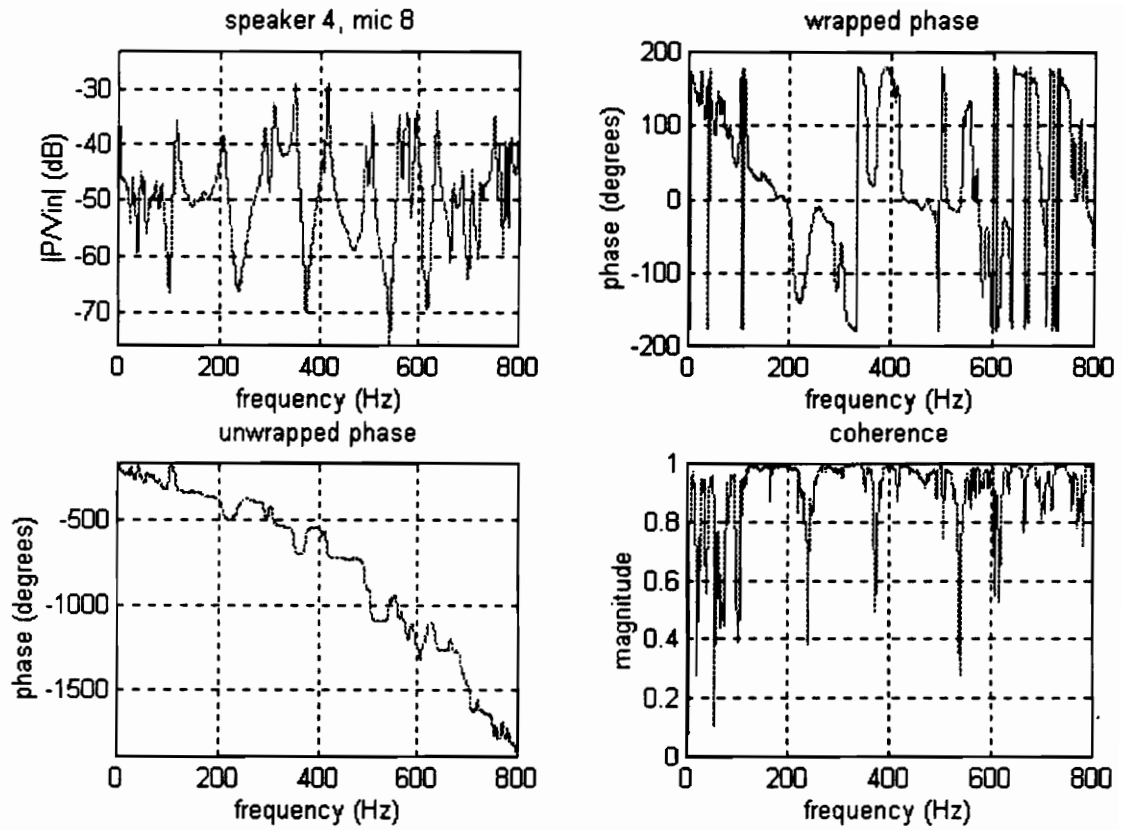


Figure A.35 Speaker 4, Microphone 8

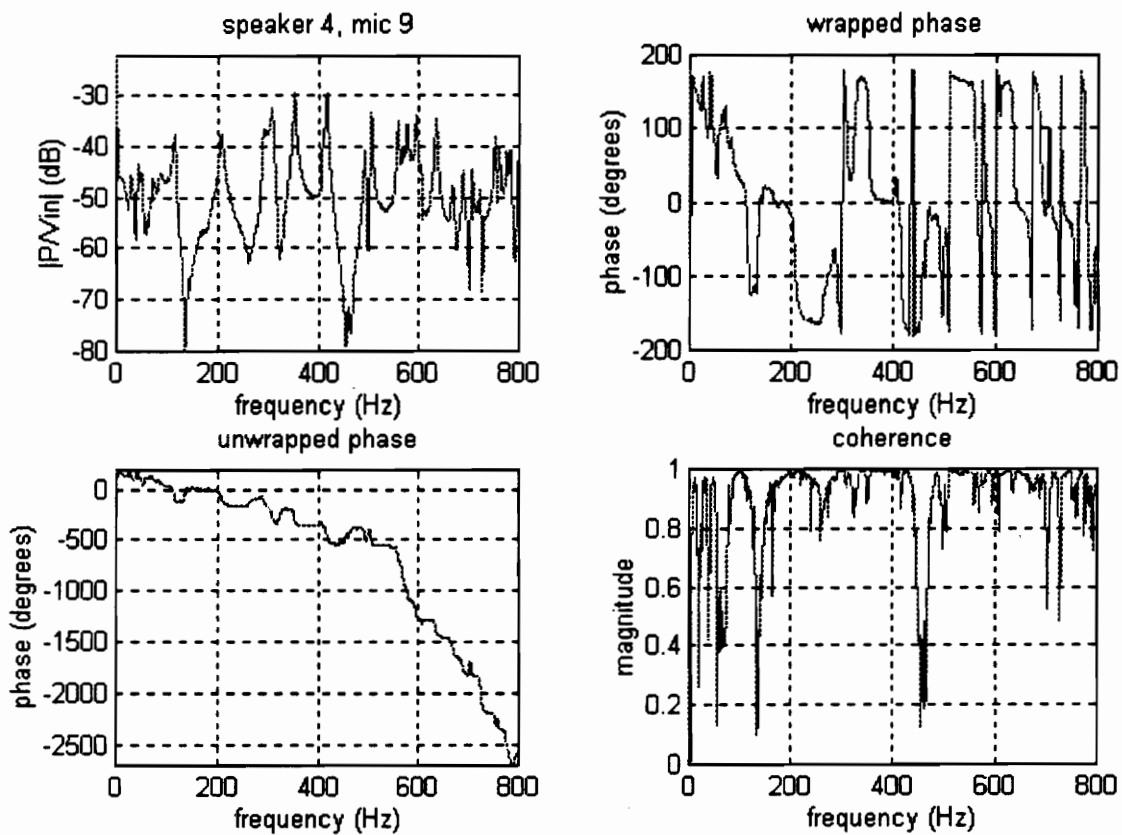


Figure A.36 Speaker 4, Microphone 9

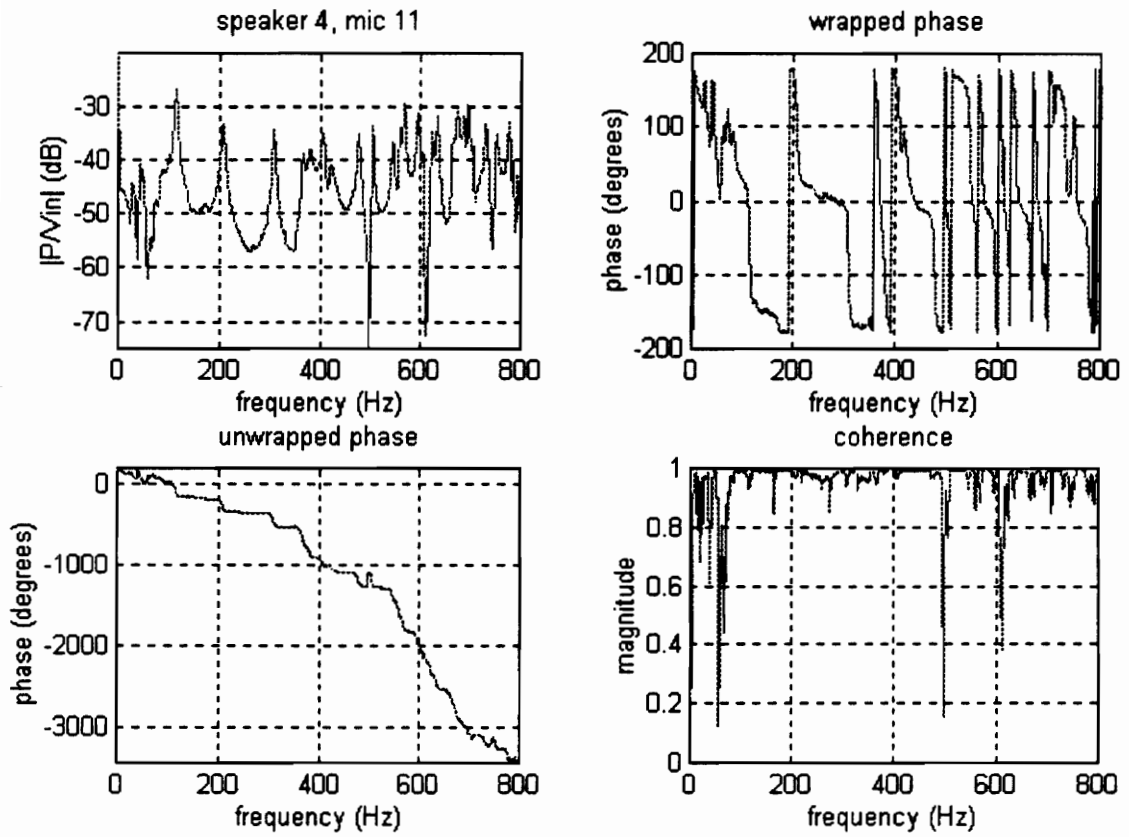


Figure A.37 Speaker 4, Microphone 11

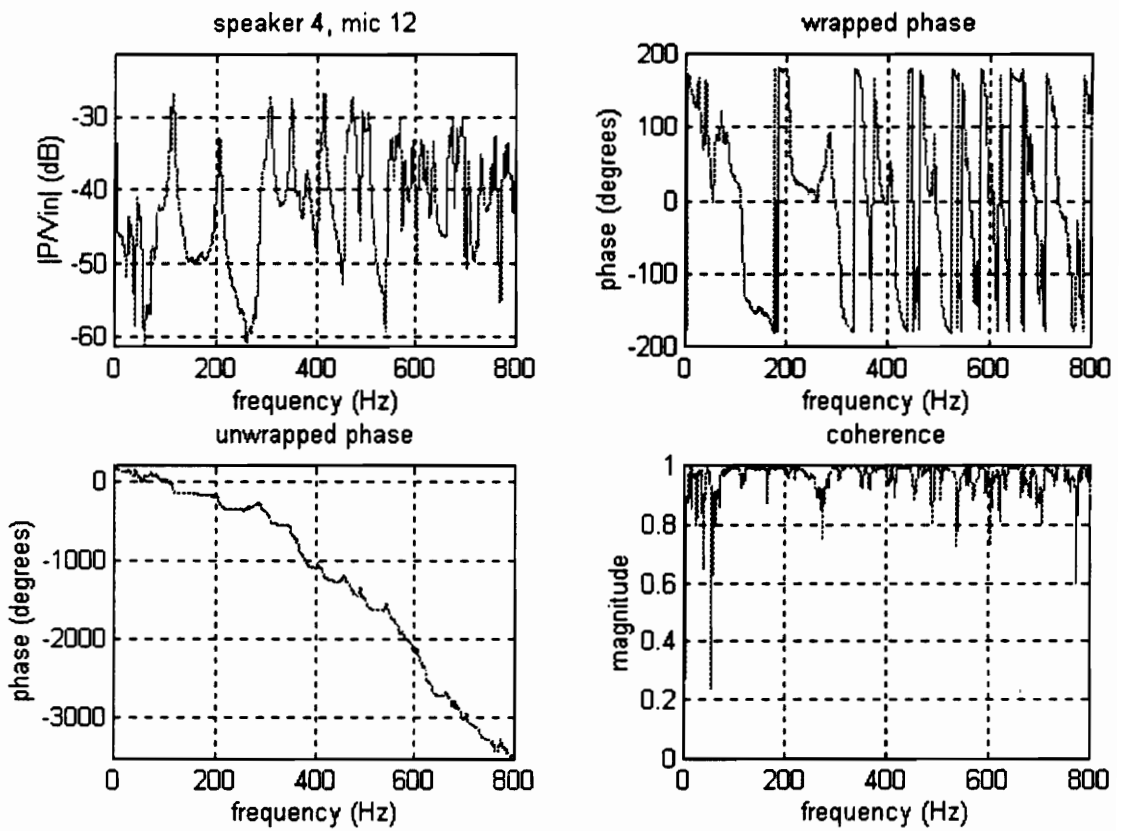
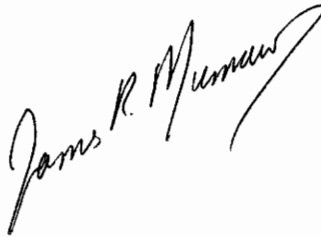


Figure A.38 Speaker 4, Microphone 12

Vita

James Mumaw was born on January 4, 1972 in Falls Church, Va. He graduated from George C. Marshall High School in Falls Church, Virginia in 1990, and entered the College of Engineering at Virginia Tech that same year. He worked as a co-op for Dupont in Martinsville, Virginia for the equivalent of one year. He graduated from the department of Mechanical Engineering with a B.S. degree in 1995, and immediately began working towards his M.S. degree. In addition to his research, he worked as a Graduate Teaching Assistant for the mechanical engineering lab. He also worked on several projects related to noise control engineering. He completed his M.S. degree in December, 1996 and wondered what he would do next.

A handwritten signature in black ink, reading "James R. Mumaw". The signature is written in a cursive style and is positioned diagonally across the page.